Shapes and rotational properties of thirty asteroids from photometric data

Johanna Torppa and Mikko Kaasalainen

University of Helsinki, Observatory, P.O.Box 14, FIN-00014 Helsinki, Finland

tel: +358-9-19122802, Fax +358-9-19122952

Email: jtpesone@astro.helsinki.fi, Mikko.Kaasalainen@astro.helsinki.fi

Tadeusz Michalowski, Tomasz Kwiatkowski,

and Agnieszka Kryszczyńska

Astronomical Observatory, Adam Mickiewicz University, ul. Słoneczna 36, 60-286 Poznań, Poland

Peter Denchev

Institute of Astronomy, Rozhen National Observatory, P.O. Box 136, 4700 Smolyan, Bulgaria

Richard Kowalski

Quail Hollow Observatory, 7630 Conrad St. Zephyrhills, Florida, USA

Pages: 57

Figures: 64

Tables: 2

Running head: Models of thirty asteroids

Correspondence to: Mikko Kaasalainen, University of Helsinki, Observatory, P.O.Box 14, FIN-00014 Helsinki, Finland

Abstract

We have analyzed photometric lightcurves of 30 asteroids, and present here the obtained shapes, rotational periods and pole directions. We also present new photometric observations of five asteroids. The shape models indicate the existence of many features of varying degrees of irregularity. Even large main-belt asteroids display such features, so the resulting poles and periods are more consistent than those obtained by simple ellipsoid-like models. In some cases the new rotational parameters are rather different from those obtained previously, and in a few cases there were no proper previous estimates at all.

Key words: asteroids, rotation; photometry; surfaces, asteroids

1 Introduction

Recent studies have demonstrated the usefulness of photometric lightcurves in detailed modelling of asteroids (Kaasalainen and Torppa 2001, hereafter KT; Kaasalainen et al. 2001 and 2002b, hereafter P I and P II; Mottola and Lahulla 2000; Pravec and Hahn 1997; Ďurech 2002). To date, we have applied new methods of lightcurve inversion (KT, P I) to model some 80 main-belt, near-Earth, and Trojan asteroids (this paper; P I and II; Kaasalainen et al. 2002a; Slivan et al. 2003; Kaasalainen et al., in preparation). The bulk of the data were collected from Uppsala Asteroid Photometric Catalogue (UAPC), fifth update (Lagerkvist et al., 2001), but several recent observations from various observers have been included in the construction of a number of models.

In this paper we present pole, period and shape results for 30 main-belt asteroids; models and new observations of several near-Earth asteroids will be discussed in a separate paper (Kaasalainen et al., in preparation). More models will be steadily obtained as further observations are made: there are tens of asteroids that need no more than a few additional lightcurves for at least a preliminary inversion analysis. It is thus important to conduct long-term observing projects of MBAs to obtain good geometry coverages. An example of such a project is the one carried out at Poznań Observatory for several targets since 1997. Here we include new data for four MBAs from that project; more will be analyzed in the future.

Another important new factor in photometry is the fast developing amateur-professional connection. Well-equipped amateurs can now readily provide quality observations down to 15th magnitude or even fainter. They represent a considerable resource of telescope time. What is more, this telescope time is extremely flexible. As an example of this, we present rapid-response observations needed to complete the datasets of 37 Fides and 129 Antigone: several hours of densely measured data could be acquired within a few days' notice. It seems that this practice, with collectively coordinated target alert lists, will form the backbone of asteroid photometry in the future.

In Section 2 we describe more closely the data and some aspects of the modelling procedure. Section 3 contains the models for 2 Pallas, 6 Hebe, 8 Flora, 9 Metis, 12 Victoria, 17 Thetis, 18 Melpomene, 19 Fortuna, 21 Lutetia, 23 Thalia, 37 Fides, 42 Isis, 55 Pandora, 63 Ausonia, 69 Hesperia, 85 Io, 88 Thisbe, 107 Camilla, 129 Antigone, 135 Hertha, 201 Penelope, 230 Athamantis, 250 Bettina, 337 Devosa, 349 Dembowska, 372 Palma, 511 Davida, 584 Semiramis, 675 Ludmilla, and 694 Ekard. New observations of 21 Lutetia, 37 Fides, 85 Io, 129 Antigone, and 135 Hertha are presented in Section 4. In Section 5 we sum up the paper and discuss some future prospects

of the analysis of photometric and complementary data.

2 Data and modelling procedure

The comments and clarifications given in P I and II naturally apply here as well, but we emphasize a couple of points and add a few remarks on the practical side of the inversion procedure.

2.1 Observations

The average numbers of data points and observing geometries (apparitions) of the asteroids analyzed here are somewhat smaller than those of P II, which is one reason why we find more double poles here than in P II. Another reason is that such solutions are inevitable (regardless of the method, if only disk-integrated data are available) when the asteroid moves very close to the plane of the ecliptic. In such cases the inversion procedure produces two equally good poles (with roughly equal ecliptic latitudes and longitudes close to 180° apart), while the corresponding shapes are mirror images of each other. Our survey of the UAPC catalogue has earmarked many asteroids for which well-constrained shape solutions or sufficiently unambiguous pole solutions could not be obtained just yet; these we have left to wait for more observations.

Even for the analyses presented here, we could not afford to be quite as choosy with our data as in P I and II. For example, lightcurves reported in composite form were included in the data sets to get a sufficiently large amount of information, and only extremely noisy curves were rejected. The final rms value from χ^2 basically indicates how noisy the data are since our models typically fit the data down to the noise level.

2.2 Shape solutions and scattering model

All the shape models presented here are convex as this is the most robust solution to the inverse problem. The coverage of the solar phase angle is as important as that of the aspect angle. Near opposition the global shadowing effects of the surface are negligible, and the data are not very informative. If at least part of the data are observed at solar phase angles of some 20 degrees or more, a reliable convex model can be obtained. An important aspect of the convex model is that any possible albedo variegation is automatically embedded in it, and we have a direct indicator for the amount of albedo asymmetry on the surface (P II).

Nonconvex features can in principle be resolved, but even large nonconvexities require very high

solar phase angles to show in disk-integrated photometric data (Ďurech and Kaasalainen 2003). We can reliably say that lightcurves of main-belt asteroids very seldom contain nonconvexity information. If no such information is available, we prefer a convex model, stripped by Occam's razor of imaginary topographic details (but if illustrative purposes dominate over scientific ones, a possible nonconvex model is always easy to create). This is also the main reason why we can confidently say whether a reported lightcurve of a main-belt asteroid is false or not. If there simply is no shape/period/pole solution that can reproduce a lightcurve at least reasonably well, the observations or their records are very probably incorrect.

As in P II, we carried out the inversion using both a combination of the Lommel-Seeliger and Lambert light-scattering laws and the Hapke scattering model. When using the Hapke model, absolute-magnitude lightcurves were used for regularization as described in P I, so that all reliable information content of the absolute brightnesses was utilized. Since the scattering parameters cannot be unambiguously determined using the available data (see also S. Kaasalainen et al. 2003), there is no reason to report the used parameter values here. We just mention that they were consistent with the 'typical' values for the corresponding asteroid classes. Since the detailed light-scattering part of the problem very effectively separates from the rotation/shape part (P I), we plan to analyze the former in the future along the lines discussed in S. Kaasalainen et al. (2003) by using the data from all analyzable objects in our UAPC survey. It should be noted that, due to the scarcity of well-measured points densely covering suitable ranges of solar phase angle (particularly close to opposition), a meaningful detailed light-scattering analysis is possible only for a much smaller group of targets than for which rotation/shape analysis is feasible. In most cases, the available absolute calibrated magnitudes are best used for consistency checks (and potential removal of pole ambiguities).

The inferred rotational properties were not sensitive to the scattering model or its parameters (when restricted to reasonable limits). The global features of the shape solution were also stable, although we noticed that particularly for mildly featured (low-amplitude) and noisy data the dimension along the rotational axis was not strongly constrained. This is due to the fact that we had to consider most lightcurves relative as there were few cases where magnitudes were accurately absolute and given in a standard magnitude system. (After all, if one observed only flat lightcurves it would be impossible to determine the degree of flattening of the originating spheroid from relative or inaccurate absolute photometry.) Therefore the shape can be stretched or squeezed in the vertical direction, typically up to some $\pm 10\%$ depending on the chosen scattering

model and the number of shape parameters. Accurate absolute photometry and scattering models would constrain the degree of flattening better, but the best way to fix the vertical dimension is to use data complementary to disk-integrated photometry.

3 Models

In this section we briefly describe the adopted models. For each object dimensional ratios a/b and b/c are given. They are the averages of the semiaxis ratios of the best-fitting triaxial ellipsoid dimensions and the corresponding ratios of the greatest three-dimensional extents of the object. The a dimension is always chosen as the biggest one when c is along the rotational axis. The b/c ratio is the one least constrained by any inversion procedure (see above). The dimensions are mostly in reasonable agreement with the previously obtained usually rather widely dispersed ellipsoidal model ratios (when applicable).

In Table I we give values for some quantities characterizing the adopted model and the observations. The first column indicates the object, and columns two to five give the rotational properties and the goodness of fit: β and λ are the ecliptic latitude and longitude of the model's pole direction in degrees, P is asteroid's sidereal rotational period in hours, and *rms* the root-mean-square value of the fit in magnitudes. β is defined such that the asteroid always rotates in the positive direction around the pole. Thus negative values of β indicate retrograde rotation. Columns six to nine describe the data: T_{tot} is the total time span of the observations in years, N_{app} the number of apparitions observed, α the solar phase angle range of the observations in degrees and N_{cur} the number of lightcurves used in inversion.

3.1 Error estimates

As in P I and II, error estimates for the pole and the period were determined by investigating the stability of the obtained values when varying initial values as well as scattering models and parameters. This creates a distribution of possible solutions, which we prefer to a formal error estimate from one fit. From our experience with various simulations, we have found it a good rule of thumb to include solutions with χ^2 up to some 5% (and certainly not more than 10%) larger than the best one in the 'solution area'. The shape solutions within this area are very similar, and the pole and period error margins can easily be estimated. Lightcurve fits of the solutions outside this area are usually already noticeably worse by eye. Indeed, here eye judgement can often be

far sharper than χ^2 estimates, particularly when it is a matter of the accurate reproduction of only a few points or some features that show very little in the somewhat insensitive total χ^2. The $\pm$-figure for the pole direction is always a rough estimate as the pole solution distribution on the celestial sphere can seldom be described by a simple shape. Also, we prefer *one* error estimate for the pole direction (in arc) to separate $\Delta\beta, \Delta\lambda$-values as $\Delta\lambda$ has no meaning at high latitudes, and there is no particular reason why β and λ should be chosen as the main axes for the solution distribution.

The pole distribution of acceptable solutions is usually steep. In some cases the error margin seems to be only about $\pm 2^\circ$, but it would be too optimistic to adopt that value due to all the systematic uncertainties and insufficiencies in both model and data. This is why we have simply adopted the custom that, if not otherwise stated, the pole error is $\pm 5^\circ$ as in P II. Simulations and the 'ground truth' cases of P I support this practice. Due to the inherent insufficiency of the model, we do not think that more refined distribution analyses can give much more meaningful estimates. It seems that simple multiples of 5° can well serve for practical purposes. It is important to note that the solution error is clearly dominated by the systematic data and model effects (underlined by the number and range of observing geometries) rather than observational noise. As a rule, the 'pseudosolution' distribution due to noise (obtained by, e.g., the Monte-Carlo method of creating additional pseudo-datasets by simulating random data noise within a given level) is tighter and less realistic than our solution bounds. The usual rule of thumb of errors applies here as well: the safe side error estimate is at least twice the standard one (i.e. $\pm 10^\circ$ for the pole rather than $\pm 5^\circ$).

The rotational period is given in the accuracy in which it could be determined (i.e., of the order of the last unit digit). The error is usually between $0.01 - 0.1$ times the basic resolution interval $P^2/(2\,T)$ (where P is the rotation period and T the length of the total observation time span), corresponding to a rotational phase shift of a few degrees between the first and the last lightcurves (see P I). Unless otherwise explained, when we say that a given pole direction is preferred to other options (typically those around $\lambda + 180^\circ$), we mean that the latter yield χ^2s at least 10% larger than the best direction (usually much larger than that). An occasional property of datasets of less than some twenty lightcurves is that an unphysical shape model may reach as good a fit as the adopted one, usually at different but sometimes even relatively nearby rotational parameters. Though such a model is easy to discard, this indicates that one should be wary of shape details and the apparent pole error, and generally regard solutions from such datasets as preliminary.

3.2 Descriptions

In Figs. 1 to 60 are shown the model shapes of each asteroid from two directions (equatorial views at longitudes 90° apart), and four selected model lightcurve fits to the data. In lightcurves the angle α is the solar phase angle, and θ_0 and θ the polar aspect angles of the Sun and the Earth. Note that the lightcurves are plotted in the natural physical dimension of relative intensity: this always scales the plots correctly, and, contrary to the traditional magnitude convention, has a well-defined zero line. The curves cover one full rotation period (all points are folded within it).

In the following descriptions of models, the term 'first' does not indicate a preference for either model: it refers to the pole solution with the smaller ecliptic longitude. 'Second' corresponds to the other solution. Though moderate albedo variegation was detected in some cases, none of them called for explicit albedo spot modelling such as in P II or in Kaasalainen et al. (2002a). For each target we state the approximate IRAS diameter and taxonomic class.

2 Pallas (520 km, B)

Pallas is, as expected of an asteroid of this size, a rather classical pseudo-ellipsoidal figure, characterized by a/b=1.1 and b/c=1.05. Pallas reaches very high ecliptic latitudes, so the two pole solutions are, roughly speaking, the pro- and retrograde versions of one pole direction area instead of the more typical roughly isolatitudinal $\lambda + 180°$-ambiguous pair of targets with orbits at low ecliptic latitudes. Despite the abundance of solar phase angles of at least 20°, neither of the two pole solutions was clearly better – this is probably due to the featureless shape. We slightly prefer the first pole as its fit is somewhat better by eye, and the convergence on it is more robust; the shape solutions from the two options are very similar. There seems to be moderate albedo variegation on the surface as the albedo asymmetry factor (see P II) is equivalent to about 1% of the surface area (values larger than $1-2$% typically call for explicit albedo spot modelling). Some of the lightcurves from the 60's and 70's clearly contained significant systematic errors. The model shape and lightcurve fits corresponding to the first pole are shown in Figs. 1 and 2.

6 Hebe (190 km, S)

For Hebe, the dimensions a/b=1.1 and b/c=1.1 are very coarse as Hebe really seems to be a rather angular, roughly cut body. Again, there is indication of moderate albedo variegation, so some of the large, flat features on the model may well be indentations accompanied by albedo markings. The model shape and lightcurve fits are shown in Figs. 3 and 4.

8 Flora (140 km, S)

Flora's shape is quite regular, which was expected since the lightcurves included no special features. Axis ratios are a/b=1.0 and b/c=1.2. The model shape and lightcurve fits are shown in Figs. 5 and 6.

9 Metis (170 km, S)

Metis has some sharp shape features, and one end is smaller than the other. There also seems to be a large planar area on the southern/northern pole region (first/second solution, respectively). Object of this size might be expected to be more regular, but our results are similar with previous studies, which have indicated presence of strong albedo or shape features (Nakayama et al., 2000, Storrs et al., 1999). The dimensions of Metis are a/b=1.2 and b/c=1.4. Both pole solutions gave good fits and shapes are roughly mirror images. Figs. 7 and 8 represent the model obtained with the first pole.

12 Victoria (120 km, S)

The shape model of Victoria contains slightly irregular features. Its dimensional ratios are a/b= 1.3 and b/c=1.3. The other hemisphere is not well observed, a fact which decreases the accuracy of the model. The solution is shown in Figs. 9 and 10. The sharp features are consistent with the radar observations by Mitchell et al. (1995).

17 Thetis (90 km, S)

Thetis' data produce two, quite regular mirror image shape solutions that are slightly elongated with a/b=1.3 and b/c=1.0, with some planar features. The model shape and lightcurve fits shown in Figs. 11 and 12 are obtained with the first pole.

18 Melpomene (150 km, S)

For Melpomene a/b=1.2 and b/c=1.2. The two pole solutions produce nearly mirror images. The convex model is not smooth, but consists of planar areas, which suggests an irregular, non-convex shape. Significant elongation and brightness variegation has also been suggested by Storrs et al. (1999). The second solution is shown in Figs. 13 and 14.

19 Fortuna (230 km, G)

Fortuna moves very close to the ecliptic plane, so two mirror pole and shape solutions are inevitable. Some albedo variegation is present, and the quite smooth and regular figure is charac-

terized by a/b=1.2 and b/c=1.05. The model shape and lightcurve fits (corresponding to the first pole) are shown in Figs. 15 and 16.

21 Lutetia (100 km, M)

Lutetia is characterized by some sharp and irregular shape features, with rough global dimensions a/b=1.2 and b/c=1.2. No albedo variegation was detected to accompany the rough shape features. The model shape and lightcurve fits (corresponding to the first pole) are shown in Figs. 17 and 18.

23 Thalia (110 km, S)

Thalia's shape is very regular without planar areas or sharp corners. Dimensional ratios are a/b=1.1 and b/c=1.3. The pole error is $\pm$15 degrees. The solution is shown in Figs. 19 and 20.

37 Fides (110 km, S)

Fides is quite spherical, with a/b=1.1 and b/c=1.05, yet the model shape is locally rather rugged. There is also indication of moderate albedo variegation, so large impact markings are probable. The model shape and lightcurve fits (corresponding to the first pole) are shown in Figs. 21 and 22.

42 Isis (110 km, S)

Isis would seem to be somewhat like Fides in appearance, with a/b=1.1, b/c=1.0, and considerable local irregularities. Consistent with this, some albedo markings are probable. We prefer the second pole somewhat because of the more realistic appearance of its shape model. This and some model fits are shown in Figs. 23 and 24.

55 Pandora (70 km, M)

Pandora is characterized by a/b=1.2 and b/c=1.2. Neither considerable irregularities nor albedo variegation seem to be present. Appararently the ecliptic latitudes of the orbit, though not larger than 9°, are high enough to distinguish between the pole solutions as the potential $\lambda - 180°$-solution gives a noticeably worse fit. The model shape and lightcurve fits are shown in Figs. 25 and 26.

63 Ausonia (110 km, S)

Ausonia is an elongated object, as is seen from the axis ratios a/b=1.9 and b/c=1.0. Data do not cover well both hemispheres, so there may be shape features this very regular model does not reveal. Moderate albedo asymmetry was indicated. Figs. 27 and 28 represent the first solution. Hestroffer et al. (private communication) prefer the first pole as it is more consistent with interferometric observations with the FGS mode of the Hubble Space Telescope (Tanga et al. 2003).

69 Hesperia (140 km, M)

Hesperia's dimensional ratios are a/b=1.1 b/c=1.4. There are some planar areas on the surface, possible markings of nonconvexities. This solution is shown in Figs. 29 and 30.

85 Io (160 km, C)

Even though Io's ecliptic latitudes are high, it is hard to say which pole solution is the correct one. This is due to the almost spherical, smooth shape with a/b=1.1, b/c=1.0, and the fact that some lightcurves are very noisy. No albedo variegation was detected. The model shape and lightcurve fits (corresponding to the first pole) are shown in Figs. 31 and 32.

88 Thisbe (200 km, C)

Dimensional ratios of Thisbe are a/b=1.1 and b/c=1.2. The model displays some large planar regions, indicated by sharp features in some lightcurves. Slight equatorial albedo asymmetry was detected. The solution is shown in Figs. 33 and 34.

107 Camilla (240 km, C)

Camilla is rather regular and slightly elongated, with a/b=1.4 and b/c=1.2. The small satellite (Storrs et al. 2001) is too faint to have any effect on the lightcurves. The mirror pole (+77,230) gives a worse fit and is not listed in Table I, but it cannot be completely ruled out. The adopted solution is shown in Figs. 35 and 36.

129 Antigone (130 km, M)

Antigone was a slightly baffling case until we obtained the 2002 lightcurve that confirmed the solution. The uncertainty was due to a group of six erroneous lightcurves from the 70's and 80's. Their faultiness was in principle easy to confirm as for each of them there was a corresponding curve from a nearby epoch and practically the same geometry that was fitted very well with the adopted solution. Also, in each case the curve shapes were fine, it was just that the reported epochs

were clearly incorrect. Nevertheless, it was important to have the fresh lightcurve to confirm the result. We also found an indication of moderate albedo variegation. The shape is rather regular, with a/b=1.3 and b/c=1.0. The adopted solution is shown in Figs. 37 and 38.

135 Hertha (80 km, M)

Hertha seems to be a somewhat flattened object, with a/b=1.1 and b/c=1.5. The model depicts a rather regular shape containing a large flat region in the pole area. There are signs of slight albedo variegation. The model shape and lightcurve fits (corresponding to the first pole) are shown in Figs. 39 and 40.

201 Penelope (70 km, M)

The shape model of Penelope is somewhat elongated and quite regular, but it shows a slight oval asymmetry as well as some large flat regions (possibly marking large indentations) in the middle. These could be due to a contact-binary structure. Similar features are much stronger in, e.g., 44 Nysa (Kaasalainen et al. 2002a). The global dimensions are approximated by a/b=1.5 and b/c=1.1. The model shape and lightcurve fits (corresponding to the first pole) are shown in Figs. 41 and 42.

230 Athamantis (110 km, S)

Athamantis has a very long rotation period, and the period is also almost exactly resonant with that of the Earth. This shows in our dataset's coverage of rotational phases, so we must still call our model preliminary. The model dimensions are roughly a/b=1.1 and b/c=1.1. We slightly prefer the first pole as it gives a somewhat more realistic-looking shape. This solution is depicted in Figs. 43 and 44.

250 Bettina (90 km, M)

As with Pallas, Bettina's two pole options are not the typical $\lambda + 180°$ mirror poles, but the pro- and retrograde versions of the same rotation axis. Indeed, the ecliptic orbit latitudes over 10° resolve the former ambiguity. The pro/retro-ambiguity remains because of the simple shape (with dimensions a/b=1.3 and b/c=1.0) and mostly small solar phase angles. The model shape and lightcurve fits corresponding to the second pole are shown in Figs. 45 and 46.

337 Devosa (60 km, M)

The analysis of Devosa was not very easy due to the sparsely covered rotational phases and some very noisy lightcurves. We found a solution that fits the data quite well, but the shape cannot be called very tightly constrained. The model's global dimensions are a/b=1.2 and b/c=1.5. Moderate albedo variegation was also detected. The solution is shown in Figs. 47 and 48.

349 Dembowska (140 km, V)

Dembowska's dimensional ratios are a/b=1.3 and b/c=1.4. The shape solution contains a few planar sections, suggestive of nonconvexities. This is also consistent with the detection of moderate equatorial albedo asymmetry. Of the two pole solutions, the second one is shown in Figs. 49 and 50.

372 Palma (200 km, C)

Palma appears to be a somewhat rugged but basically rather spheroidal body, with a/b=1.1 and b/c=1.3. The amplitudes of the lightcurves were very low, but the good aspect angle coverage and the high ecliptic orbit latitudes singled out a good solution. Since there were no signs of albedo asymmetry, the lightcurves are likely to be caused mostly by the rugged appearance rather than albedo variegation. The model is shown in Figs. 51 and 52.

511 Davida (340 km, C)

For Davida, the dimensional ratios are a/b=1.2 and b/c=1.3. The shape is rather regular with no sharp features. The solution is shown in Figs. 53 and 54.

584 Semiramis (60 km, S)

This irregular object has dimensional ratios a/b=1.3 and b/c=1.2. The large flat area on one side may be an indication of a nonconvex feature. The solution is shown in Figs. 55 and 56.

675 Ludmilla (350 km, S)

Ludmilla's dimension ratios are a/b=1.3 and b/c=1.1. We slightly prefer the second pole as it gives a somewhat smoother shape result, expected of an asteroid of this size. One equatorial end of the otherwise regular model appears rather flat. This solution is shown in Figs. 57 and 58.

694 Ekard (90 km, C)

Ekard is another globally quite regular body that shows many local planar regions. The dimensions are a/b=1.2 and b/c=1.1. The model and lightcurve fits are shown in Figs. 59 and 60.

4 New observational data

4.1 Sample observations from long-term campaign

Photometric measurements of four asteroids (21 Lutetia, 85 Io, 129 Antigone, and 135 Hertha) from 23 nights were performed at two observatories. Most of these observations were obtained at Borowiec Station of the Poznań Observatory (Poland). The observing system consists of a 0.4–m Newton reflector, a KAF–400 CCD camera and R filter (see Michałowski et al., 2000). A standard reduction of the frames as well as the aperture photometry were performed with the CCLRS STARLINK package. Due to non–photometrical weather conditions no reduction to the standard system was done.

On 30 January 1998, the asteroid 135 Hertha was also observed at Rozhen Observatory (Bulgaria). A 0.6–m Cassegrain telescope equipped with a single–channel photometer was used. Reduction has been carried out with standard algorithms as described in Denchev et al. (1998).

Table II contains the aspect data for the asteroids observed. The results of our observations are presented in Figs. 61–63 as composite lightcurves. For convenient viewing, the lightcurves have been composited with the synodical periods shown in the graphs. The abscissae are the rotational phases with the zero points corrected for light–time.

4.2 Small telescopes for rapid response and flexible telescope time

Today, a well-equipped amateur can obtain lightcurves with better quantity and quality of data points than professional observers in the pre-90's before CCDs. This has profound implications for asteroid photometry. The observing possibilities are very flexible, and the response to an observation request can be rapid. As an example of this, lightcurves for 37 Fides and 129 Antigone were obtained at Quail Hollow Observatory on 6 January 2003 and 26 November 2002, respectively. The instrument was a fully automated 18 cm Maksutov telescope, equipped with an SBIG ST-7E CCD. Data reduction was performed with Brian Warner's Canopus software (`http://www.MinorPlanetObserver.com`). The observations were relative unfiltered photometry in order to obtain as high a signal-to-noise ratio as possible for these bright targets (both brighter than 12 mag). In this way, we wanted to exploit the small-telescope possibilities to the maximum, and the experiment turned out to be very positive. The data could well be used to complete two slightly insufficient datasets so that reliable models could be constructed. The lightcurves for 37 Fides and 129 Antigone are shown in Fig. 64 together with the model fits, and their aspect data

are included in Table II.

5 Conclusions and future work

As in P II, the obtained models show that while very large global-scale irregularities become more abundant as the size decreases, even objects larger than 100 kilometres in diameter may have significant large-scale shape features. The corresponding rotational models take such features into account and thus give consistent values for rotation periods and pole directions. On the other hand, peculiar-looking lightcurve features can often be explained with rather simple shape 'perturbations'. Striking albedo features, in particular, are very seldom needed to explain the observed lightcurves. This is consistent with spacecraft images and simple physical considerations: asteroid surfaces are not likely to be covered with extensive albedo markings of high contrast. Albedo spots visible to the eye in the disk-resolved probe images are usually negligible in disk-integrated sense. An interesting class seems to be that of 'chipped apples' such as 37 Fides that are literally roughly spheroidal. The rough features are perhaps outcomes of strong impacts on originally almost classic equilibrium-like shapes.

We have now carried out photometric inversion analyses for a total of about 80 asteroids. Though the shape results are closer to the real shapes than triaxial ellipsoids, they should be treated with care. One must keep in mind that they are still rough global representations of the real topographies that can be resolved accurately only with spacecraft flybys. New lightcurves will always serve to improve the models. Particularly in the case of asteroids that have been analyzed with rather minimal datasets, the pole solutions can change with new data a larger amount than the estimated error for the original dataset. This is typical for any observational science, but such systematic effects are very difficult to predict in advance since an error estimate applies only to a given dataset. After the inclusion of new data, the fit for some of the older lightcurves may have to be allowed to get somewhat worse than would have been originally accepted, resulting in a new solution area in a new χ^2-topography. It is naturally clear that models from 4 apparitions and 20 lightcurves are liable to change more than those from, say, 7 apparitions and 40 lightcurves.

Model files (updated when applicable) for the asteroids we have analyzed are obtainable from `Mikko.Kaasalainen@astro.helsinki.fi` upon request. These files give the three-dimensional, rotational, and light-scattering data needed for viewing the asteroid models from any direction, predicting (or reproducing) lightcurves and observational aspects, etc. Additional information and links to related pages are available at `http://www.astro.helsinki.fi/~kaselain/`.

We estimate that there are at least 70 more asteroids for which sufficient datasets can be attained with one or two additional apparitions, i.e., within the next few years. In addition to this, we expect there to be several NEAs that can be modelled after just one or two apparitions – in the most extreme case, continued photometric follow-up observations after discovery may already be sufficient for a preliminary model. Thus, allocating telescope time to planned photometric observing campaigns certainly has relatively fast and extensive pay-off prospects. Dedicated, well-trained, and well-equipped amateur observers are a very important resource in this. With a global coordinated effort for small- and medium-sized telescopes, it should well be possible eventually to accumulate thousands of hours of telescope time per year, and hundreds of modelled asteroids by the end of the decade.

With this large a set of minor planet models, we can already start to perform statistical analysis. We plan to investigate cross-correlations between quantities such as size, rotation period, pole latitude, shape irregularity, deviation from an equilibrium shape, etc. This should provide us with new insights into asteroid structures and evolution (cf. the case of an asteroid family in Slivan et al. 2003). We are also extending our analysis to include complementary information supporting photometric data in order to obtain more detailed models. Such data are, e.g., interferometric (particularly HST/FGS – see Tanga et al. 2003), stellar occultation, and CW Doppler radar observations.

Acknowledgments

We thank Jukka Piironen for a list of previous models of UAPC asteroids and Brian Warner, Alan Harris, and Petr Pravec for valuable comments. Research funded by Emil Aaltonen Foundation and Jenny and Antti Wihuri Fund. The observational part of this work was supported by the Polish KBN Grant 2 P03D 007 18.

References

Denchev P., P. Magnusson, and Z. Donchev 1998, Lightcurves of nine asteroids, with pole and sense of rotation of 42 Isis, Planet. Space Sci. 46, 673–682

Ďurech J. 2002. Shape Determination of the Asteroid (6053) 1993 BW3 *Icarus 159*, 192-196.

Ďurech J. and M. Kaasalainen 2003. Photometric signatures of highly nonconvex and binary asteroids. *Astron. Astrophys.*, in press.

Kaasalainen M. and J. Torppa 2001. Optimization methods for asteroid lightcurve inversion. I. Shape determination. *Icarus 153*, 24-36.

Kaasalainen M., J. Torppa, and K. Muinonen 2001. Optimization methods for asteroid lightcurve inversion. II. The complete inverse problem. *Icarus 153*, 37-51.

Kaasalainen M., J. Torppa, and J. Piironen 2002a. Binary structures among large asteroids. *Astron. Astrophys. 383*, L19-L22.

Kaasalainen M., J. Torppa, and J. Piironen 2002b. Models of twenty asteroids from photometric data. *Icarus 159*, 369-395.

Kaasalainen S., J. Piironen, M. Kaasalainen, A. W. Harris, K. Muinonen, and A. Cellino (2003): Asteroid photometric and polarimetric phase curves: Empirical interpretation. *Icarus 161*, 34-46.

Lagerkvist, C.-I., J. Piironen, and A. Erikson 2001 (UAPC). *Asteroid Photometric Catalogue.* Fifth update, Uppsala University Press, Uppsala.

Michałowski T., W. Pych, J. Berthier, A. Kryszczyńska, T. Kwiatkowski, J. Boussuge, S. Fauvaud, P. Denchev, and R. Baranowski 2000, CCD photometry, spin and shape models of five asteroids: 225, 360, 416, 516, and 1223. Astron. Astrophys. Suppl. Ser. 146, 471-479

Mitchell D.L., S.J. Ostro, K.D. Rosema, R.S. Hudson, D.B. Campbell, J.F. Chandler, and I.I. Shapiro 1995. Radar Observations of Asteroids 7 Iris, 9 Metis, 12 Victoria, 216 Kleopatra, and 654 Zelinda. *Icarus 118, 105-131.*

Mottola S. and F. Lahulla 2000. Mutual Eclipse Events in Asteroidal Binary System 1996FG3: Observations and a Numerical Model. *Icarus 146*, 556-567.

Nakayama H., Y. Fujii, M. Ishiguro, R. Nakamura, S. Yokogawa, F. Yosida, and T. Mukai 2000, Observations of polarization and brightness variations with the rotation for asteroids 9 Metis, 52 Europa and 1036 Ganymed. *Icarus 146*, 220-231.

Pravec P. and G. Hahn 1997. Two-period lightcurve of 1994 AW1: Indication of a binary asteroid? *Icarus 127*, 431-440.

Slivan S., R. Binzel, L. Crespo da Silva, M. Kaasalainen, M. Lyndaker, and M. Krco 2003. Spin vectors in the Koronis family: Comprehensive results from two independent analyses of 213 rotation lightcurves. *Icarus 162*, 285-307.

Storrs A., B. Weiss, B. Zellner, W. Burleson, R. Sichitiv, E. Wells, C. Kowal, and D. Tholen 1999. Imaging observations of asteroids with Hubble Space Telescope. *Icarus 137*, 260-268.

Storrs A., F. Vilas, R. Landis, E. Wells, C. Woods, B. Zellner, and M. Gaffey 2001. S/2001 (107) 1, *IAUC* 7599.

Tanga P., D. Hestroffer, A. Cellino, M. Lattanzi, M. Di Martino, and V. Zappalà 2003. Asteroid observations with the Hubble Space Telescope FGS. II. Duplicity search and size measurements for 6 asteroids. *Astron. Astrophys. 401*, 733-741.

Tables

Table I. Values for some important quantities characterizing the adopted model and the observations: β and λ are the ecliptic latitude and longitude of the model's pole direction in degrees, P is asteroid's rotational period in hours and *rms* the root-mean-square value of the fit in magnitudes, T_{tot} is the total time span of the observations in years, N_{app} the number of apparitions observed, α the solar phase angle range of the observations in degrees and N_{cur} the number of lightcurves used in inversion.

Asteroid	β (deg)	λ(deg)	P (hrs)	rms(mag)	T_{tot}	N_{app}	α(deg)	N_{cur}
2 Pallas	-12	35	7.813225	0.01	1951-86	15	0-26	51
	+43	193						
6 Hebe	+45	339	7.274470	0.01	1953-93	14	1-23	39
8 Flora	+16	160	12.79900	0.01	1953-93	8	3-31	35
9 Metis	+23	181	5.07918	0.01	1949-88	15	2-24	28
	+9	359						
12 Victoria	+55	137	8.65990	0.02	1968-90	3	3-23	24
17 Thetis	+12	58	12.26603	0.02	1953-95	8	1-18	55
	+25	240						
18 Melpomene	-37	8	11.57144	0.03	1958-90	8	2-33	33
	-24	199						
19 Fortuna	+58	98	7.443223	0.02	1963-98	10	0-28	38
	+60	277						
21 Lutetia	+3	39	8.165455	0.02	1962-98	6	2-25	32
	+3	220						
23 Thalia	-55	359	12.31220	0.02	1963-94	10	2-24	41
37 Fides	-26	85	7.33350	0.01	1977-2003	5	2-23	23
	-34	264						
42 Isis	-14	120	13.59701	0.02	1970-96	7	4-17	28
	-23	294						
55 Pandora	+10	225	4.804044	0.02	1977-93	6	0-24	36
63 Ausonia	-15	120	9.29759	0.02	1976-91	7	2-22	20
	-22	304						
69 Hesperia	-45	73	5.65520	0.02	1977-93	6	0-13	33
85 Io	-45	105	6.875110	0.02	1964-97	5	2-21	29
	-14	295						
88 Thisbe	+48	207	6.04130	0.03	1977-89	6	3-18	19
107 Camilla	+51	72	4.84393	0.01	1981-89	7	2-17	26
129 Antigone	+58	207	4.957154	0.02	1971-2002	13	4-25	34

Asteroid	β (deg)	λ(deg)	P (hrs)	rms(mag)	T_{tot}	N_{app}	α(deg)	N_{cur}
135 Hertha	+58	96	8.40061	0.02	1978-2002	8	1-26	42
	+53	274						
201 Penelope	-15	84	3.74745	0.03	1980-89	7	1-24	32
	-1	262						
230 Athamantis	+27	74	23.9845	0.01	1963-84	6	2-26	36
	+28	238						
250 Bettina	-12	282	5.05442	0.03	1980-94	6	2-17	23
	+17	100						
337 Devosa	+43	209	4.65368	0.03	1977-93	7	2-27	27
349 Dembowska	+23	150	4.70121	0.03	1962-85	7	3-21	21
	0	329						
372 Palma	+2	68	8.59103	0.01	1979-94	6	5-20	28
511 Davida	+44	303	5.129367	0.03	1952-86	11	2-21	28
584 Semiramis	-39	106	5.06892	0.03	1981-91	6	6-20	16
675 Ludmilla	-36	20	7.717215	0.02	1965-93	4	3-21	33
	-54	215						
694 Ekard	-48	89	5.92200	0.02	1983-91	5	5-21	20

Table II. Aspect data for Borowiec, Quail Hollow, and Rozhen observations.

Date (UT)	r	Δ	Phase angle	λ (J2000)	β	Obs.
	(AU)	(AU)	(°)	(°)	(°)	
21 Lutetia						
1998 01 24.9	2.728	1.769	5.78	108.78	2.62	Bor
1998 01 25.9	2.729	1.774	6.19	108.56	2.62	Bor
37 Fides						
2003 01 06.3	2.436	1.776	20.18	164.17	2.90	Qho
85 Io						
1997 03 04.9	3.161	2.275	9.52	135.67	-14.38	Bor
1997 03 05.8	3.161	2.281	9.76	135.52	-14.32	Bor
129 Antigone						
1999 01 19.0	3.252	2.299	5.16	103.26	-8.40	Bor
1999 01 21.0	3.249	2.304	5.78	102.84	-8.29	Bor
2002 11 26.0	3.469	2.522	5.43	53.45	-16.68	Qho
135 Hertha						
1998 01 30.9	2.736	1.951	14.78	85.71	2.89	Roz
1998 02 23.9	2.773	2.264	19.51	85.73	2.41	Bor
1998 03 09.9	2.792	2.471	20.60	87.34	2.16	Bor
1998 03 10.8	2.793	2.485	20.64	87.49	2.14	Bor
1998 03 11.9	2.795	2.501	20.68	87.66	2.13	Bor
1998 03 19.8	2.805	2.621	20.79	89.06	2.00	Bor
1998 03 20.8	2.806	2.637	20.78	89.27	1.98	Bor
1999 03 27.0	2.807	1.828	4.78	172.30	-0.80	Bor
1999 04 05.9	2.794	1.858	8.89	170.09	-0.89	Bor
1999 04 09.0	2.790	1.873	10.07	169.49	-0.92	Bor
1999 04 29.9	2.761	2.026	16.75	166.89	-1.05	Bor
1999 04 30.9	2.759	2.036	17.00	166.84	-1.06	Bor

Table II (continued).

Date (UT)	r	Δ	Phase angle	λ (J2000)	β	Obs.
	(AU)	(AU)	(°)	(°)	(°)	
2002 03 03.8	2.872	2.230	17.16	104.25	2.01	Bor
2002 03 17.9	2.884	2.421	19.19	104.78	1.76	Bor
2002 03 18.9	2.885	2.436	19.29	104.86	1.75	Bor
2002 03 27.9	2.892	2.565	19.94	105.83	1.61	Bor
2002 03 28.9	2.892	2.580	19.98	105.97	1.59	Bor

Observatory Code: Bor - Borowiec; Qho - Quail Hollow; Roz - Rozhen

Figure captions

Fig. 1. Shape model of 2 Pallas, shown at equatorial viewing/illuminaton geometry, with rotational phases 90° apart.

Fig. 2. Four lightcurves (asterisks) and the corresponding fits (dashed lines) for 2 Pallas. The rotational phase is given in degrees, and the brightness in units of relative intensity. The aspect angle of the Earth (measured from the pole) is given by θ, and that of the Sun by θ_0. The solar phase angle is given by α.

Fig. 3. Shape model of 6 Hebe.

Fig. 4. Four lightcurves of 6 Hebe with model fits.

Fig. 5. Shape model of 8 Flora.

Fig. 6. Four lightcurves of 8 Flora with model fits.

Fig. 7. Shape model of 9 Metis.

Fig. 8. Four lightcurves of 9 Metis with model fits.

Fig. 9. Shape model of 12 Victoria.

Fig. 10. Four lightcurves of 12 Victoria with model fits.

Fig. 11. Shape model of 17 Thetis.

Fig. 12. Four lightcurves of 17 Thetis with model fits.

Fig. 13. Shape model of 18 Melpomene.

Fig. 14. Four lightcurves of 18 Melpomene with model fits.

Fig. 15. Shape model of 19 Fortuna.

Fig. 16. Four lightcurves of 19 Fortuna with model fits.

Fig. 17. Shape model of 21 Lutetia.

Fig. 18. Four lightcurves of 21 Lutetia with model fits.

Fig. 19. Shape model of 23 Thalia.

Fig. 20. Four lightcurves of 23 Thalia with model fits.

Fig. 21. Shape model of 37 Fides.

Fig. 22. Four lightcurves of 37 Fides with model fits.

Fig. 23. Shape model of 42 Isis.

Fig. 24. Four lightcurves of 42 Isis with model fits.

Fig. 25. Shape model of 55 Pandora.

Fig. 26. Four lightcurves of 55 Pandora with model fits.

Fig. 27. Shape model of 63 Ausonia.

Fig. 28. Four lightcurves of 63 Ausonia with model fits.

Fig. 29. Shape model of 69 Hesperia.

Fig. 30. Four lightcurves of 69 Hesperia with model fits.

Fig. 31. Shape model of 85 Io.

Fig. 32. Four lightcurves of 85 Io with model fits.

Fig. 33. Shape model of 88 Thisbe.

Fig. 34. Four lightcurves of 88 Thisbe with model fits.

Fig. 35. Shape model of 107 Camilla.

Fig. 36. Four lightcurves of 107 Camilla with model fits.

Fig. 37. Shape model of 129 Antigone.

Fig. 38. Four lightcurves of 129 Antigone with model fits.

Fig. 39. Shape model of 135 Hertha.

Fig. 40. Four lightcurves of 135 Hertha with model fits.

Fig. 41. Shape model of 201 Penelope.

Fig. 42. Four lightcurves of 201 Penelope with model fits.

Fig. 43. Shape model of 230 Athamantis.

Fig. 44. Four lightcurves of 230 Athamantis with model fits.

Fig. 45. Shape model of 250 Bettina.

Fig. 46. Four lightcurves of 250 Bettina with model fits.

Fig. 47. Shape model of 337 Devosa.

Fig. 48. Four lightcurves of 337 Devosa with model fits.

Fig. 49. Shape model of 349 Dembowska.

Fig. 50. Four lightcurves of 349 Dembowska with model fits.

Fig. 51. Shape model of 372 Palma.

Fig. 52. Four lightcurves of 372 Palma with model fits.

Fig. 53. Shape model of 511 Davida.

Fig. 54. Four lightcurves of 511 Davida with model fits.

Fig. 55. Shape model of 584 Semiramis.

Fig. 56. Four lightcurves of 584 Semiramis with model fits.

Fig. 57. Shape model of 675 Ludmilla.

Fig. 58. Four lightcurves of 675 Ludmilla with model fits.

Fig. 59. Shape model of 694 Ekard.

Fig. 60. Four lightcurves of 694 Ekard with model fits.

Fig. 61. Composite lightcurves of 21 Lutetia in 1998 and 85 Io in 1997.

Fig. 62. Composite lightcurves of 129 Antigone in 1999 and 135 Hertha in 1998.

Fig. 63. Composite lightcurves of 135 Hertha in 1999 and 2002.

Fig. 64. Lightcurves of 37 Fides in 2003 and 129 Antigone in 2002.

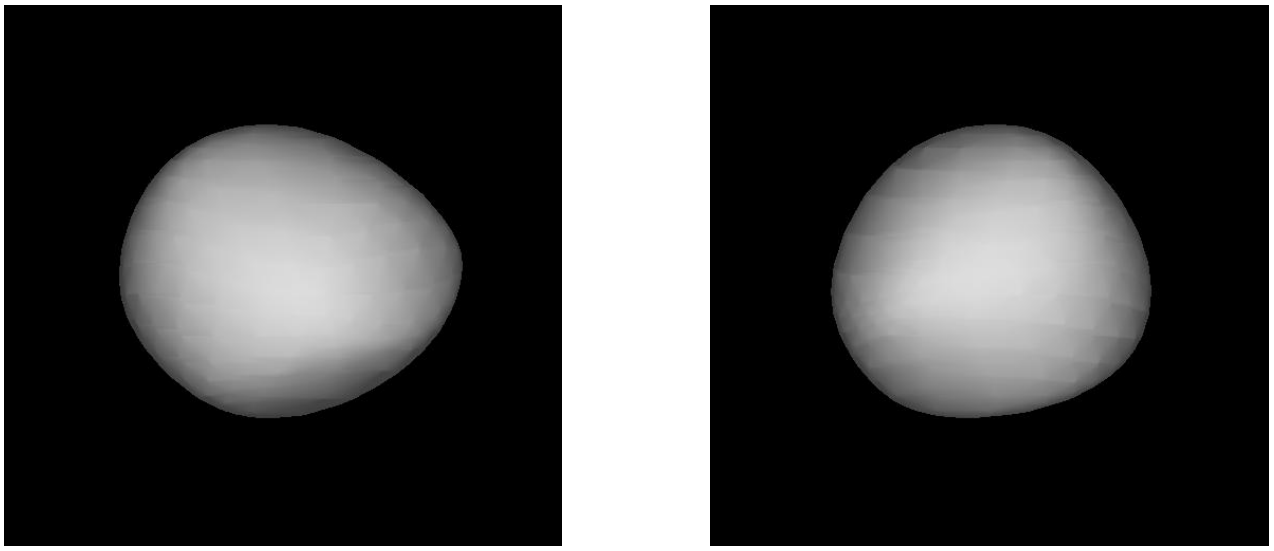

Fig. 1

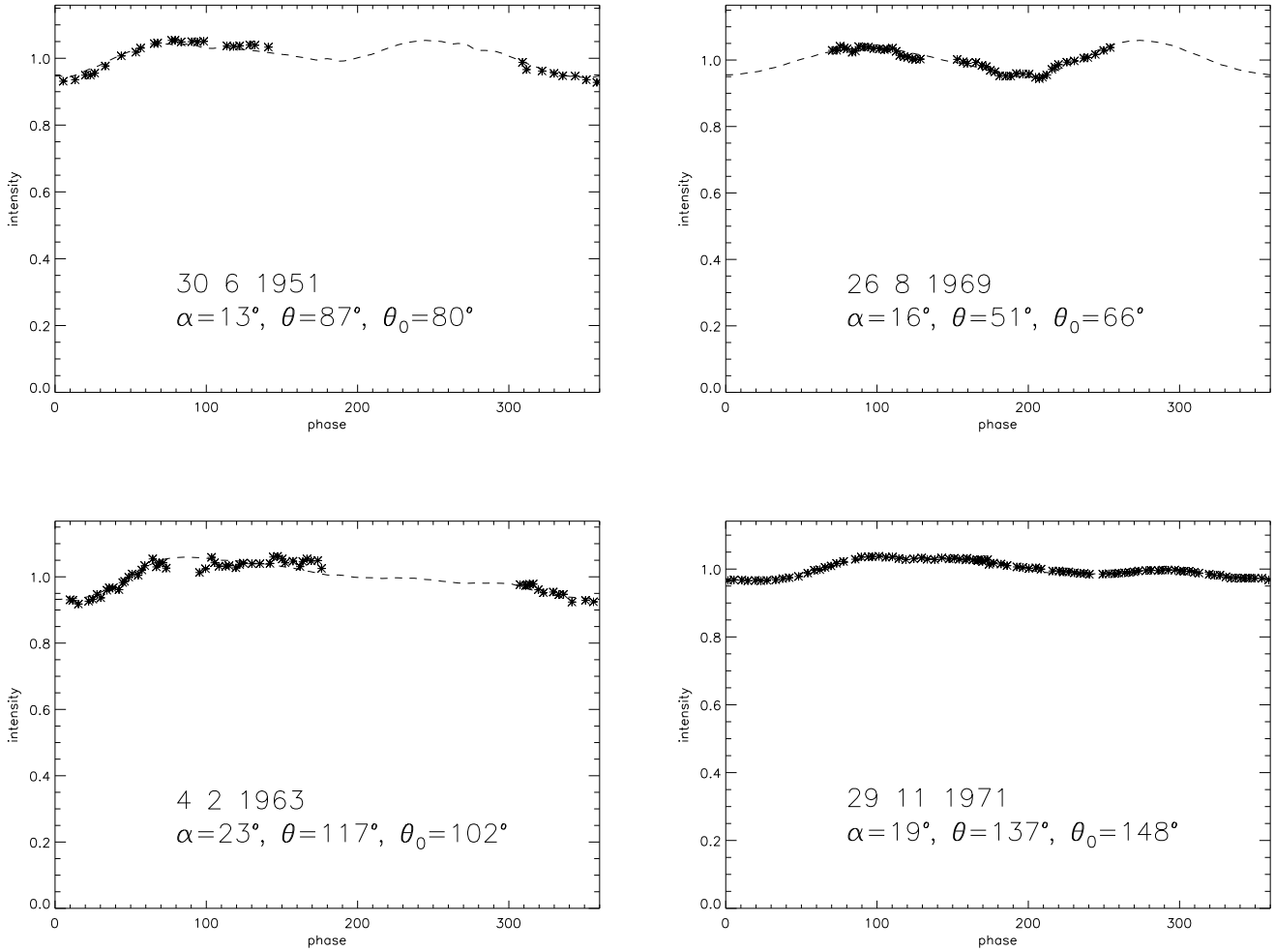
30 6 1951
α=13°, θ=87°, θ0=80°
26 8 1969
α=16°, θ=51°, θ0=66°
4 2 1963
α=23°, θ=117°, θ0=102°
29 11 1971
α=19°, θ=137°, θ0=148°
intensity
phase

Fig. 2

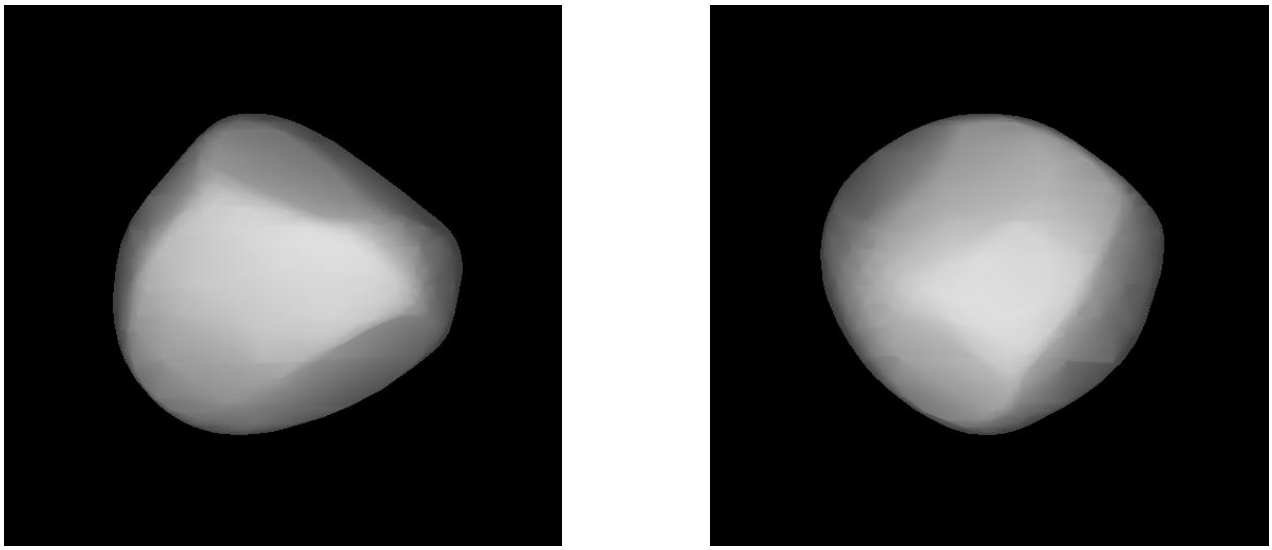

Fig. 3

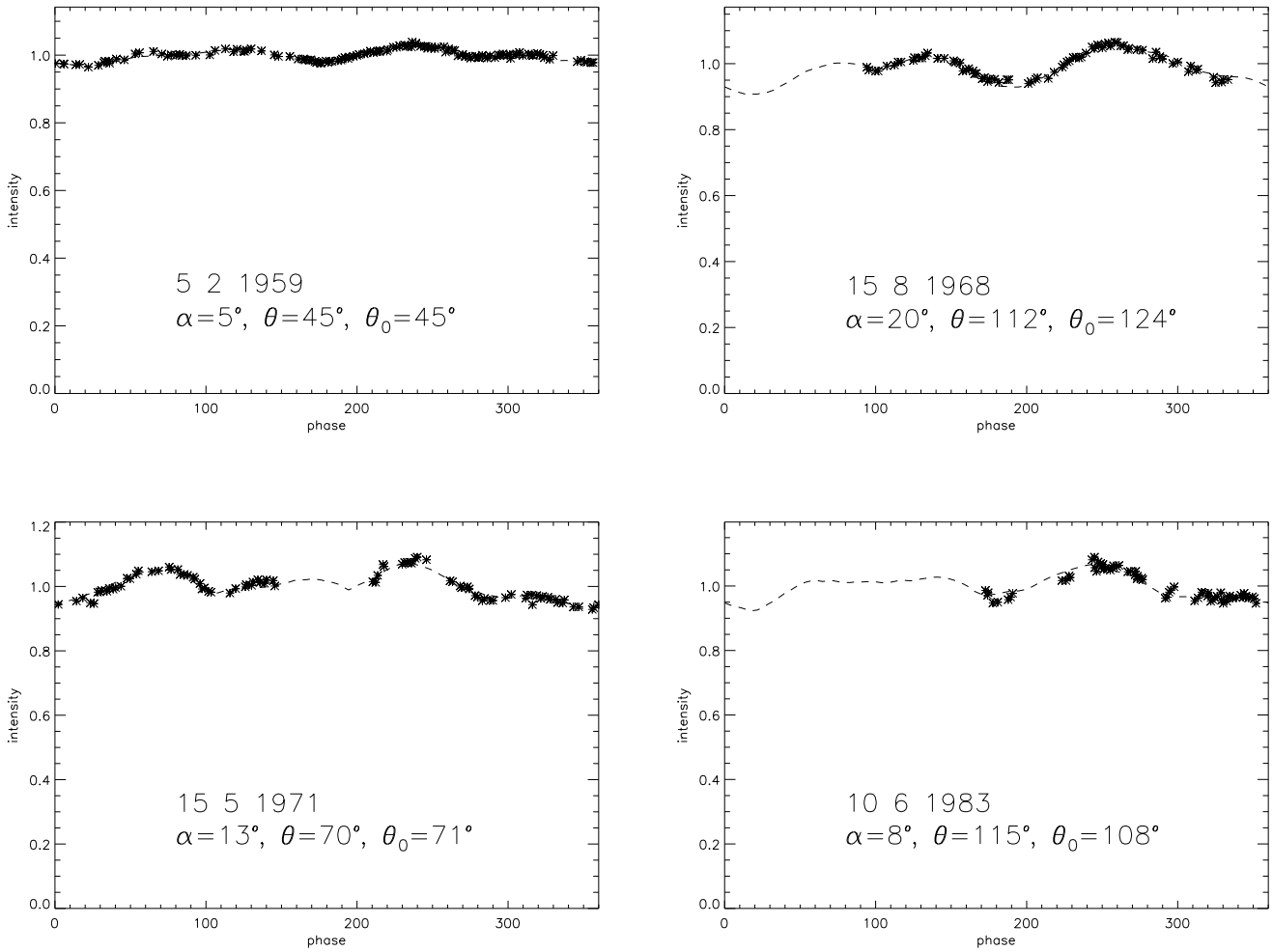
intensity
phase
5 2 1959
α=5°, θ=45°, θ0=45°
15 8 1968
α=20°, θ=112°, θ0=124°
15 5 1971
α=13°, θ=70°, θ0=71°
10 6 1983
α=8°, θ=115°, θ0=108°

Fig. 4

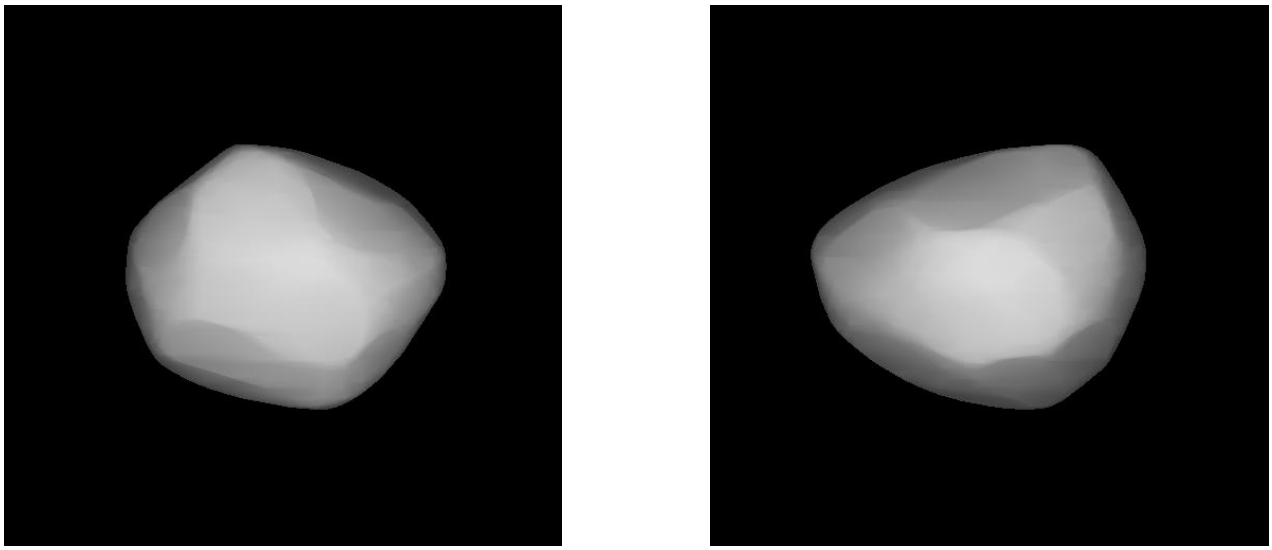

Fig. 5

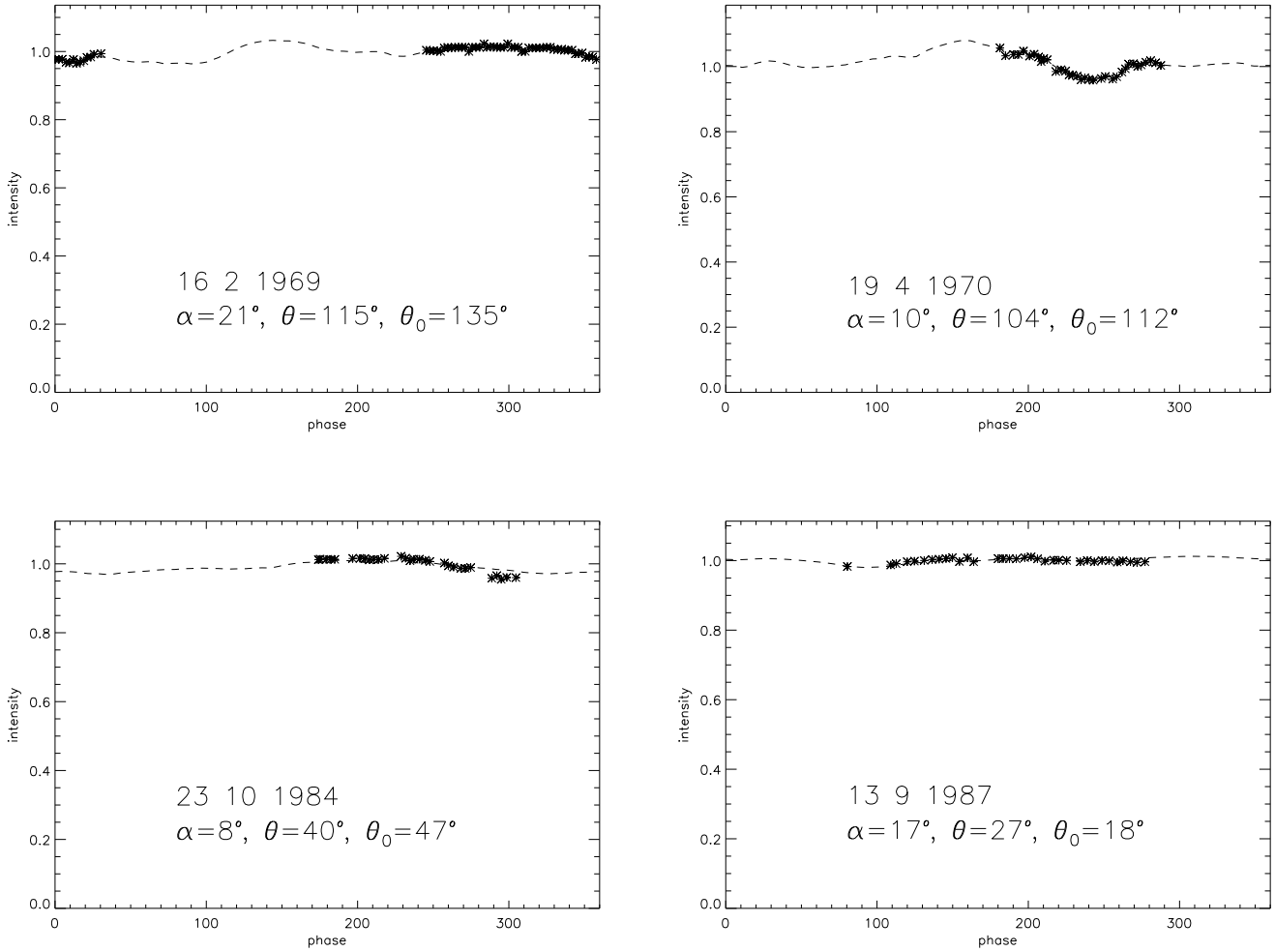
16 2 1969
α=21°, θ=115°, θ0=135°
19 4 1970
α=10°, θ=104°, θ0=112°
23 10 1984
α=8°, θ=40°, θ0=47°
13 9 1987
α=17°, θ=27°, θ0=18°
intensity
phase

Fig. 6

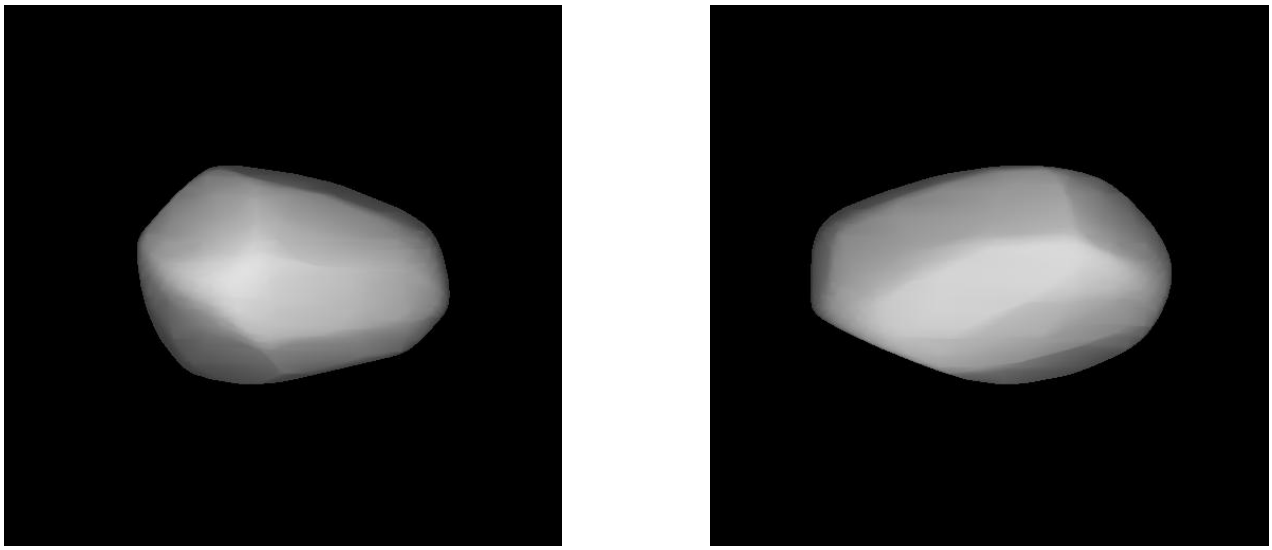

Fig. 7

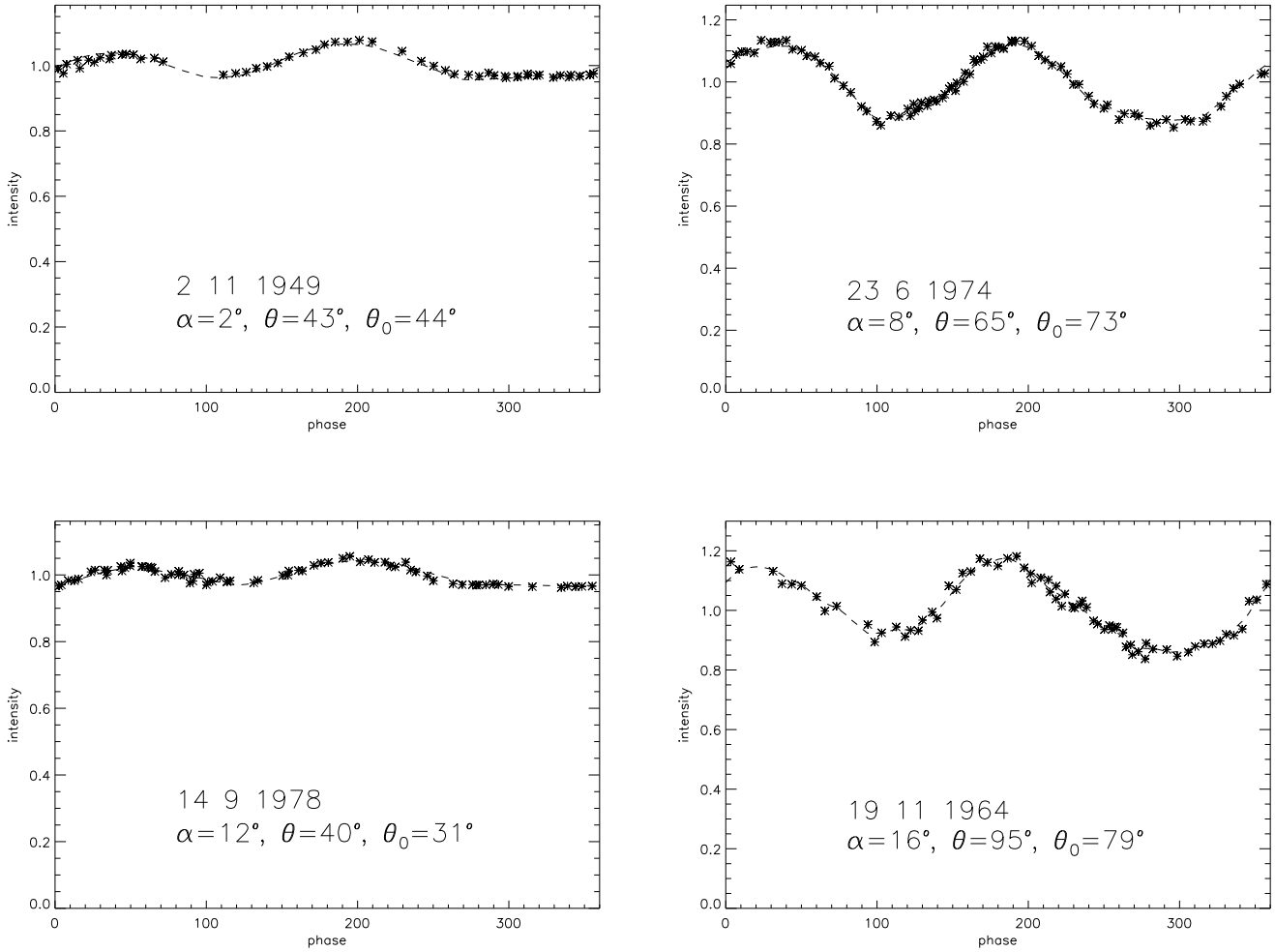
intensity
phase
2 11 1949
α=2°, θ=43°, θ0=44°
23 6 1974
α=8°, θ=65°, θ0=73°
14 9 1978
α=12°, θ=40°, θ0=31°
19 11 1964
α=16°, θ=95°, θ0=79°

Fig. 8

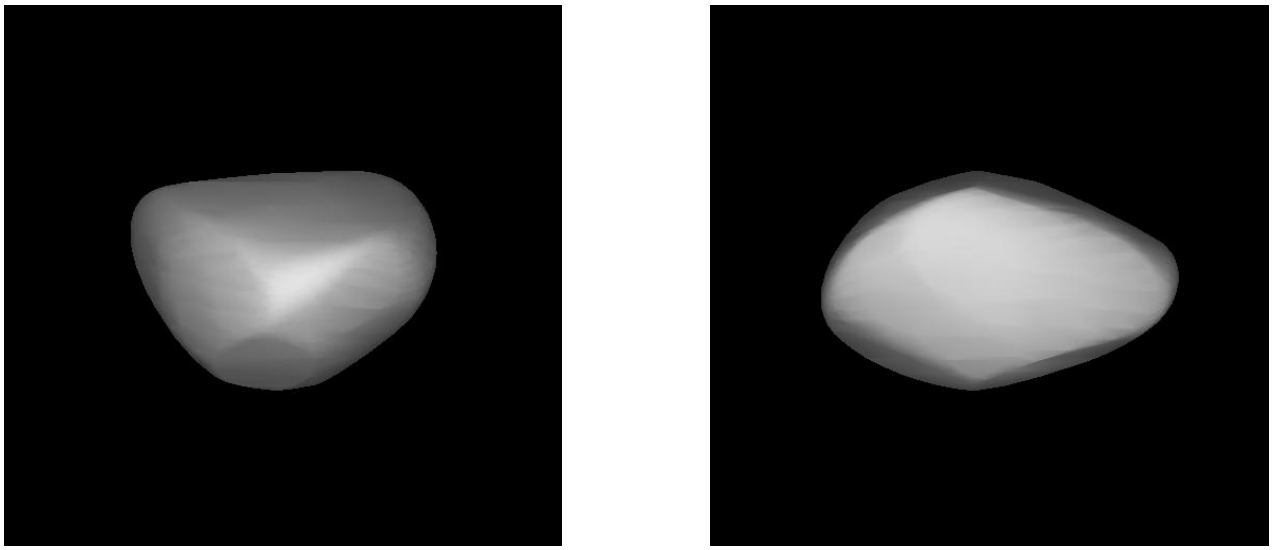

Fig. 9

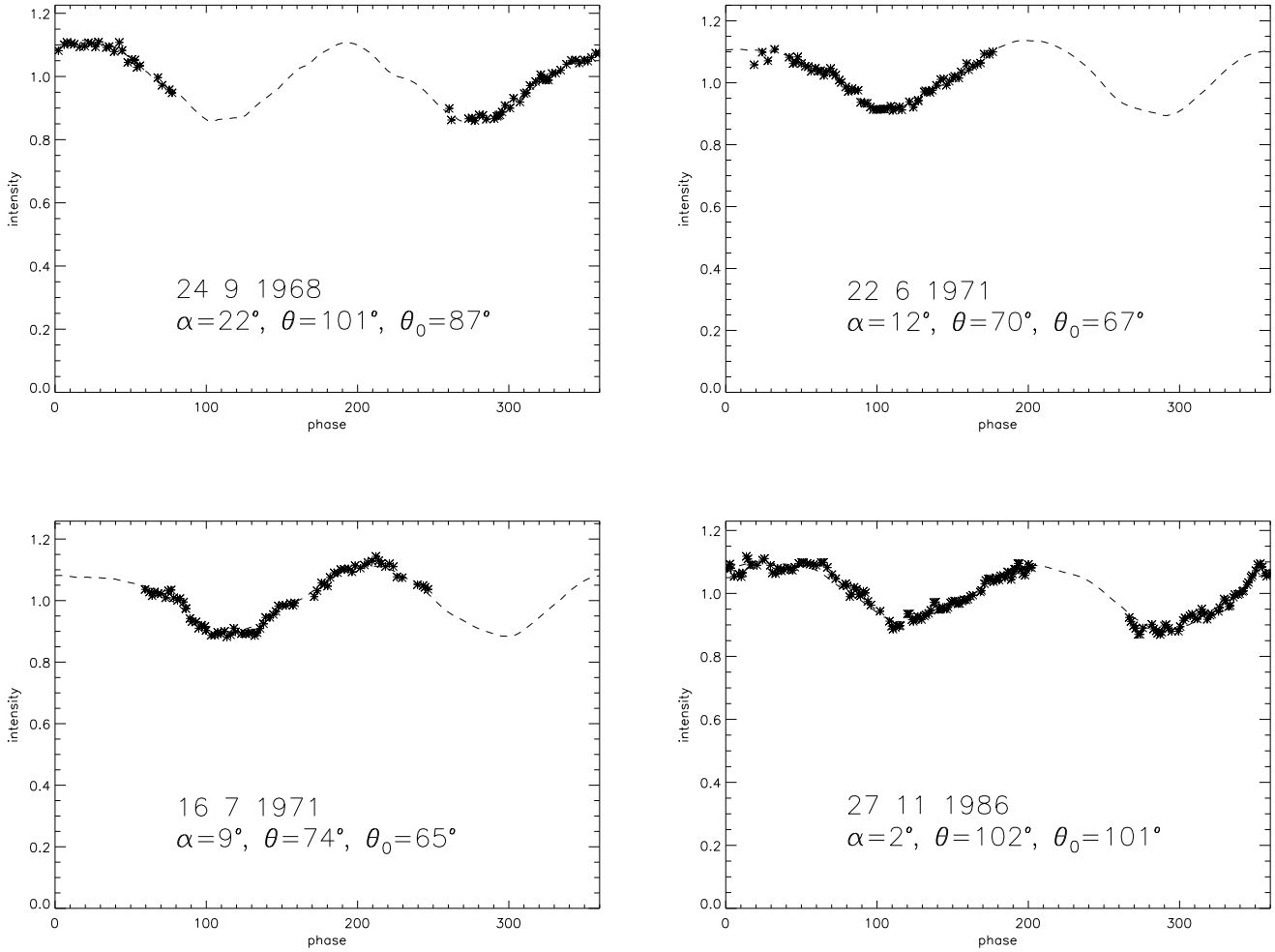
24 9 1968
α=22°, θ=101°, θ0=87°
22 6 1971
α=12°, θ=70°, θ0=67°
16 7 1971
α=9°, θ=74°, θ0=65°
27 11 1986
α=2°, θ=102°, θ0=101°
intensity
phase

Fig. 10

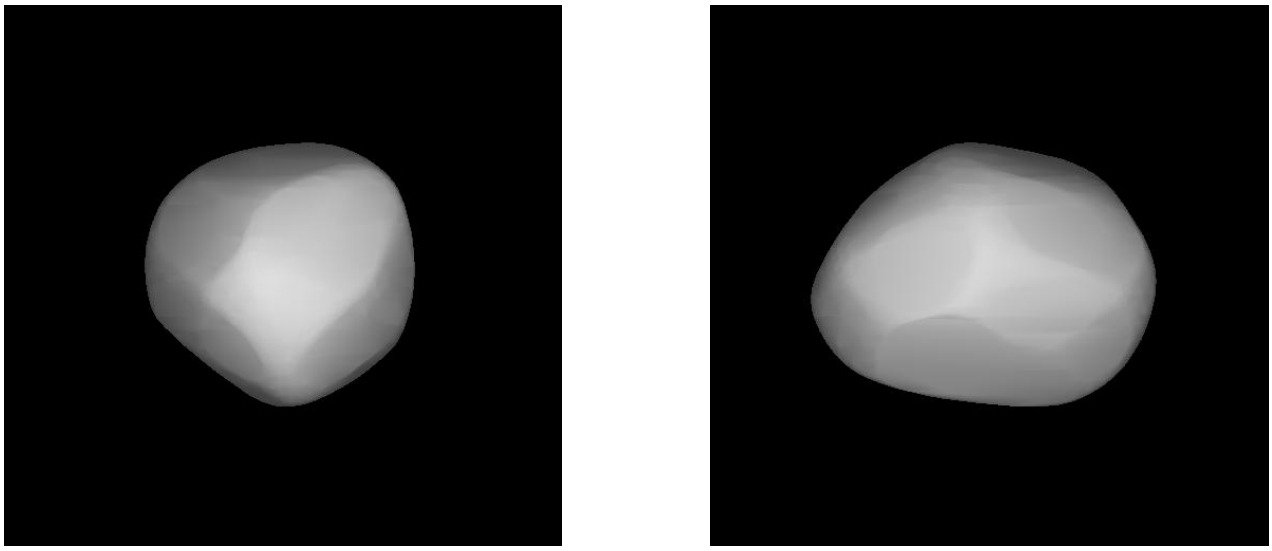

Fig. 11

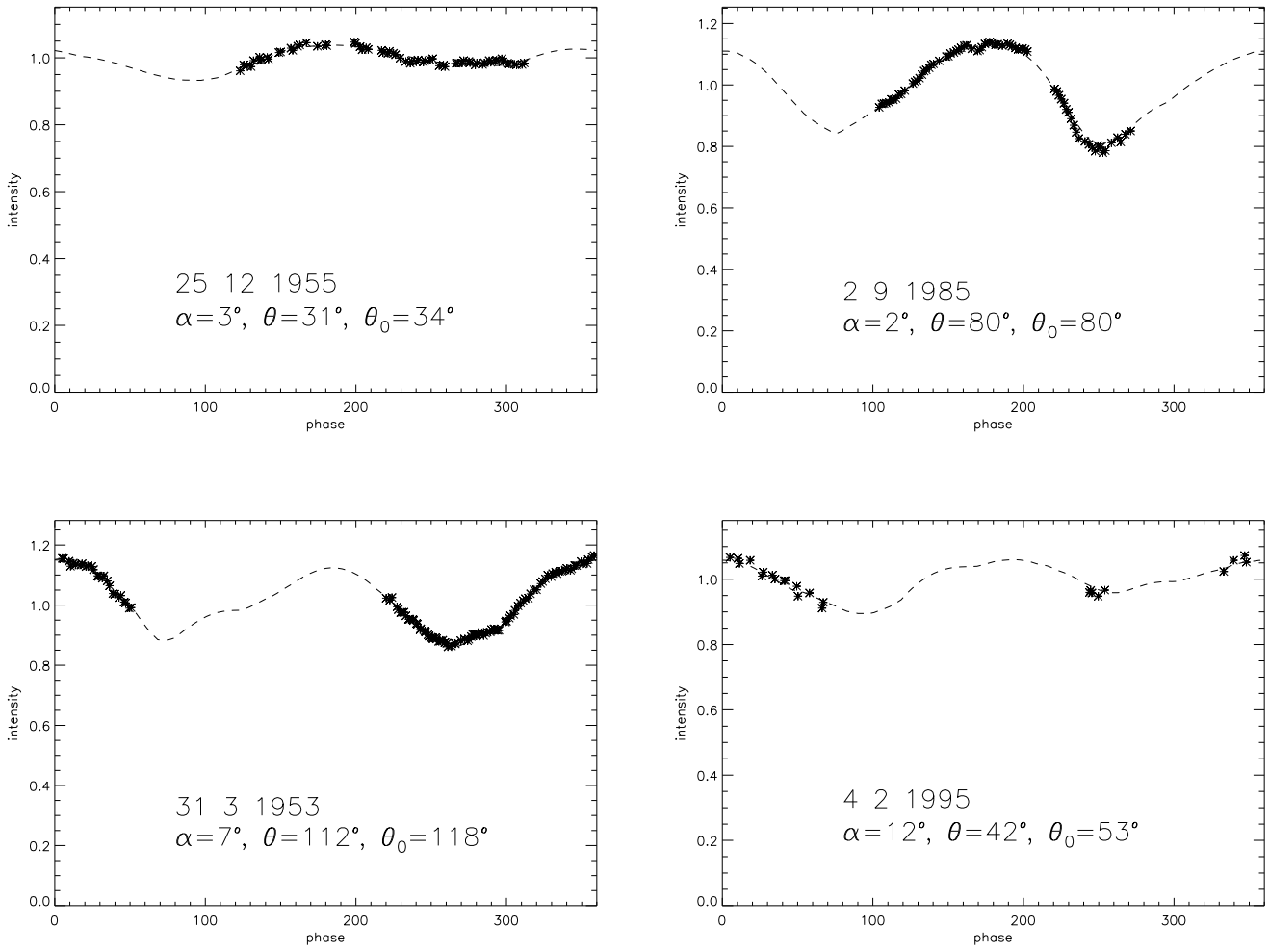
25 12 1955
α=3°, θ=31°, θ0=34°
2 9 1985
α=2°, θ=80°, θ0=80°
31 3 1953
α=7°, θ=112°, θ0=118°
4 2 1995
α=12°, θ=42°, θ0=53°
intensity
phase

Fig. 12

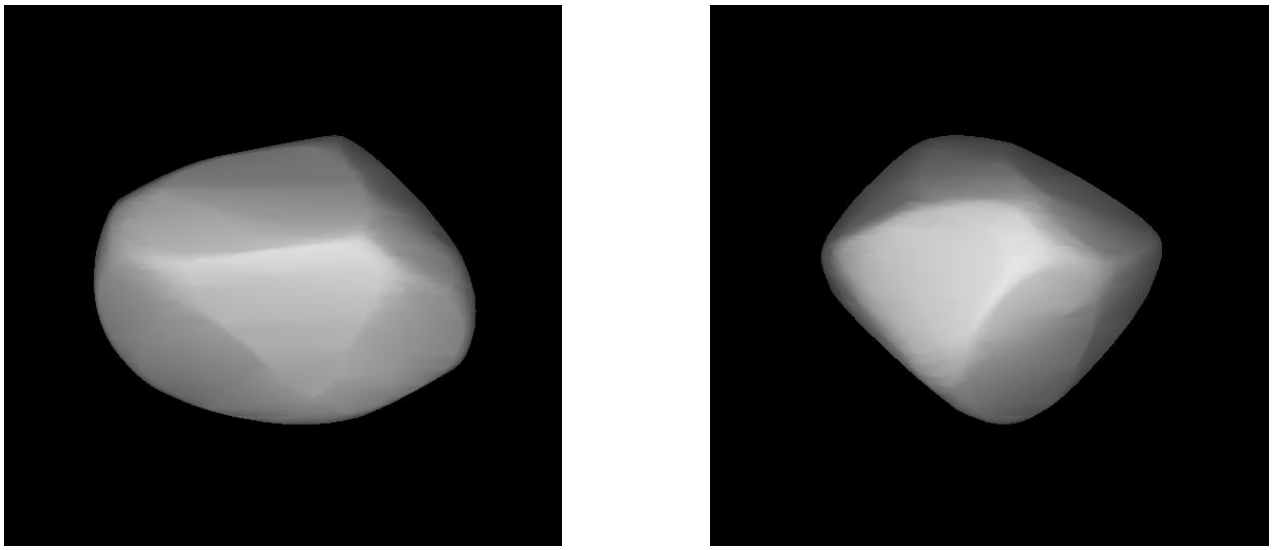

Fig. 13

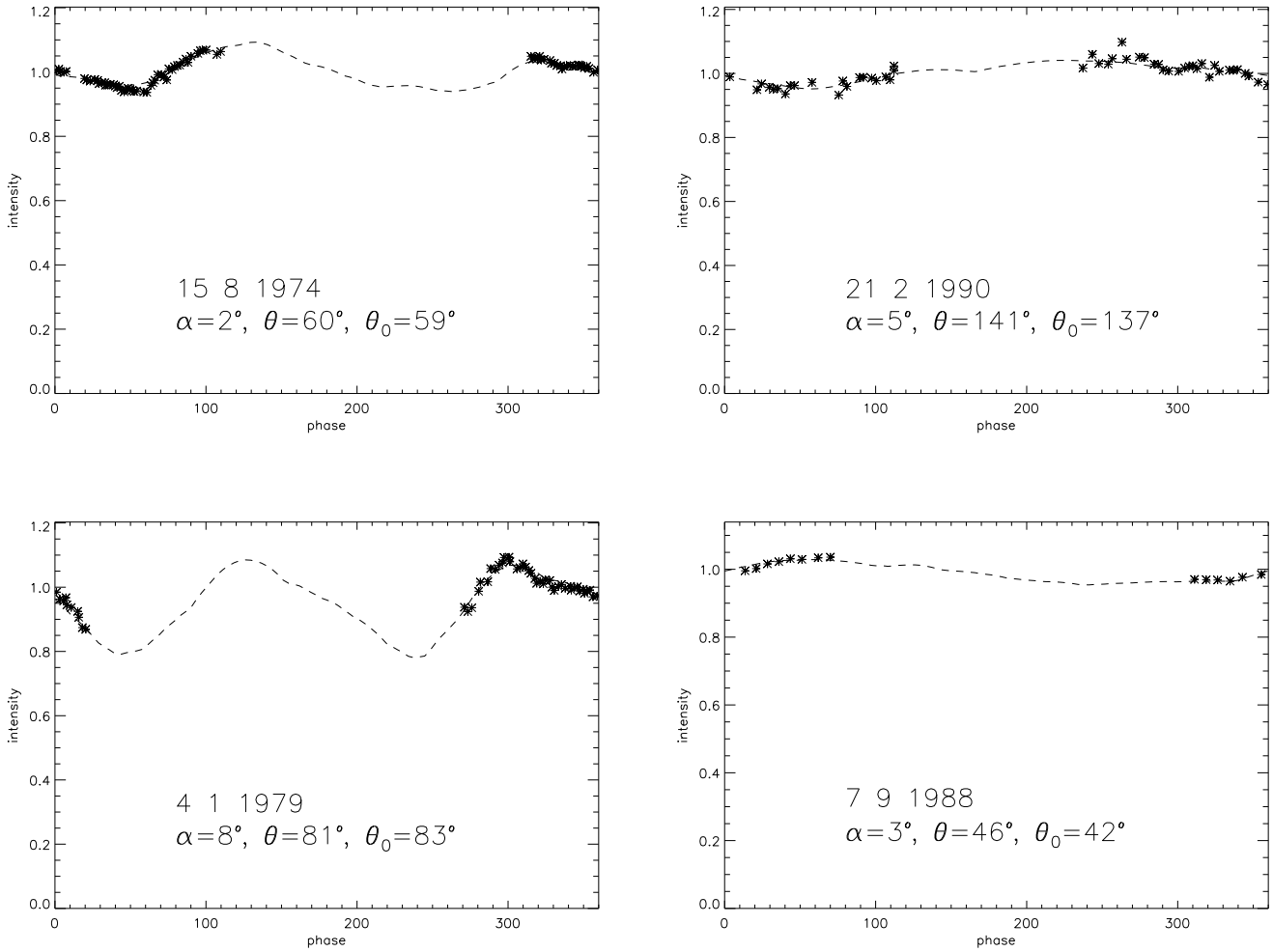
15 8 1974
α=2°, θ=60°, θ0=59°
21 2 1990
α=5°, θ=141°, θ0=137°
4 1 1979
α=8°, θ=81°, θ0=83°
7 9 1988
α=3°, θ=46°, θ0=42°
intensity
phase

Fig. 14

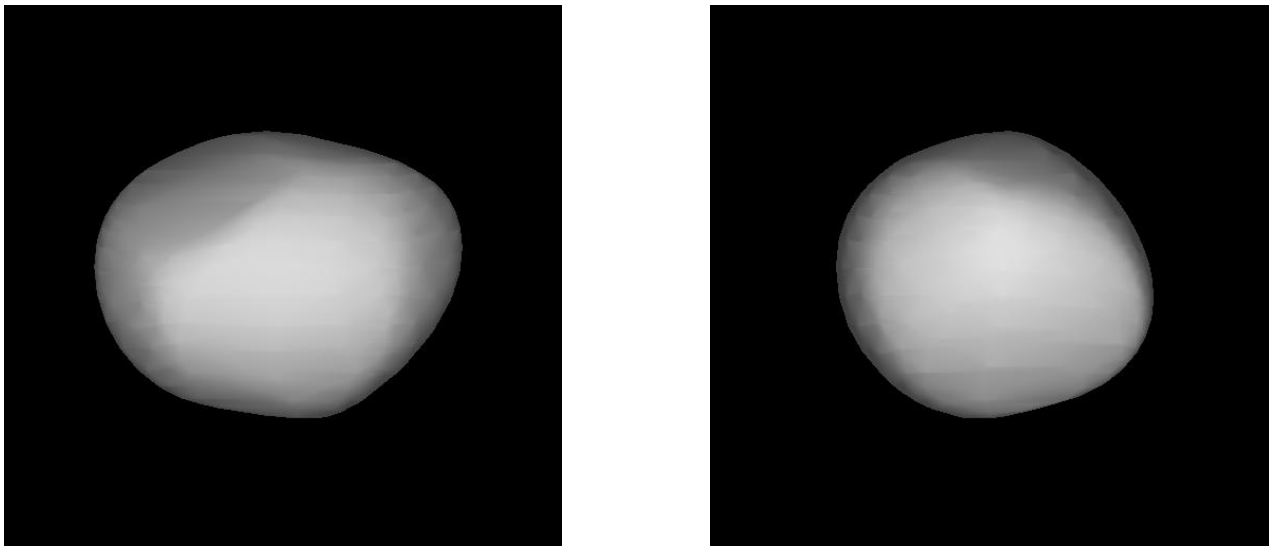

Fig. 15

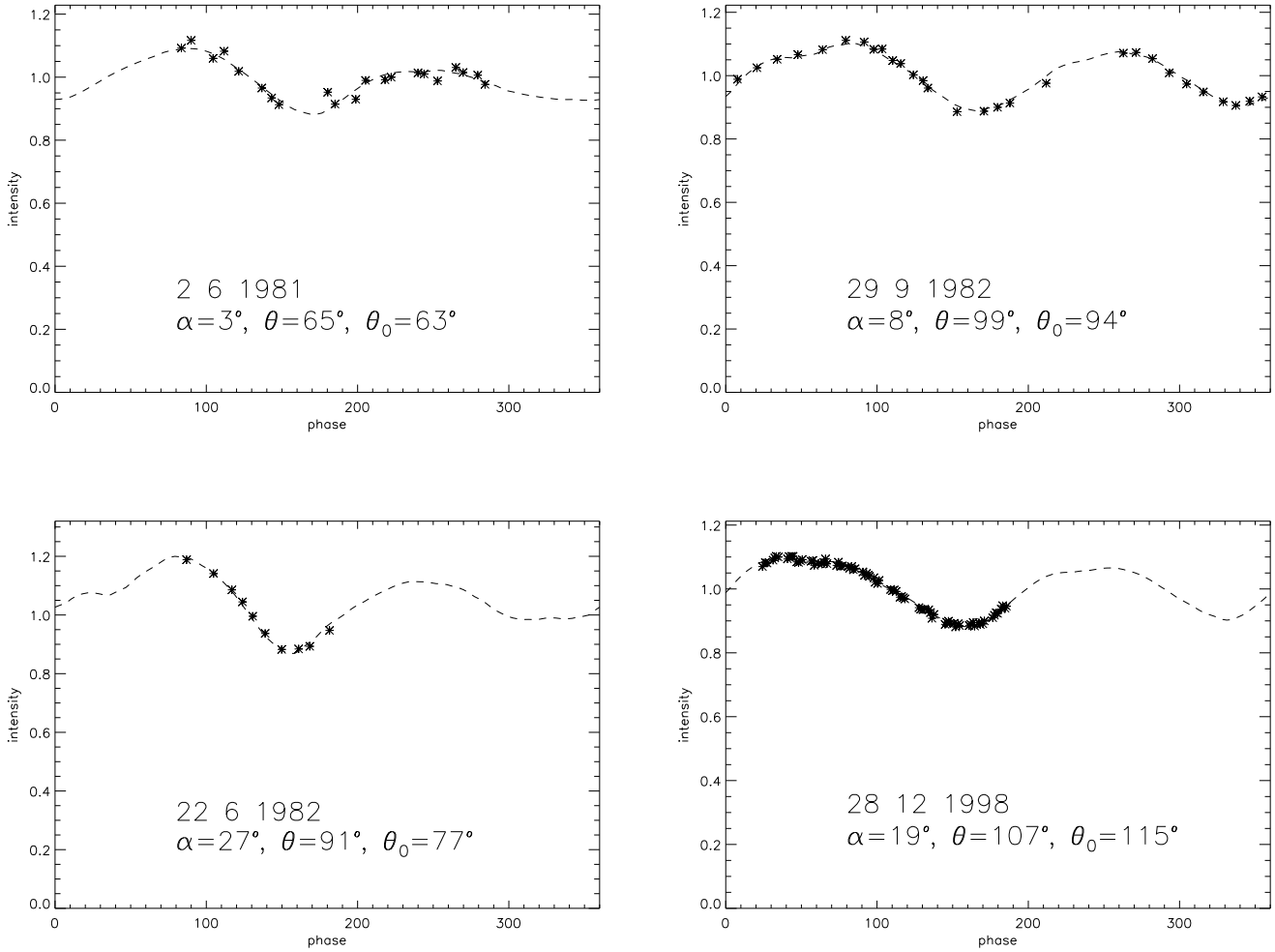
intensity
phase
2 6 1981
α=3°, θ=65°, θ0=63°
29 9 1982
α=8°, θ=99°, θ0=94°
22 6 1982
α=27°, θ=91°, θ0=77°
28 12 1998
α=19°, θ=107°, θ0=115°

Fig. 16

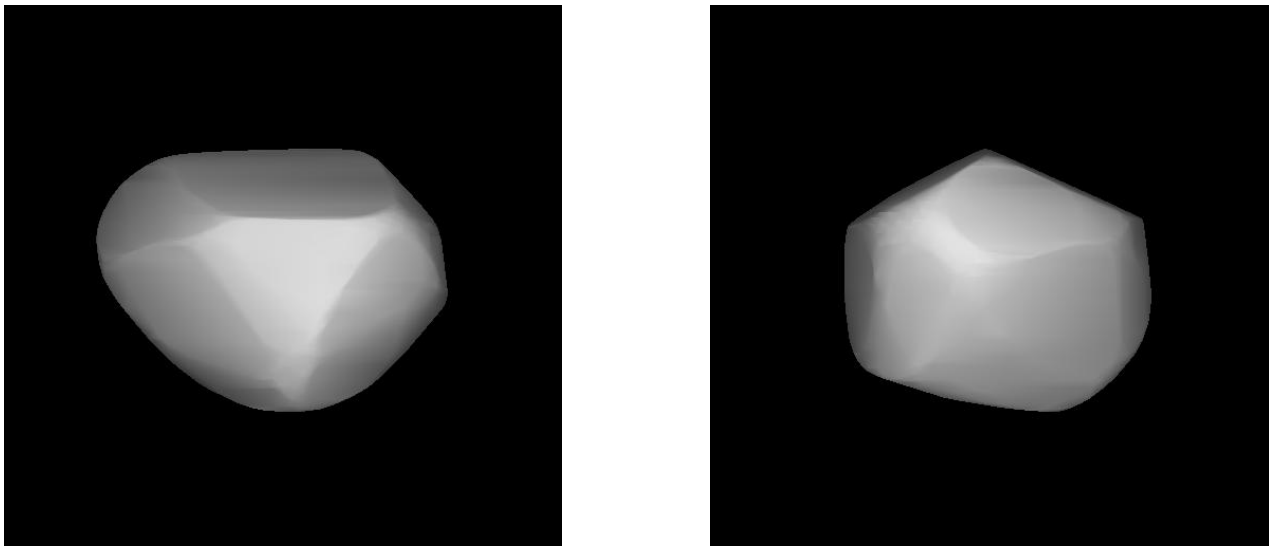

Fig. 17

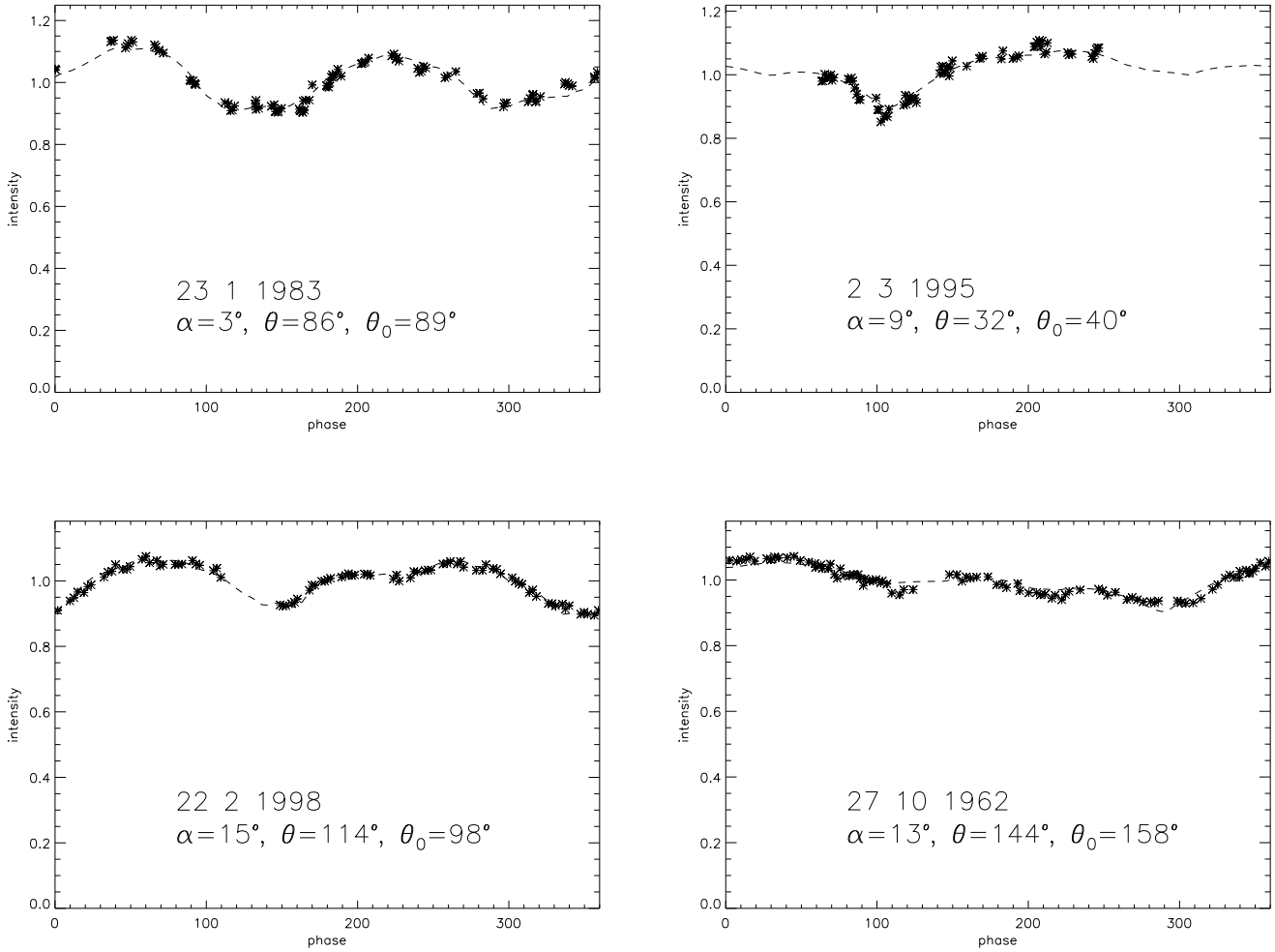
23 1 1983
α=3°, θ=86°, θ0=89°
2 3 1995
α=9°, θ=32°, θ0=40°
22 2 1998
α=15°, θ=114°, θ0=98°
27 10 1962
α=13°, θ=144°, θ0=158°
intensity
phase

Fig. 18

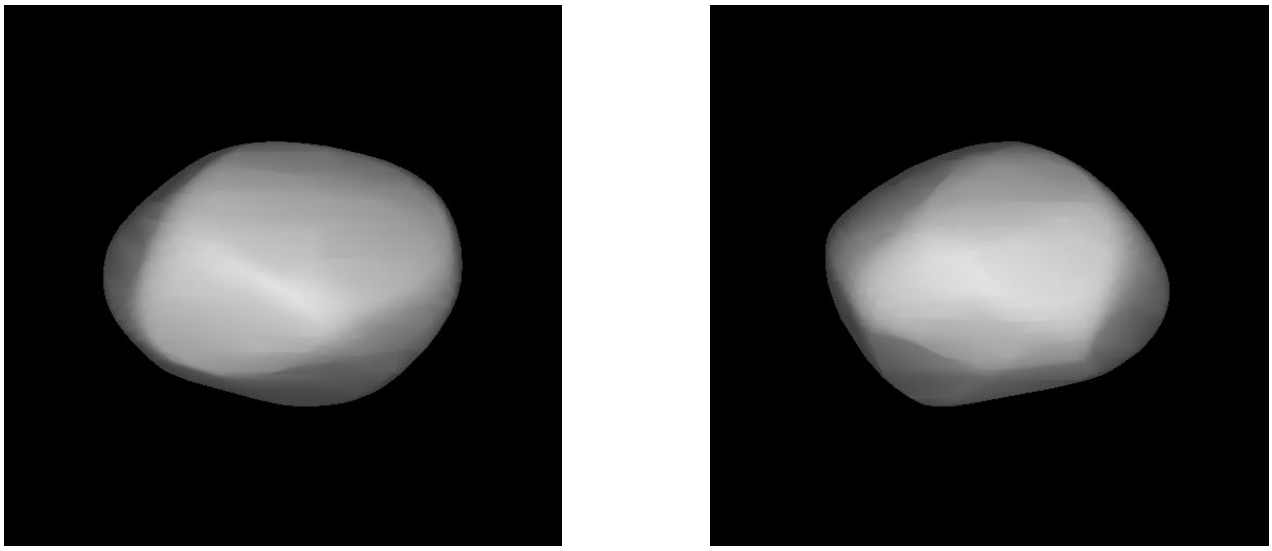

Fig. 19

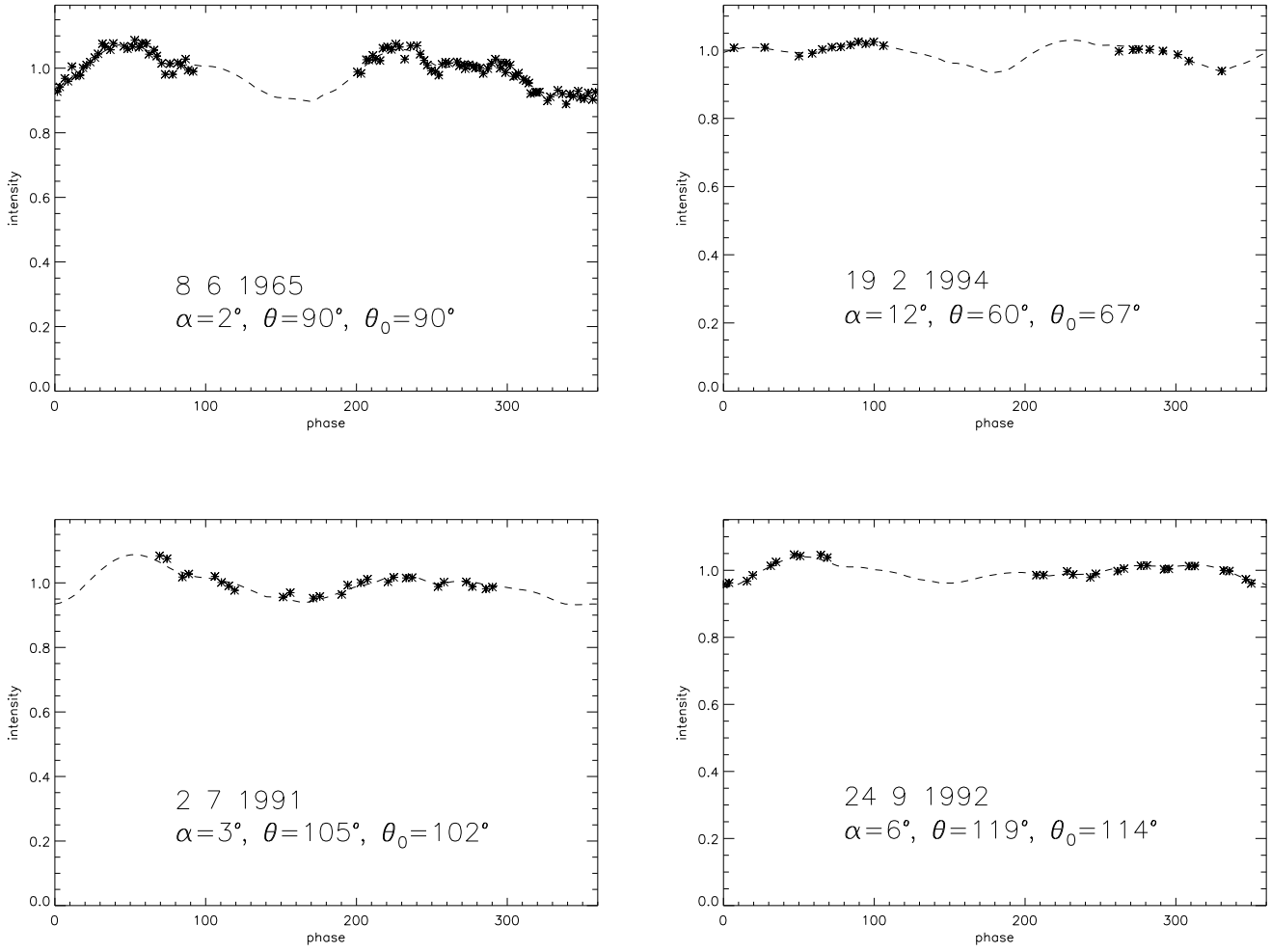
8 6 1965
α=2°, θ=90°, θ0=90°
19 2 1994
α=12°, θ=60°, θ0=67°
2 7 1991
α=3°, θ=105°, θ0=102°
24 9 1992
α=6°, θ=119°, θ0=114°
intensity
phase

Fig. 20

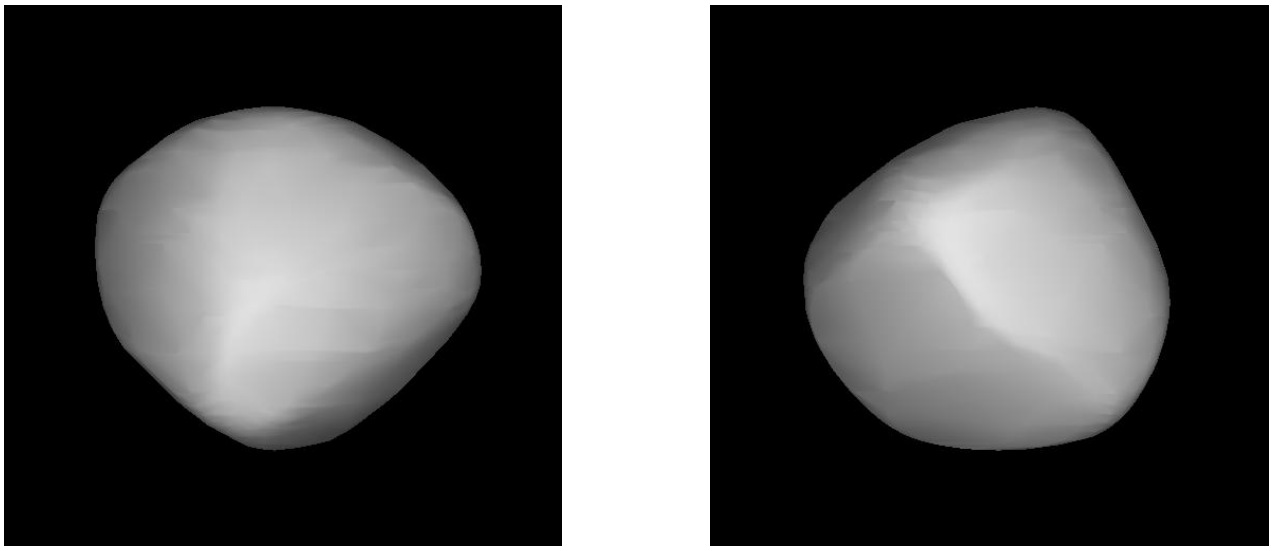

Fig. 21

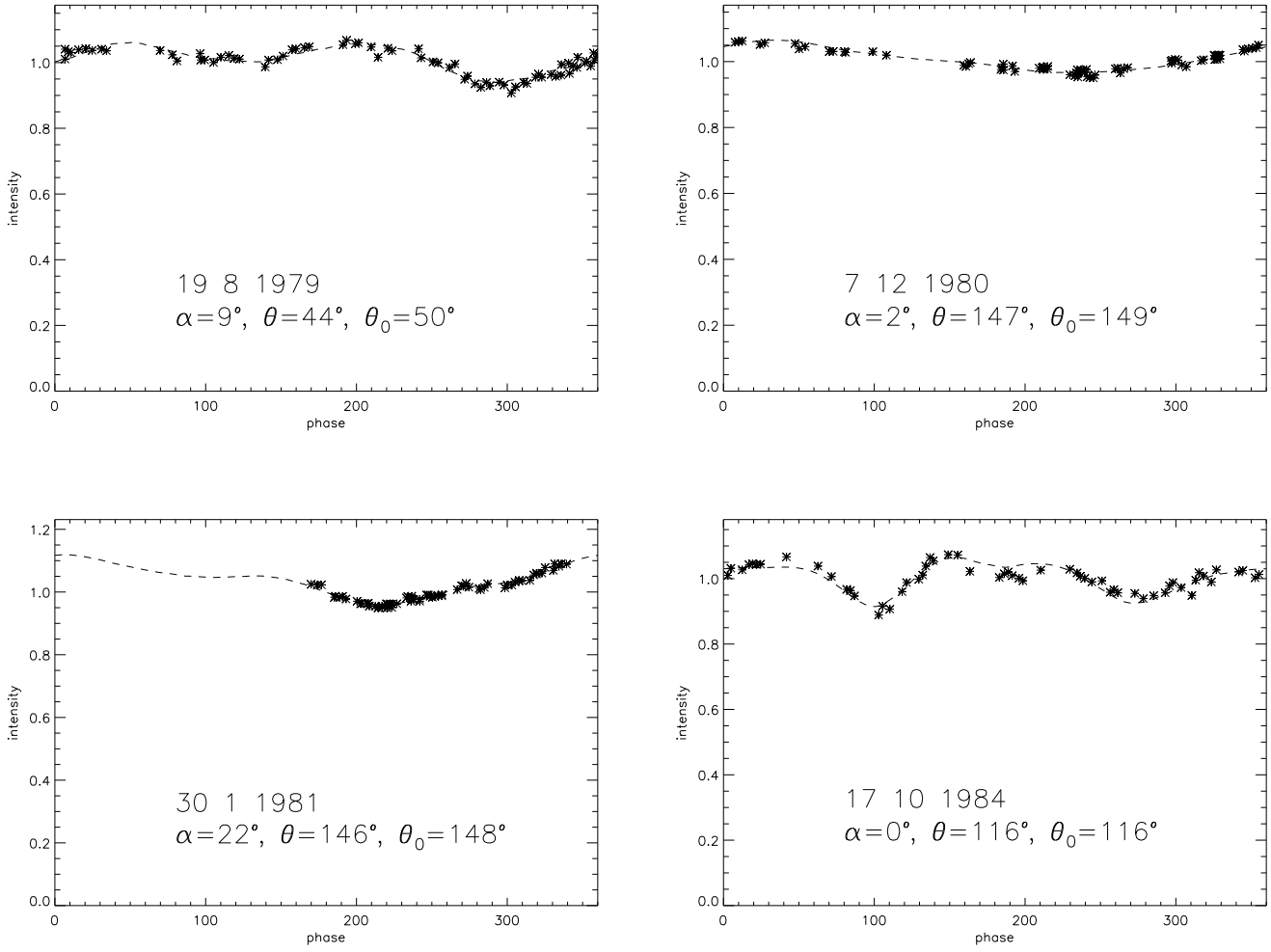
intensity
phase
19 8 1979
α=9°, θ=44°, θ0=50°
7 12 1980
α=2°, θ=147°, θ0=149°
30 1 1981
α=22°, θ=146°, θ0=148°
17 10 1984
α=0°, θ=116°, θ0=116°

Fig. 22

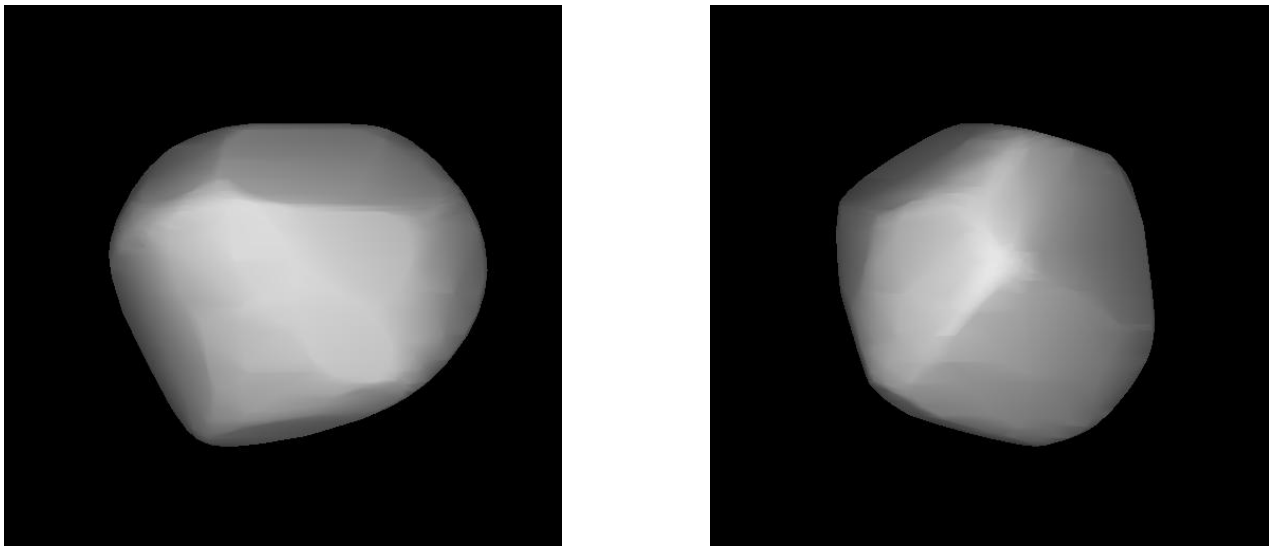

Fig. 23

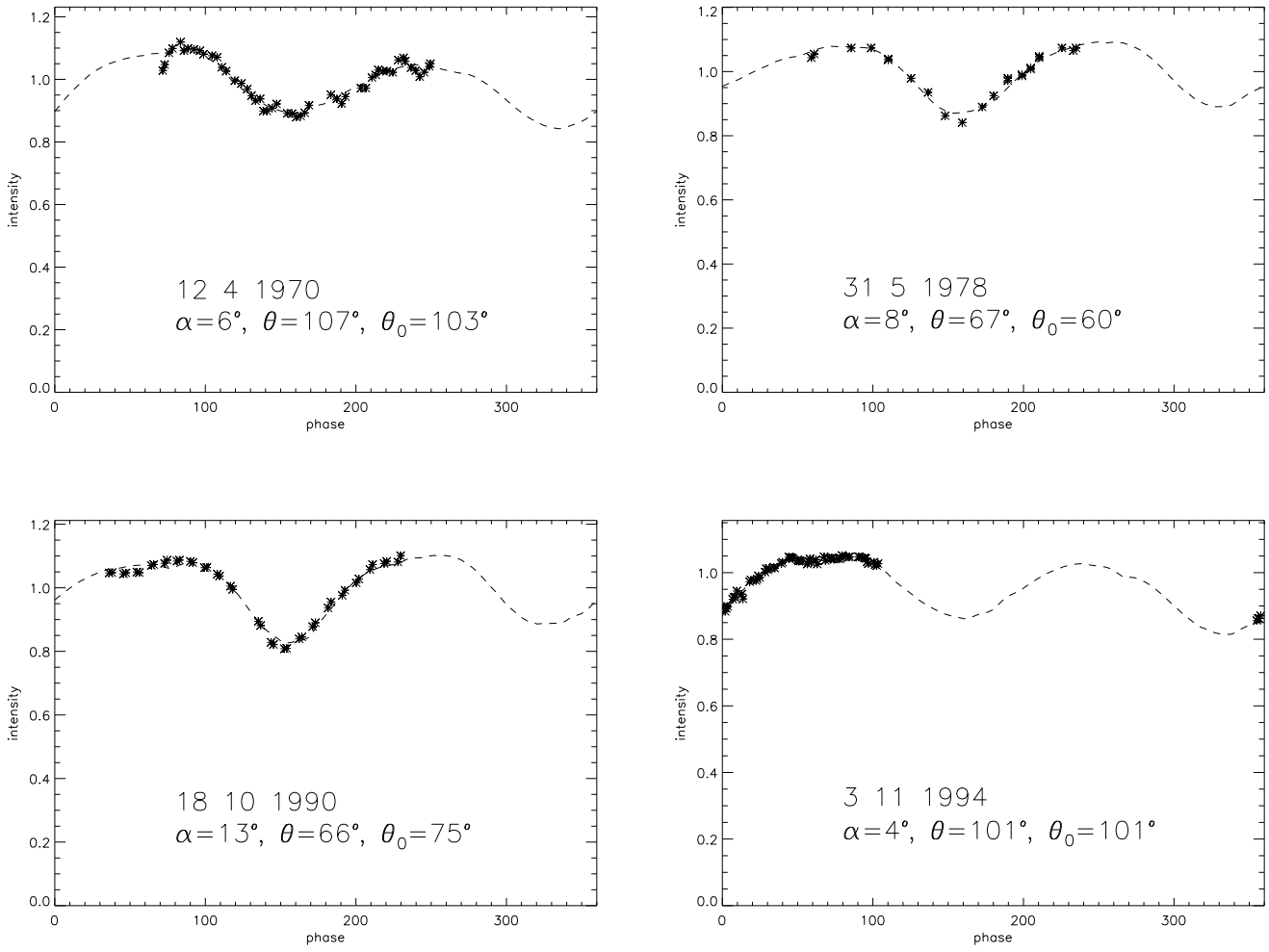
12 4 1970
α=6°, θ=107°, θ0=103°
31 5 1978
α=8°, θ=67°, θ0=60°
18 10 1990
α=13°, θ=66°, θ0=75°
3 11 1994
α=4°, θ=101°, θ0=101°
intensity
phase

Fig. 24

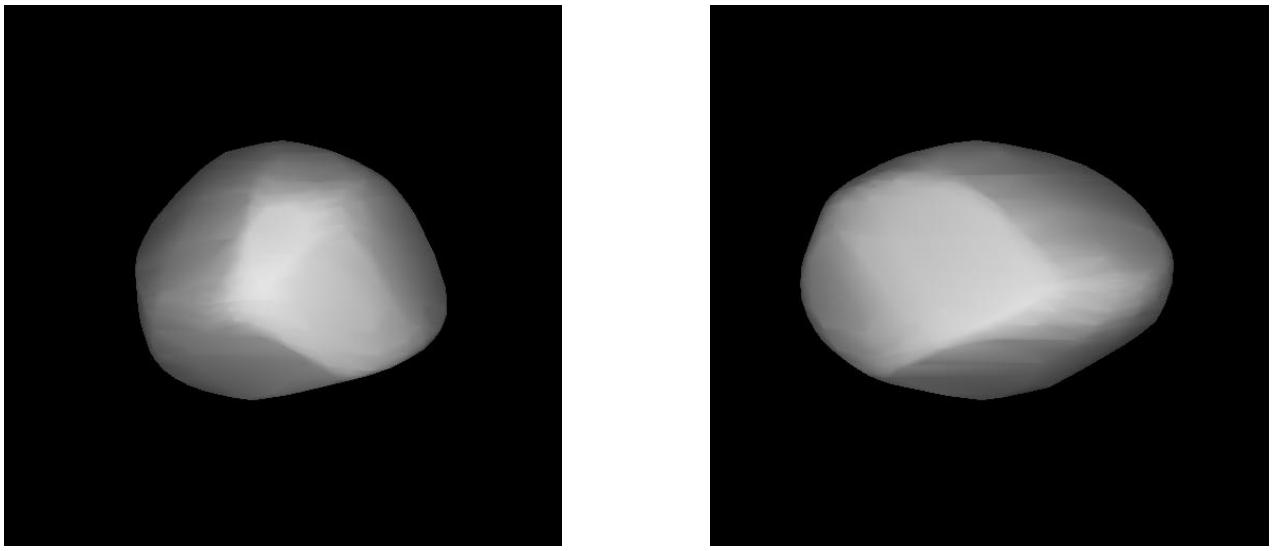

Fig. 25

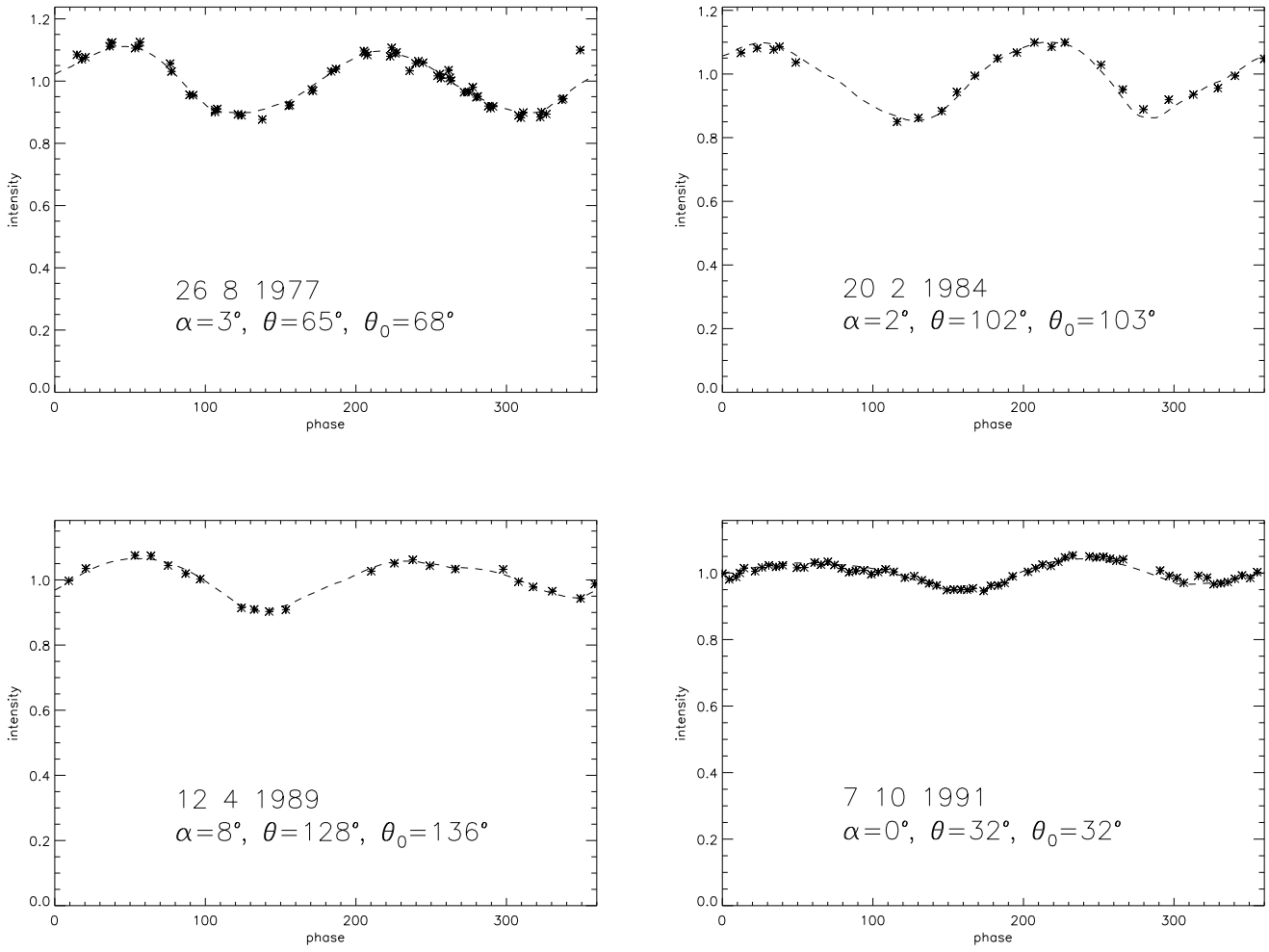
intensity
phase
26 8 1977
α=3°, θ=65°, θ0=68°
20 2 1984
α=2°, θ=102°, θ0=103°
12 4 1989
α=8°, θ=128°, θ0=136°
7 10 1991
α=0°, θ=32°, θ0=32°

Fig. 26

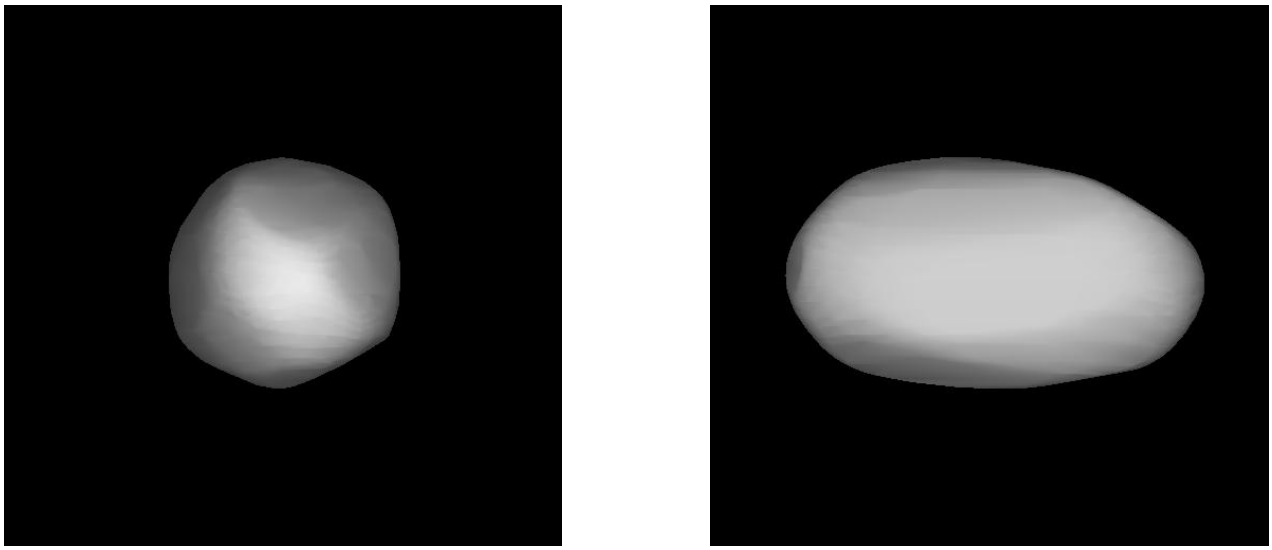

Fig. 27

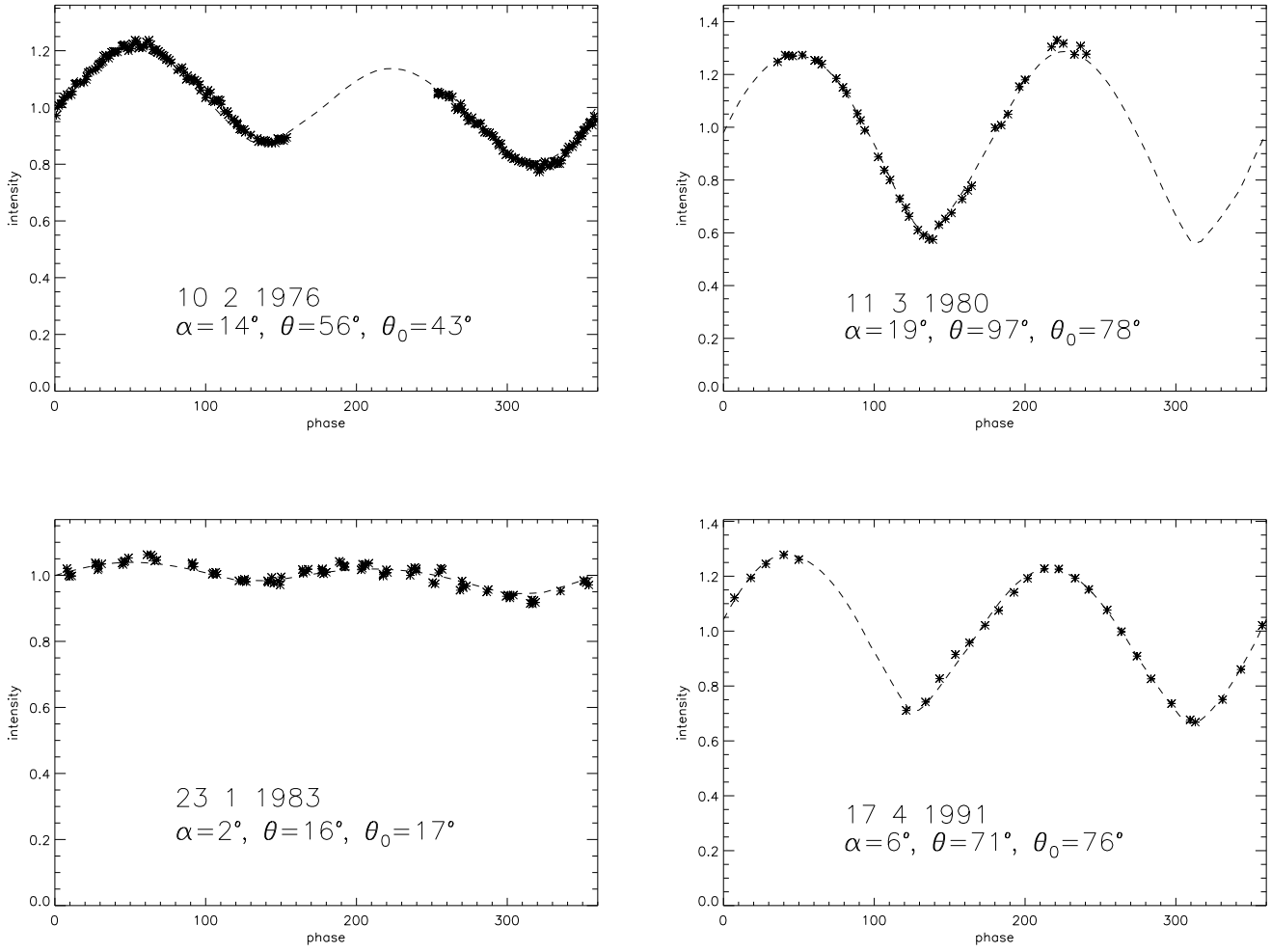
intensity
phase
10 2 1976
α=14°, θ=56°, θ0=43°
11 3 1980
α=19°, θ=97°, θ0=78°
23 1 1983
α=2°, θ=16°, θ0=17°
17 4 1991
α=6°, θ=71°, θ0=76°

Fig. 28

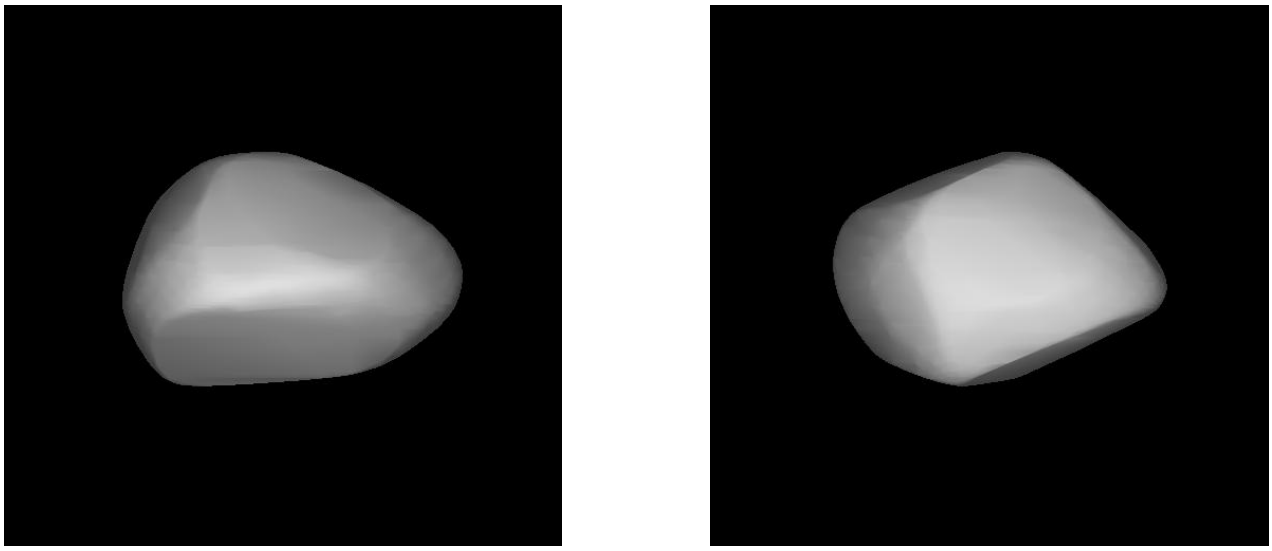

Fig. 29

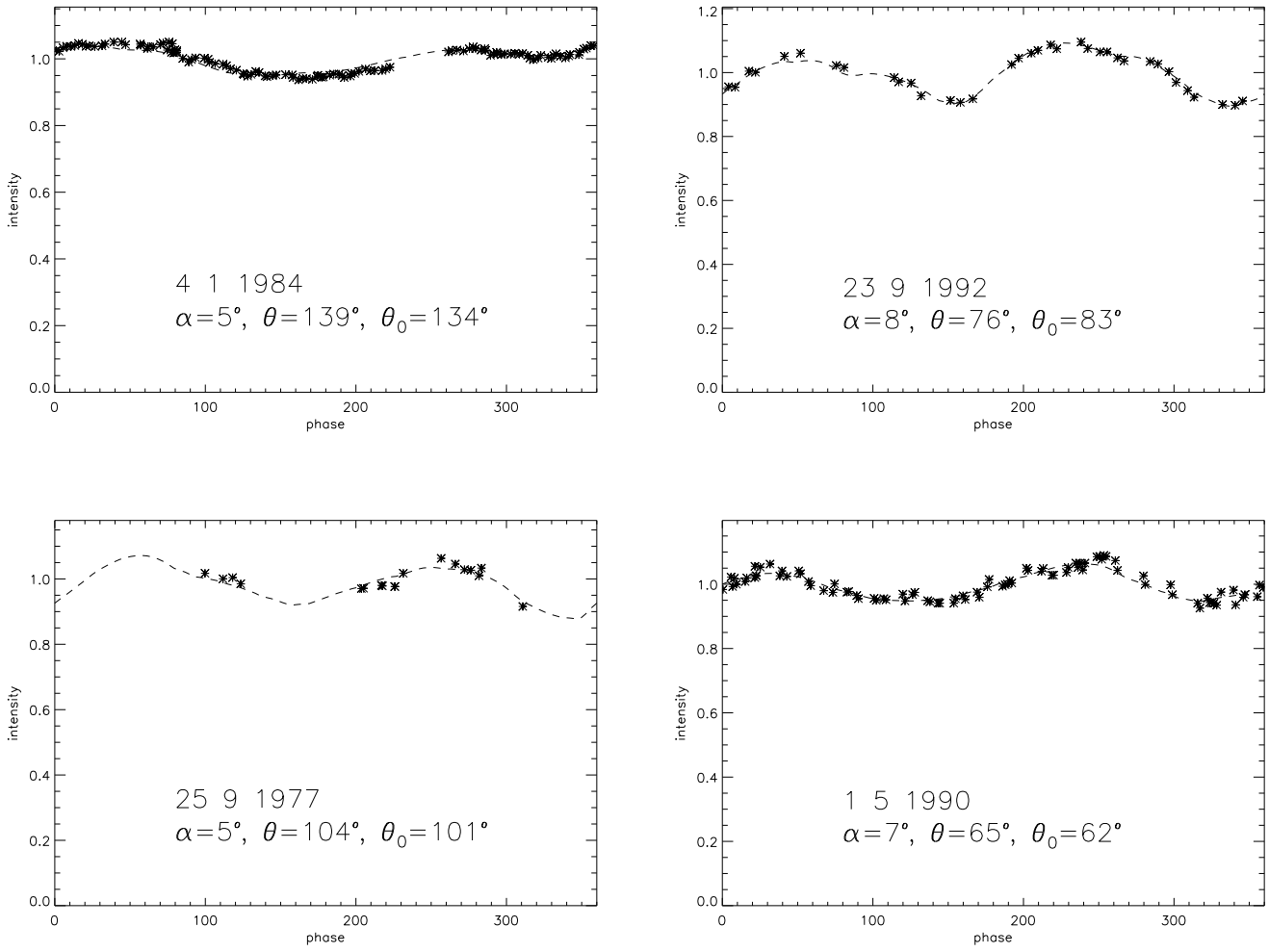
4 1 1984
α=5°, θ=139°, θ0=134°
23 9 1992
α=8°, θ=76°, θ0=83°
25 9 1977
α=5°, θ=104°, θ0=101°
1 5 1990
α=7°, θ=65°, θ0=62°
intensity
phase

Fig. 30

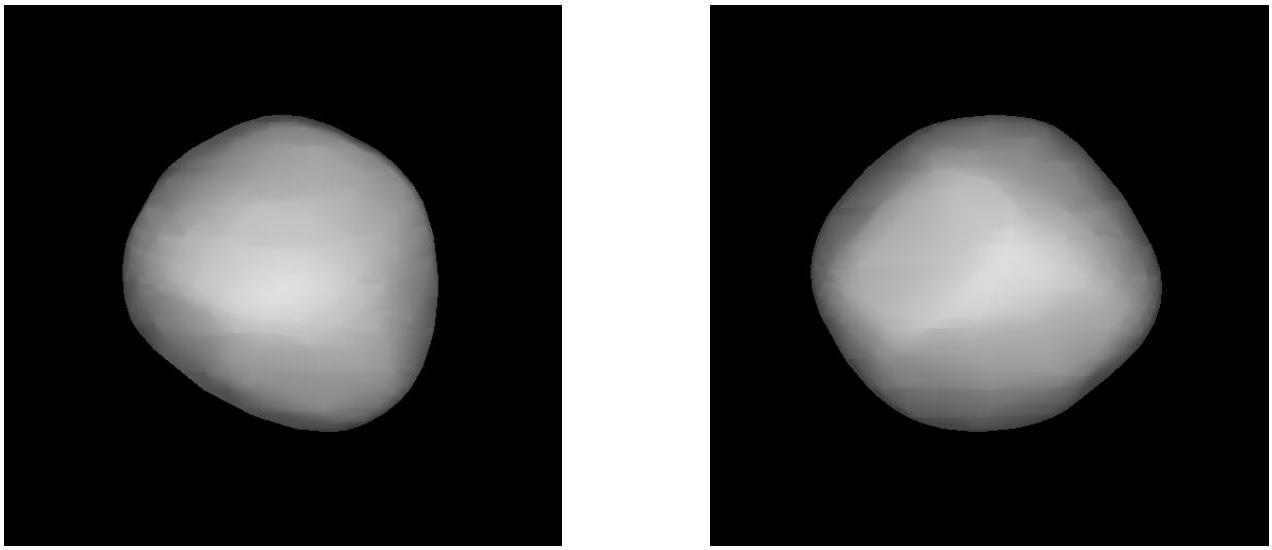

Fig. 31

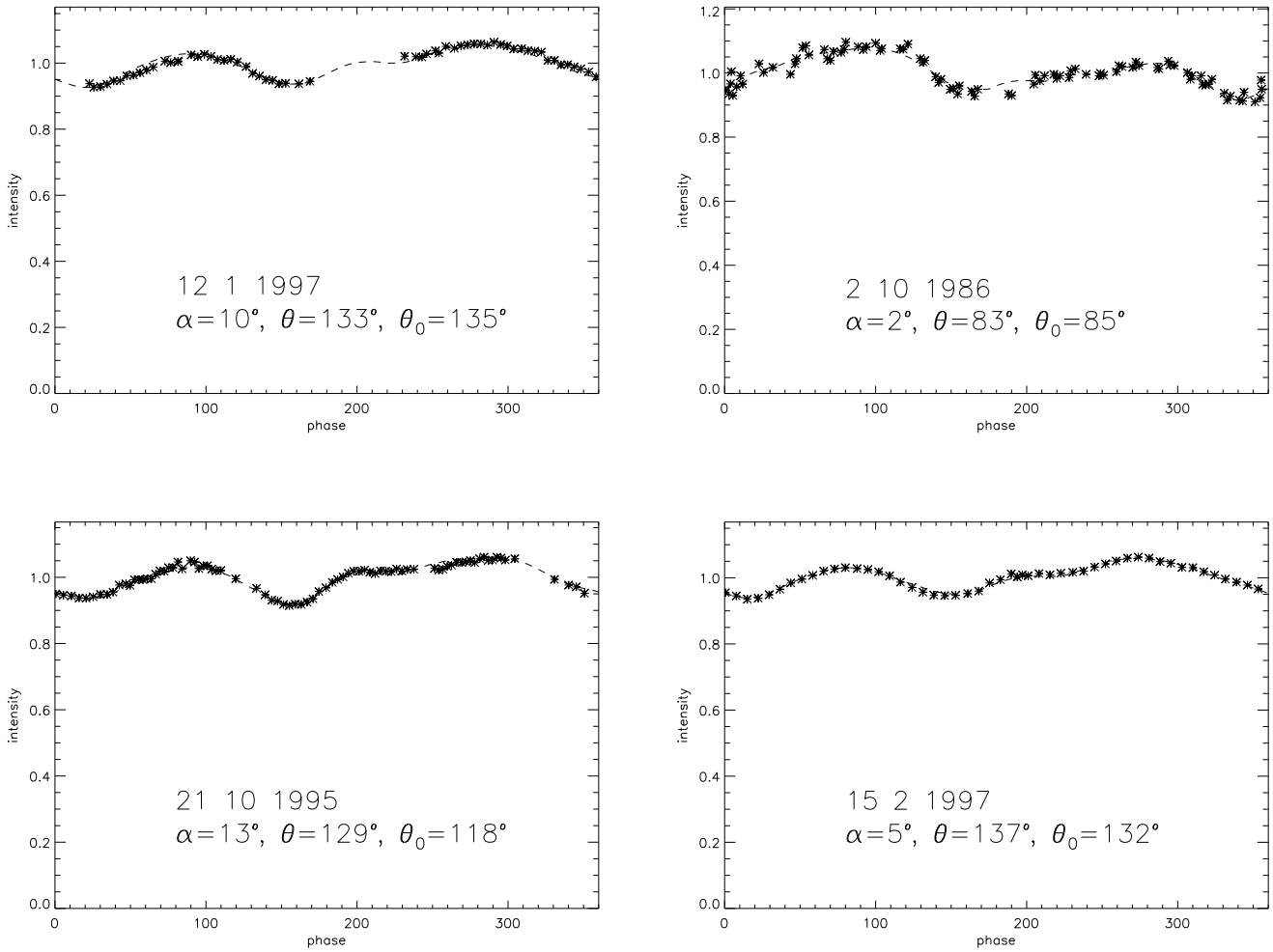
12 1 1997
α=10°, θ=133°, θ0=135°
2 10 1986
α=2°, θ=83°, θ0=85°
21 10 1995
α=13°, θ=129°, θ0=118°
15 2 1997
α=5°, θ=137°, θ0=132°
intensity
phase

Fig. 32

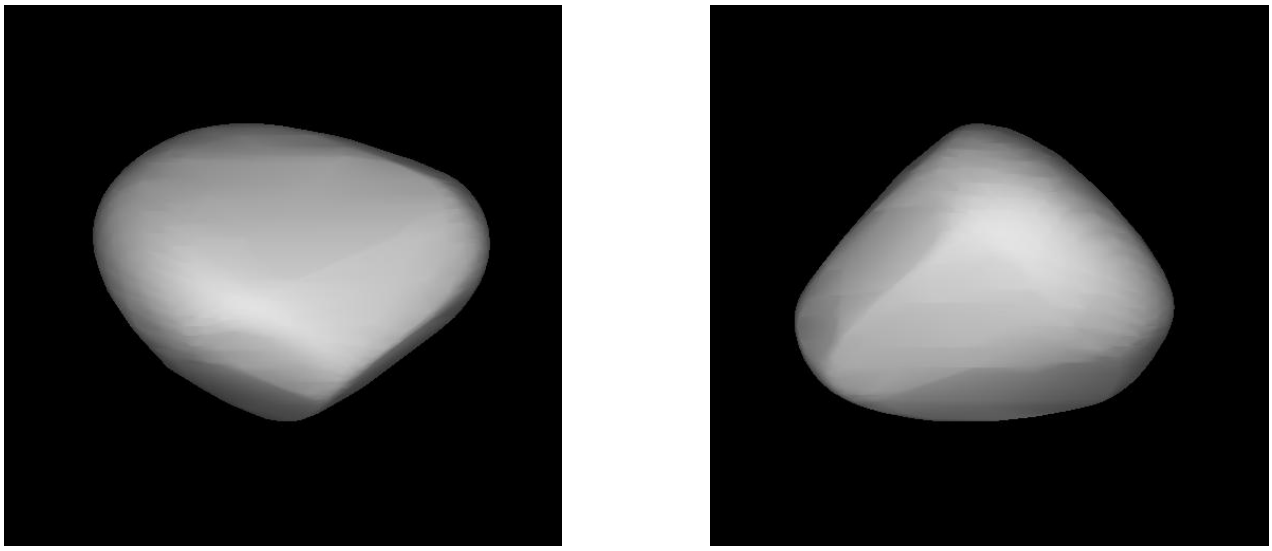

Fig. 33

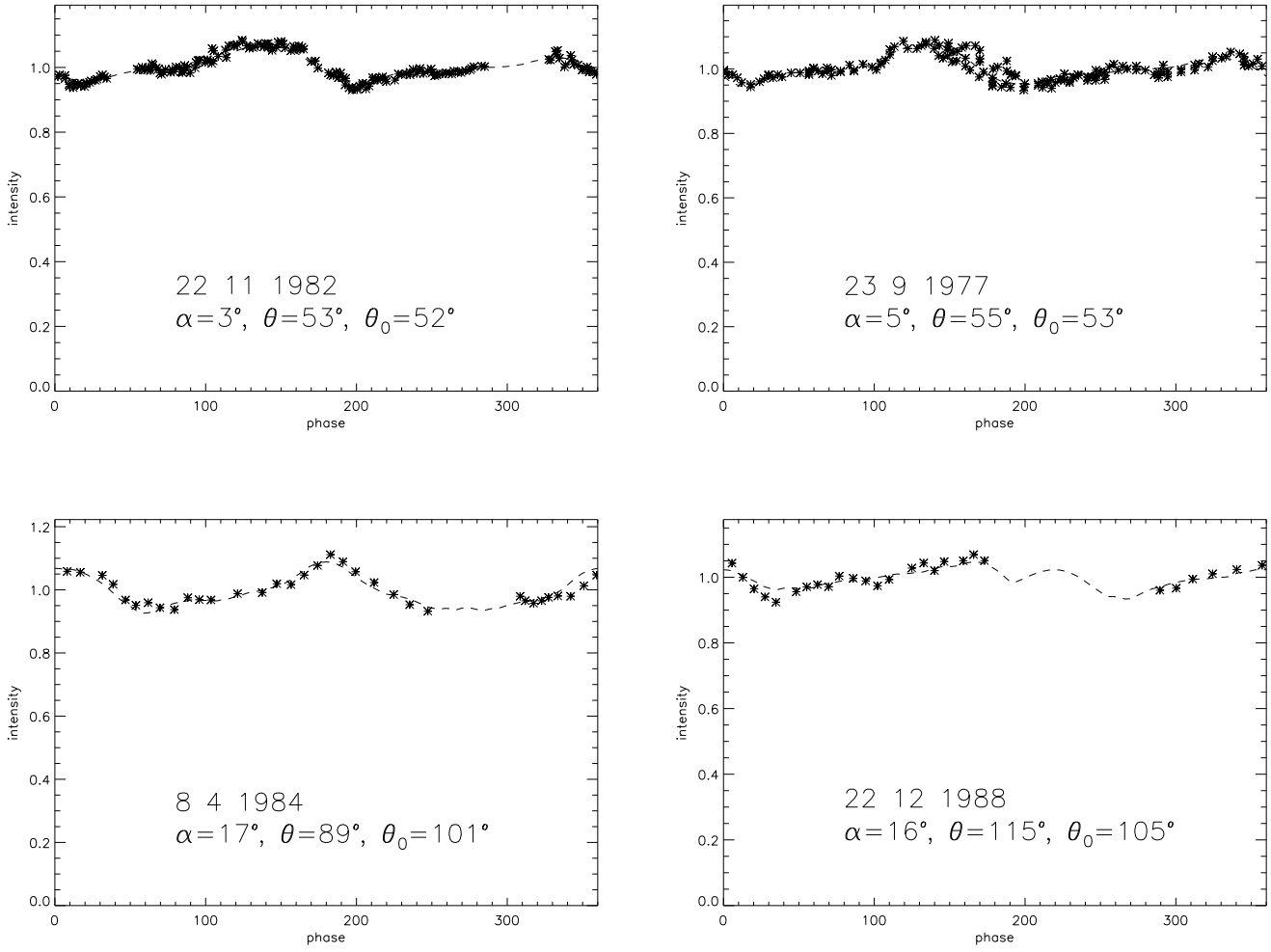
22 11 1982
α=3°, θ=53°, θ0=52°
23 9 1977
α=5°, θ=55°, θ0=53°
8 4 1984
α=17°, θ=89°, θ0=101°
22 12 1988
α=16°, θ=115°, θ0=105°
intensity
phase

Fig. 34

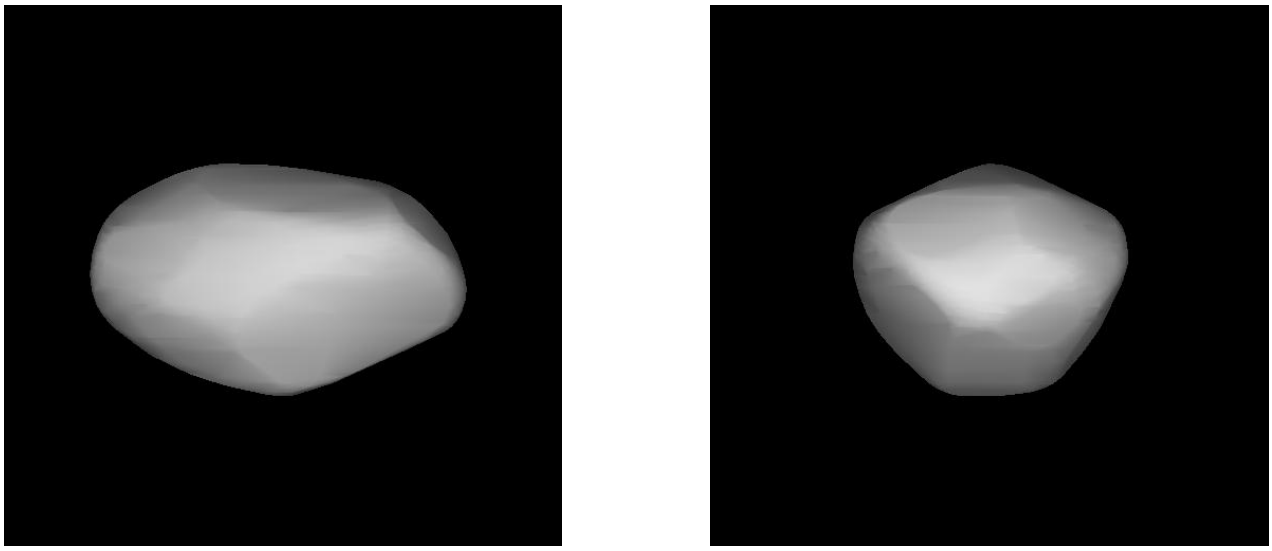

Fig. 35

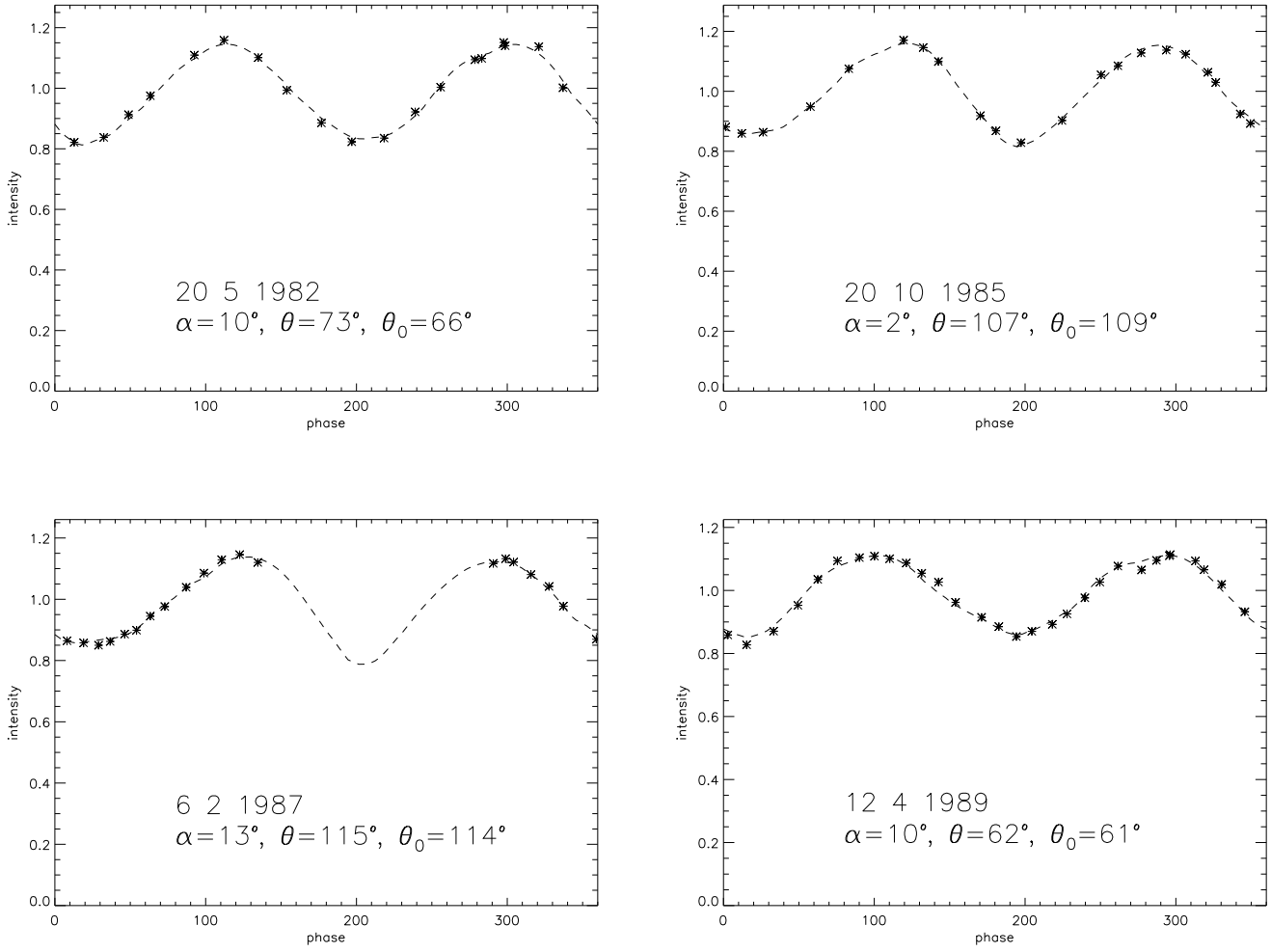
intensity
phase
20 5 1982
α=10°, θ=73°, θ0=66°
20 10 1985
α=2°, θ=107°, θ0=109°
6 2 1987
α=13°, θ=115°, θ0=114°
12 4 1989
α=10°, θ=62°, θ0=61°

Fig. 36

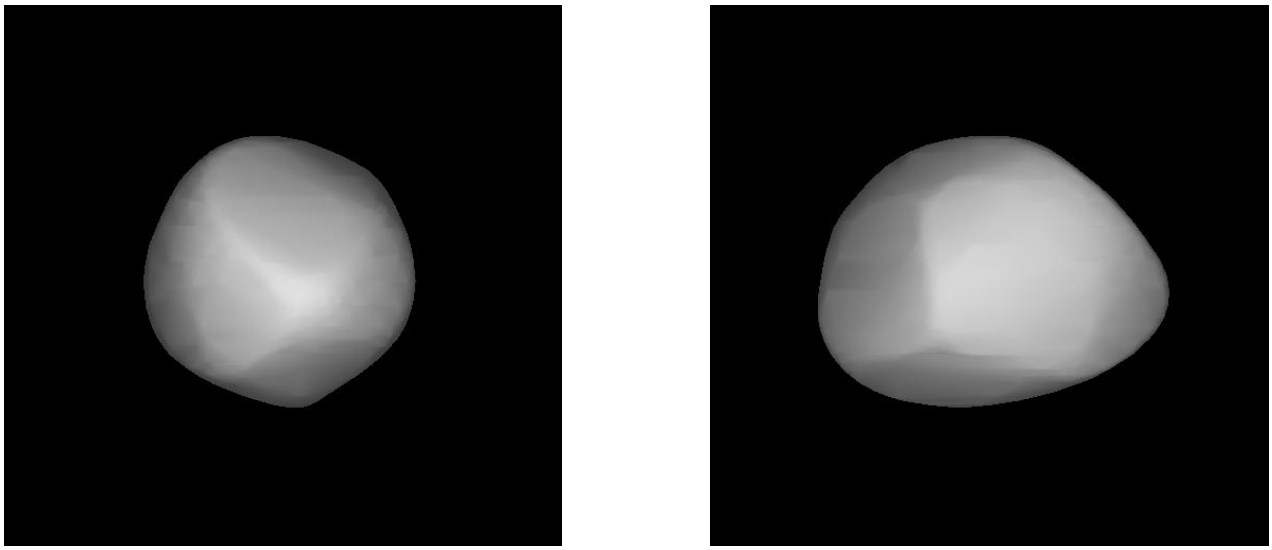

Fig. 37

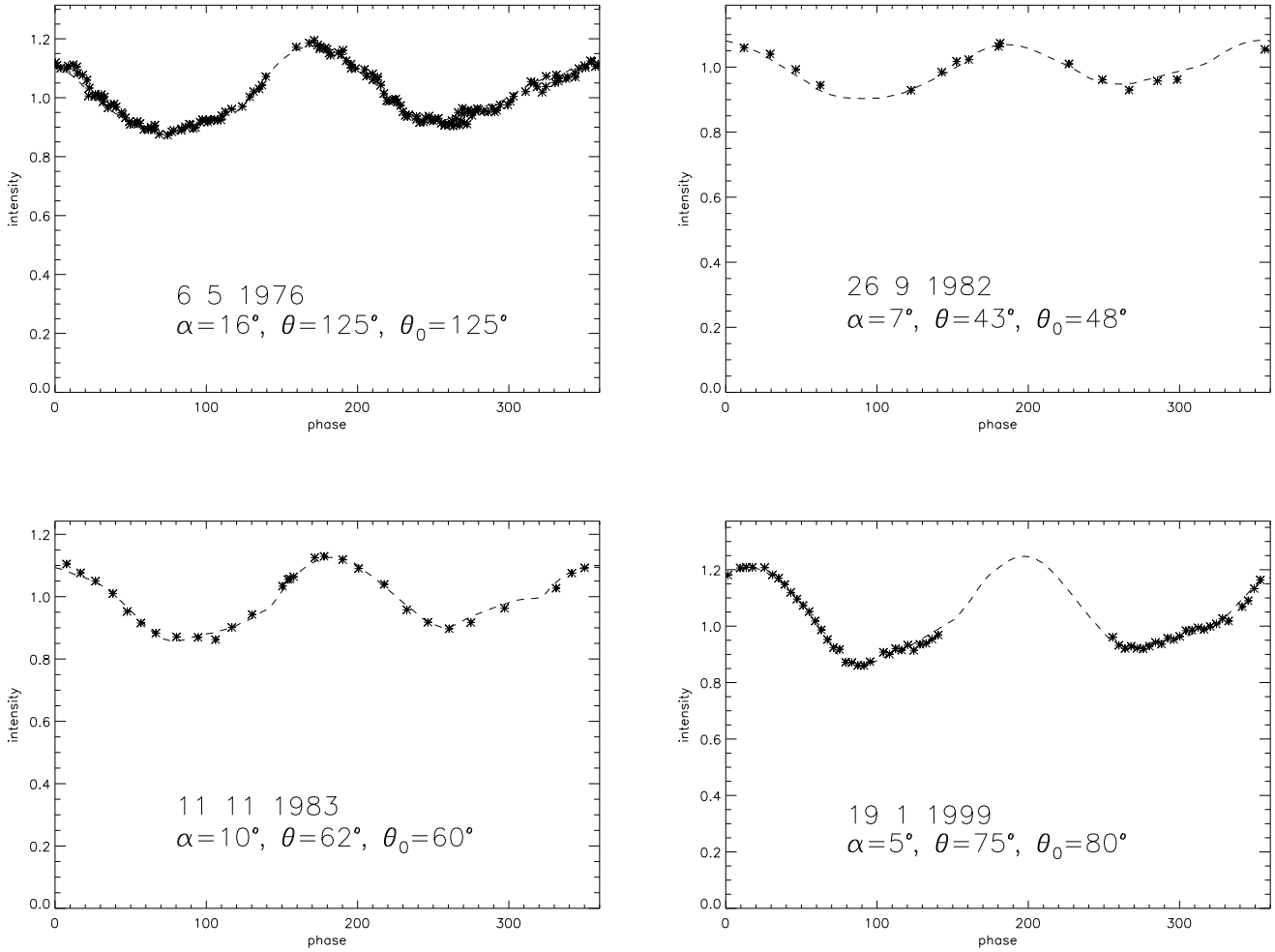
6 5 1976
α=16°, θ=125°, θ0=125°
26 9 1982
α=7°, θ=43°, θ0=48°
11 11 1983
α=10°, θ=62°, θ0=60°
19 1 1999
α=5°, θ=75°, θ0=80°
intensity
phase

Fig. 38

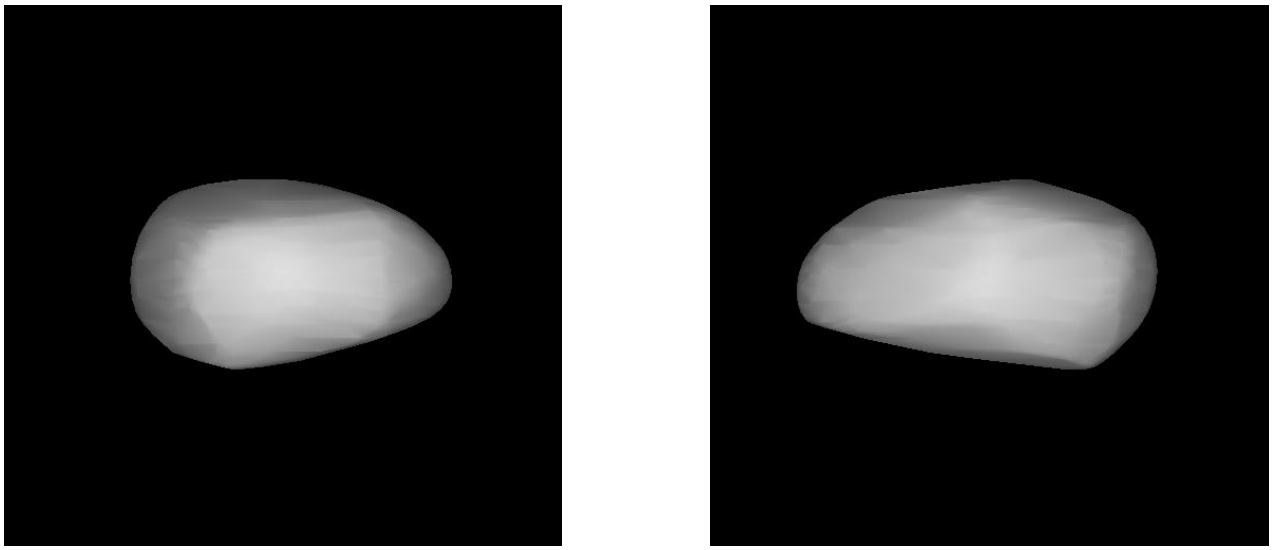

Fig. 39

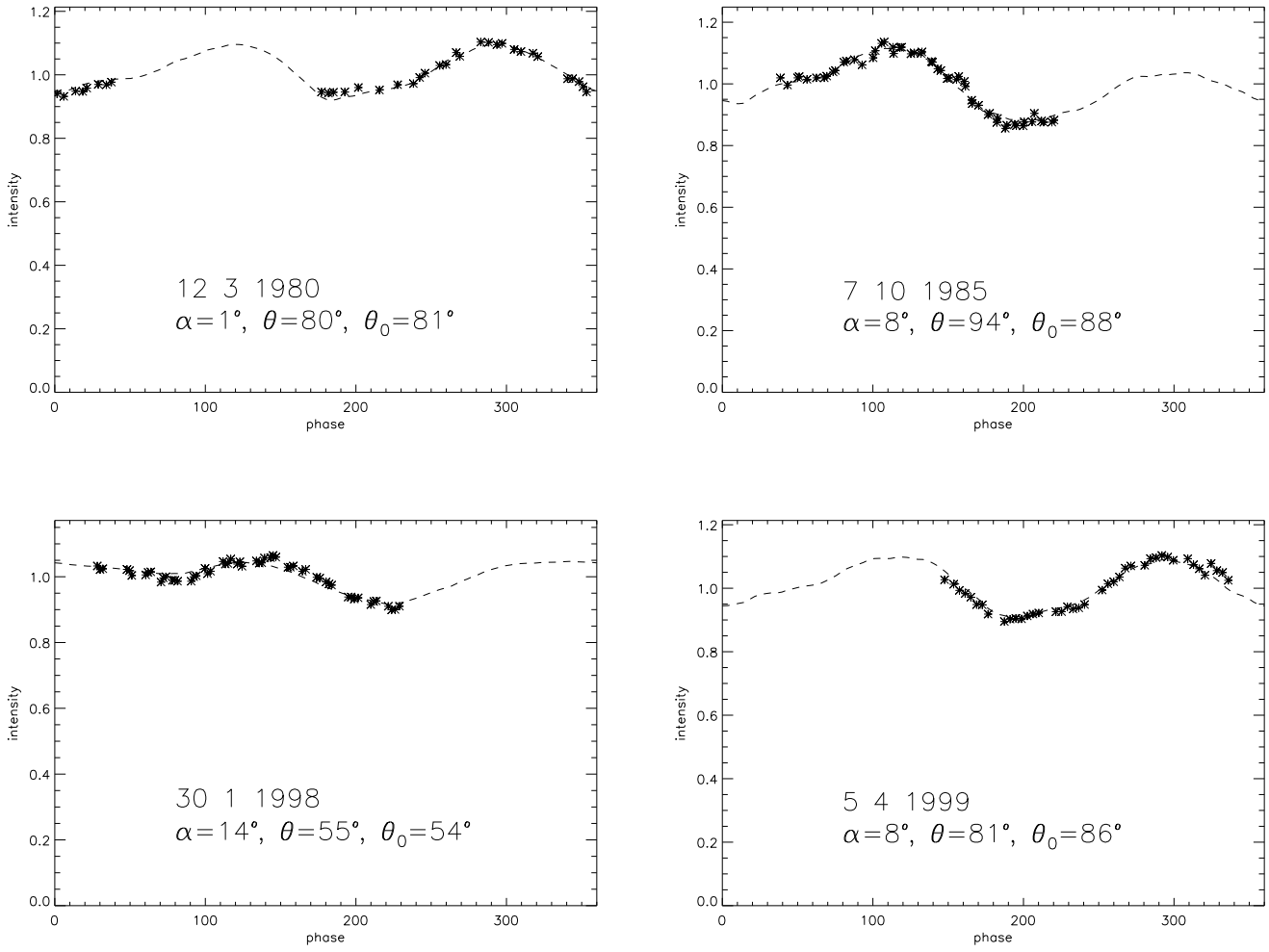
12 3 1980
α=1°, θ=80°, θ0=81°
7 10 1985
α=8°, θ=94°, θ0=88°
30 1 1998
α=14°, θ=55°, θ0=54°
5 4 1999
α=8°, θ=81°, θ0=86°
intensity
phase

Fig. 40

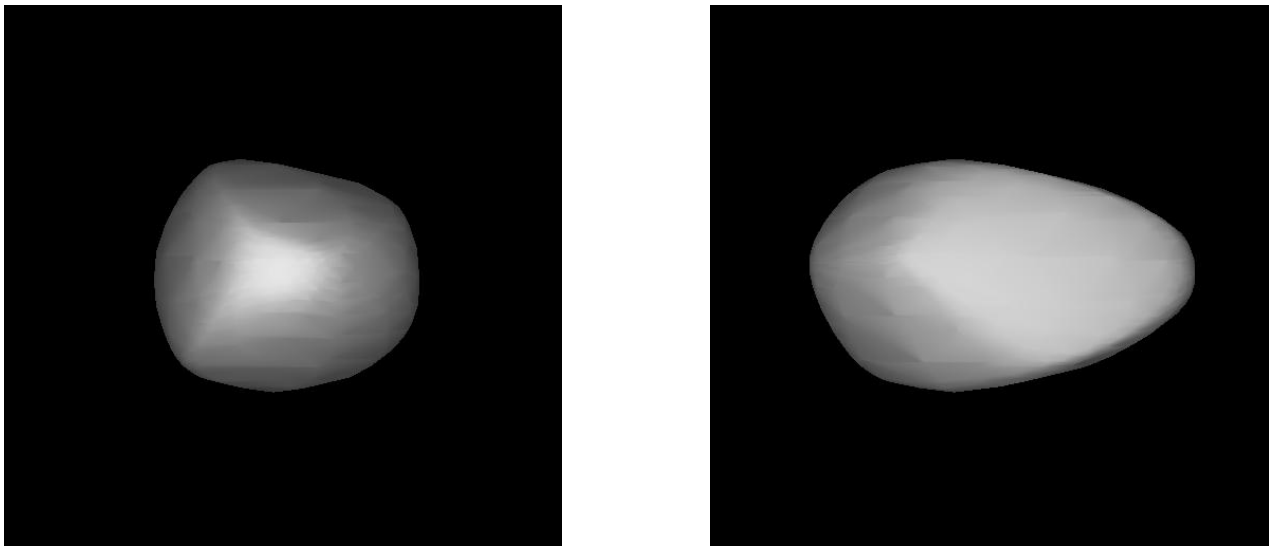

Fig. 41

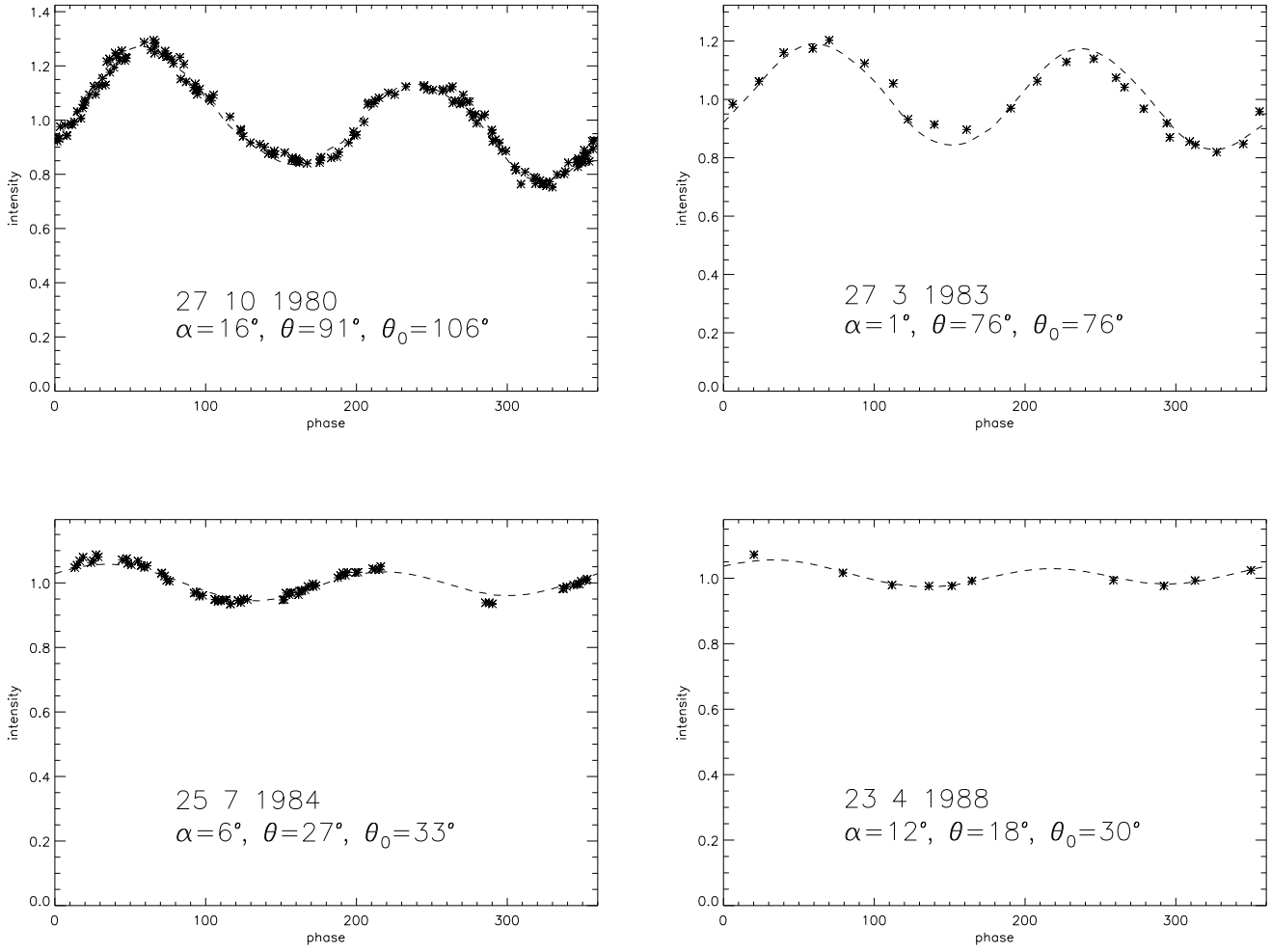
intensity
phase
27 10 1980
α=16°, θ=91°, θ0=106°
27 3 1983
α=1°, θ=76°, θ0=76°
25 7 1984
α=6°, θ=27°, θ0=33°
23 4 1988
α=12°, θ=18°, θ0=30°

Fig. 42

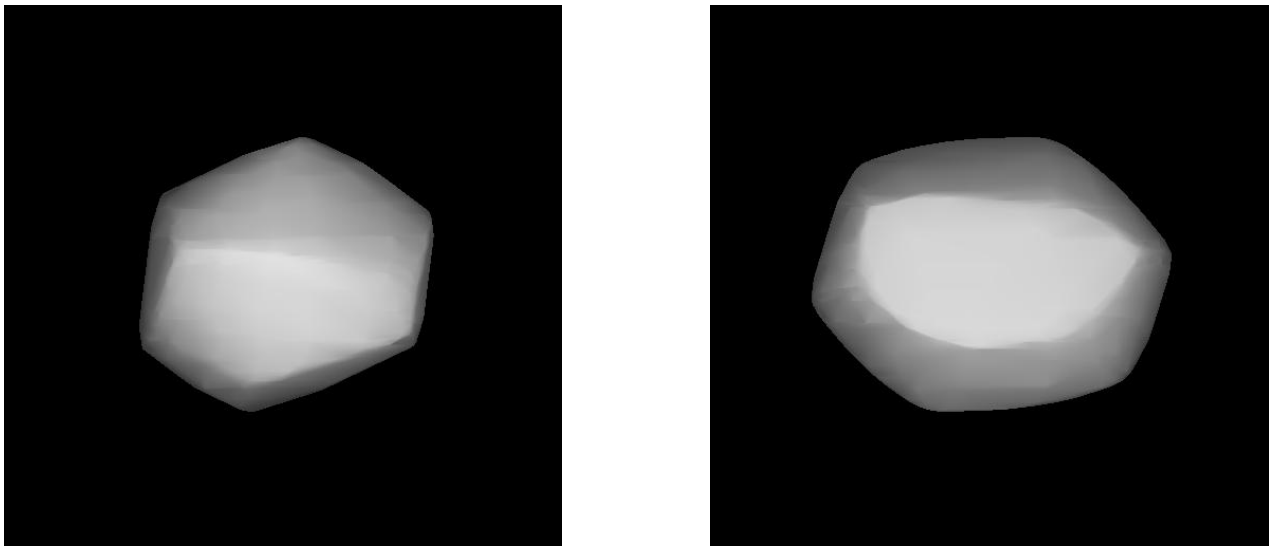

Fig. 43

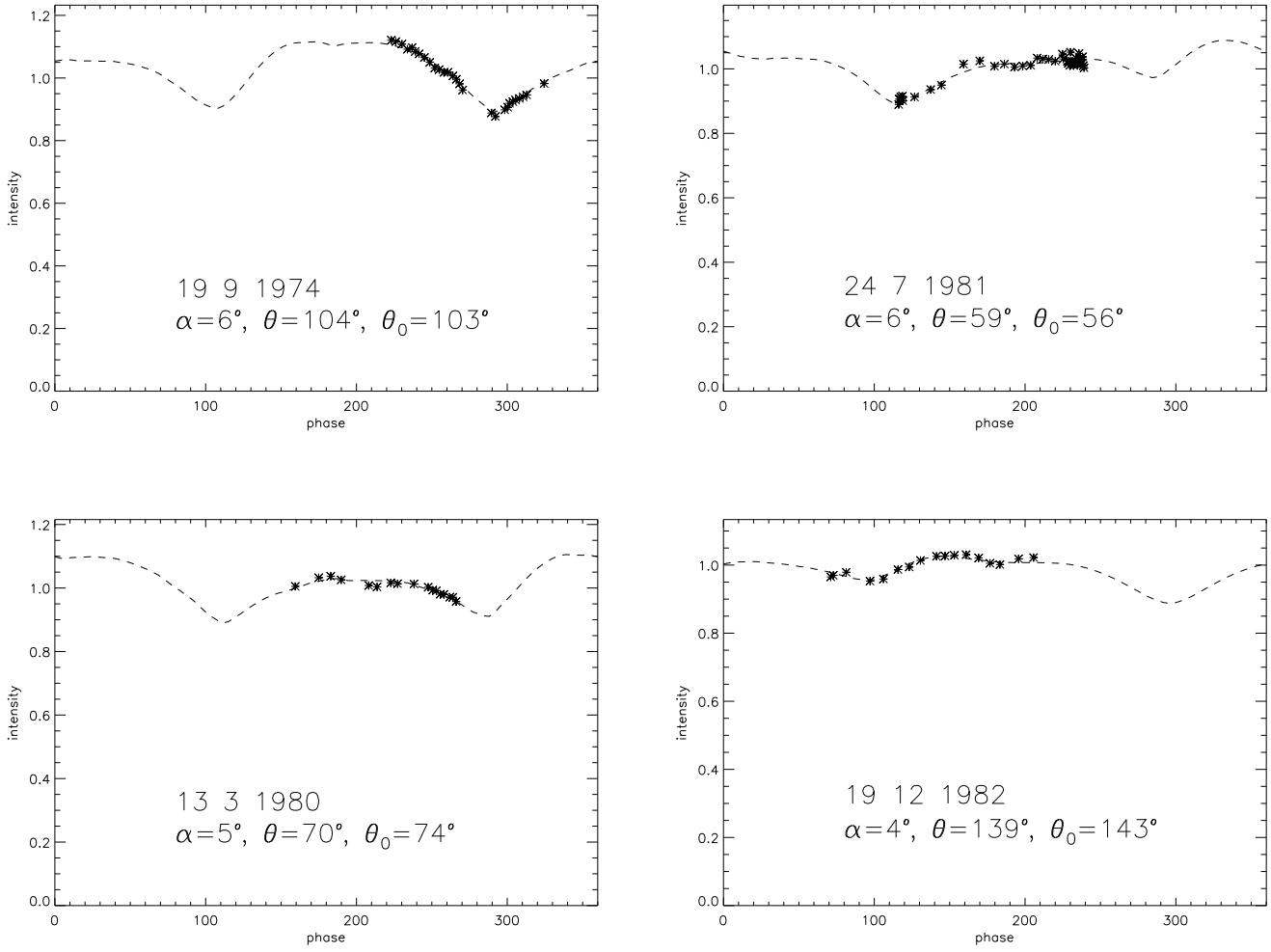
intensity
phase
19 9 1974
α=6°, θ=104°, θ0=103°
24 7 1981
α=6°, θ=59°, θ0=56°
13 3 1980
α=5°, θ=70°, θ0=74°
19 12 1982
α=4°, θ=139°, θ0=143°

Fig. 44

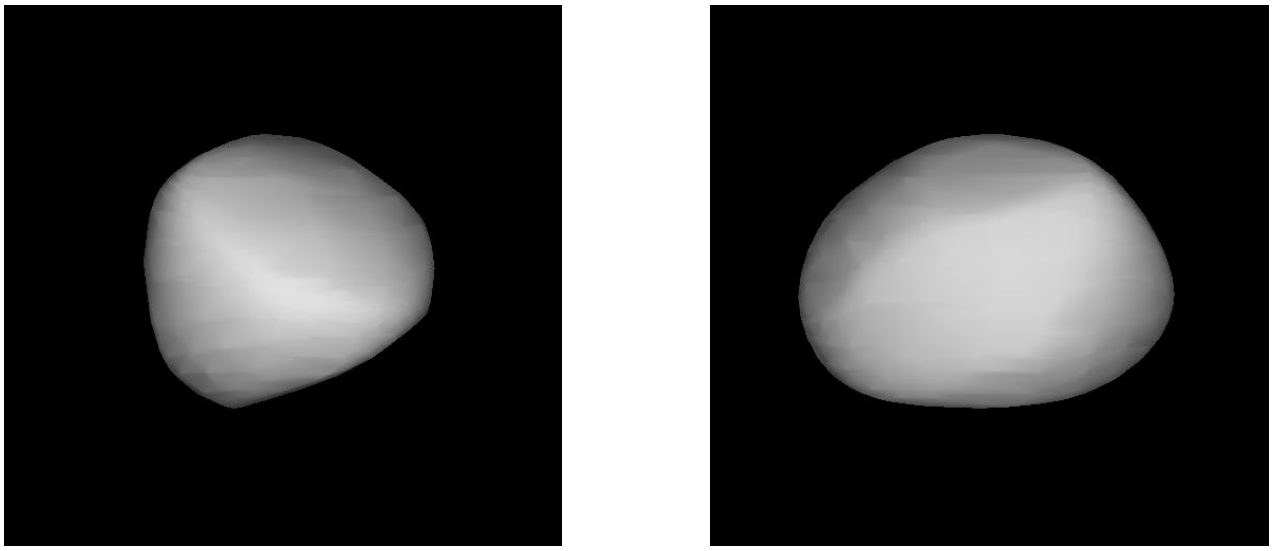

Fig. 45

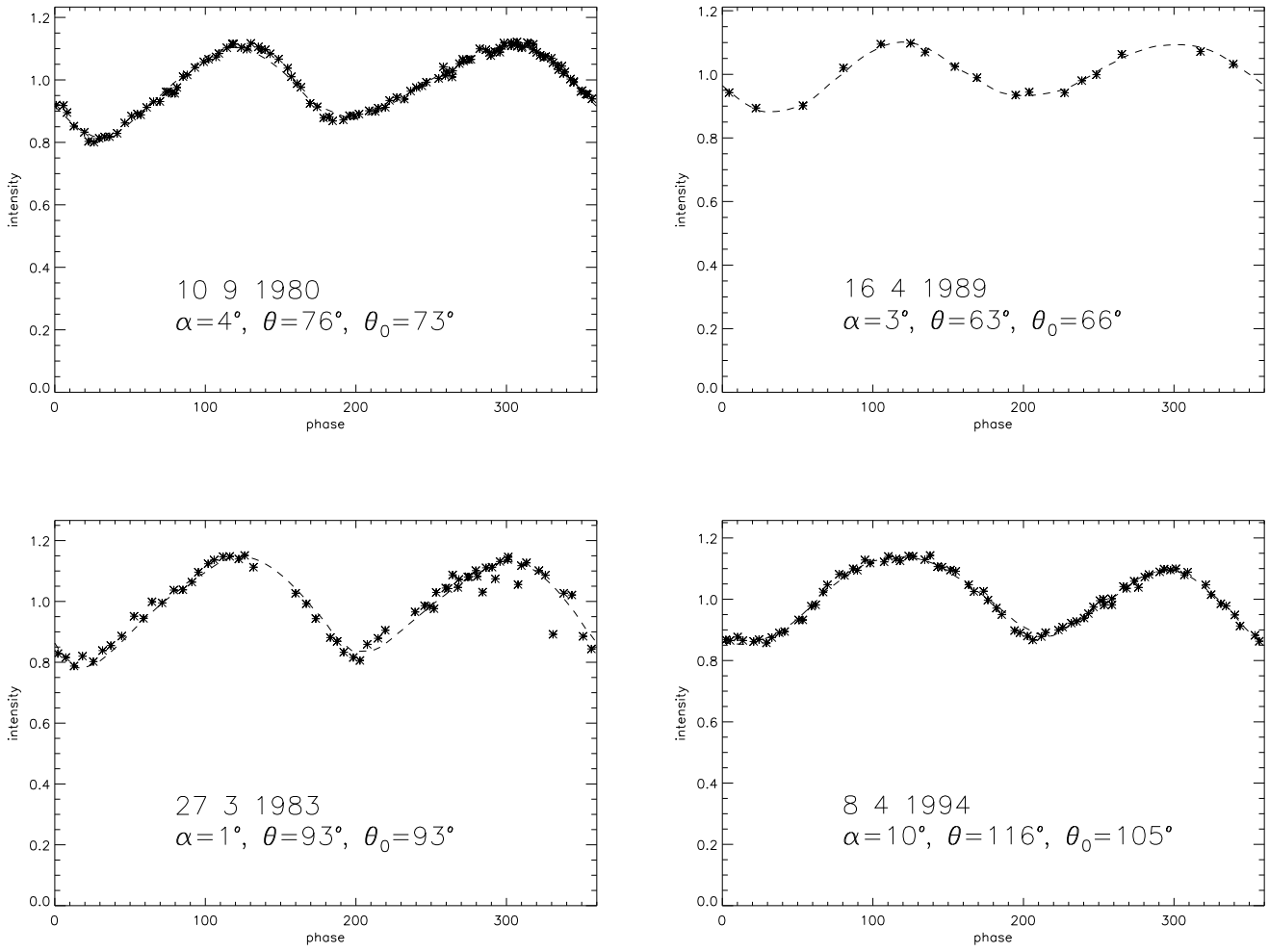
10 9 1980
α=4°, θ=76°, θ0=73°
16 4 1989
α=3°, θ=63°, θ0=66°
27 3 1983
α=1°, θ=93°, θ0=93°
8 4 1994
α=10°, θ=116°, θ0=105°
intensity
phase

Fig. 46

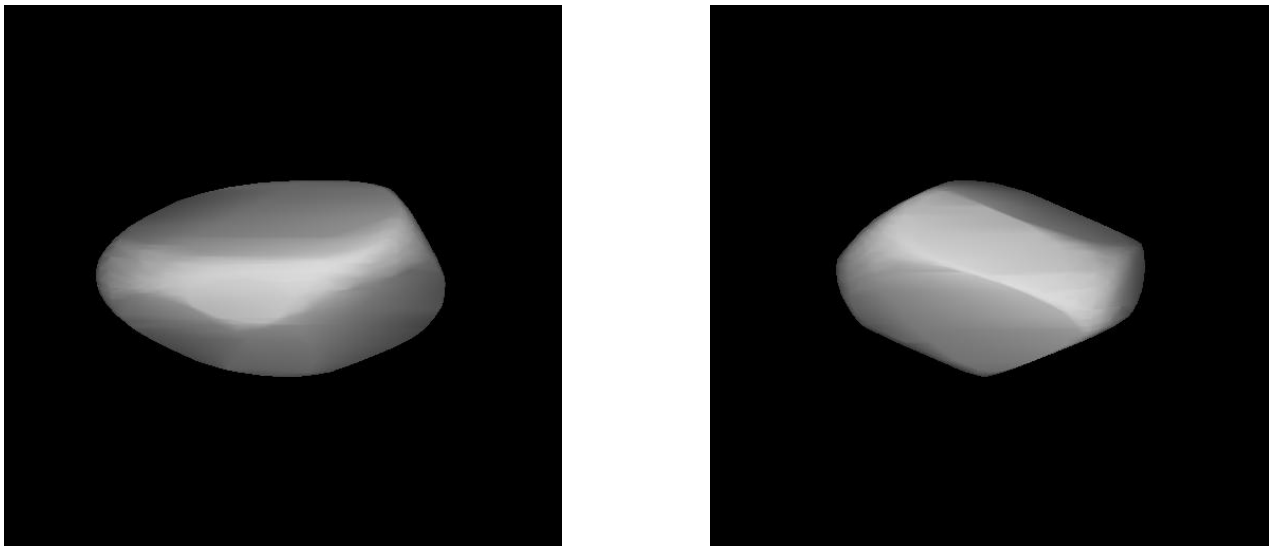

Fig. 47

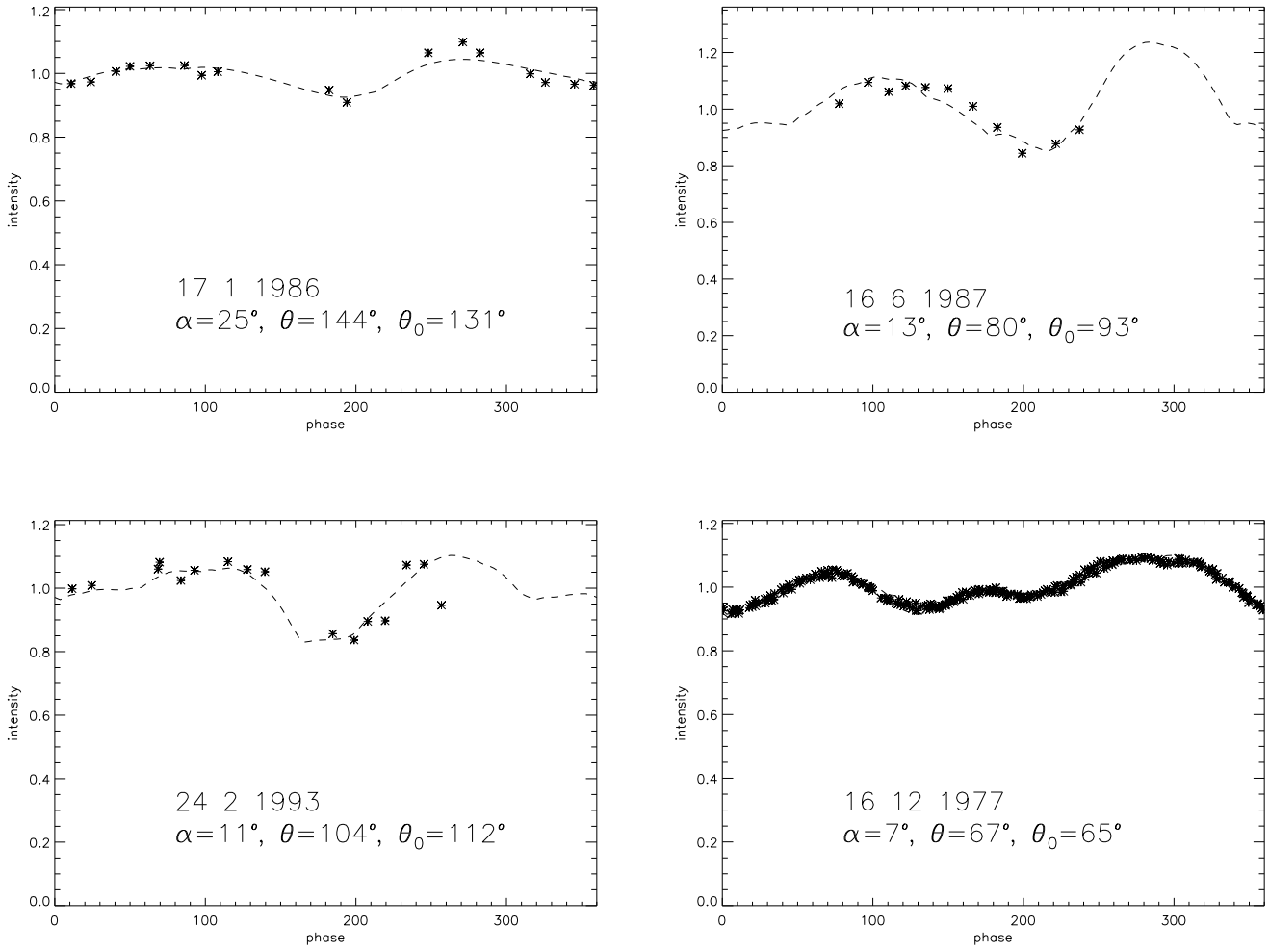
17 1 1986
α=25°, θ=144°, θ0=131°
16 6 1987
α=13°, θ=80°, θ0=93°
24 2 1993
α=11°, θ=104°, θ0=112°
16 12 1977
α=7°, θ=67°, θ0=65°
intensity
phase

Fig. 48

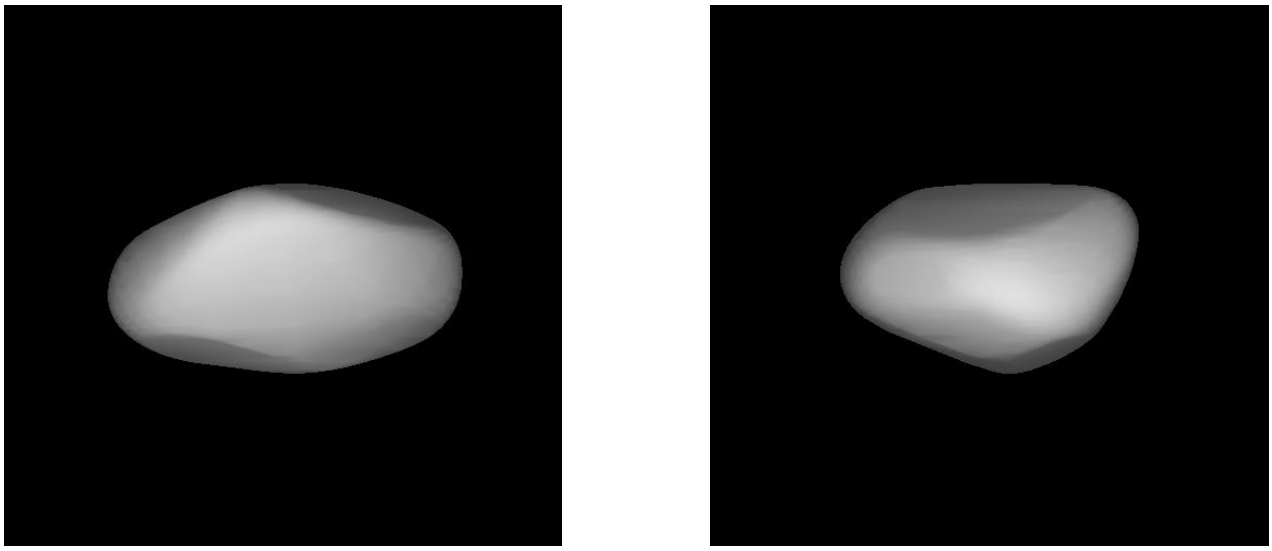

Fig. 49

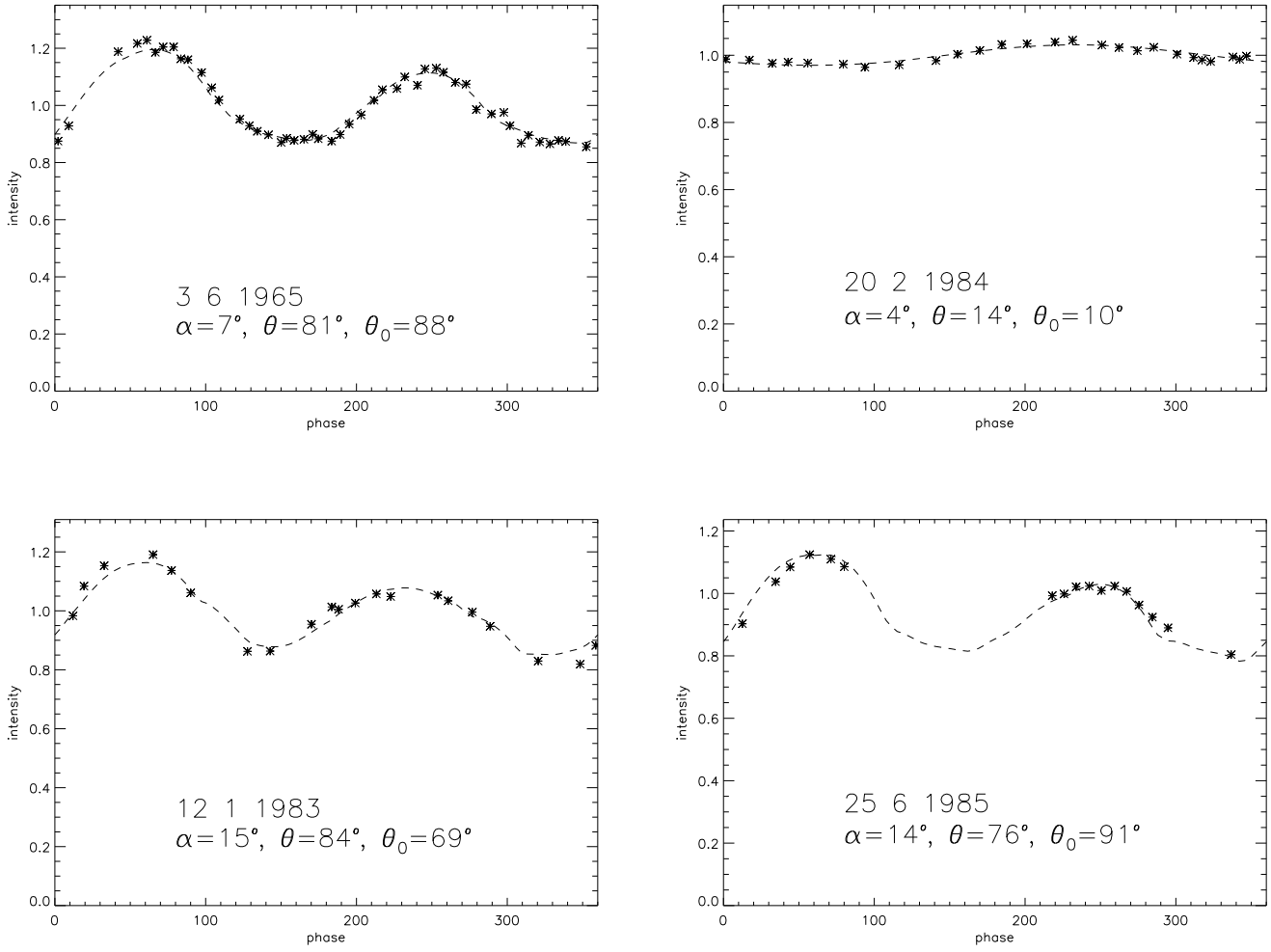
intensity
phase
3 6 1965
α=7°, θ=81°, θ0=88°
20 2 1984
α=4°, θ=14°, θ0=10°
12 1 1983
α=15°, θ=84°, θ0=69°
25 6 1985
α=14°, θ=76°, θ0=91°

Fig. 50

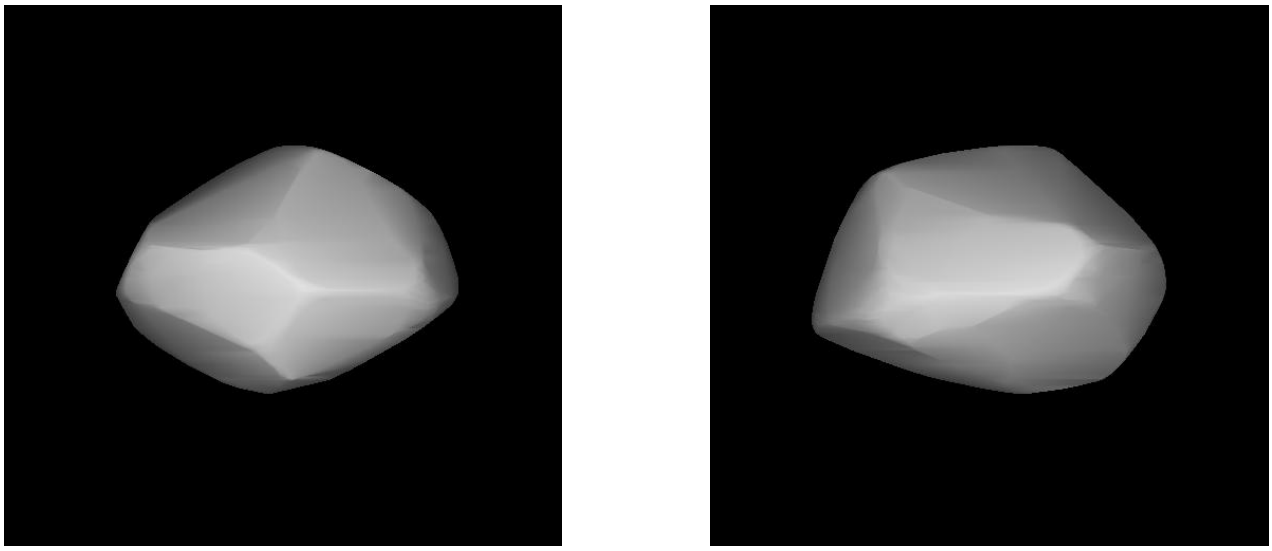

Fig. 51

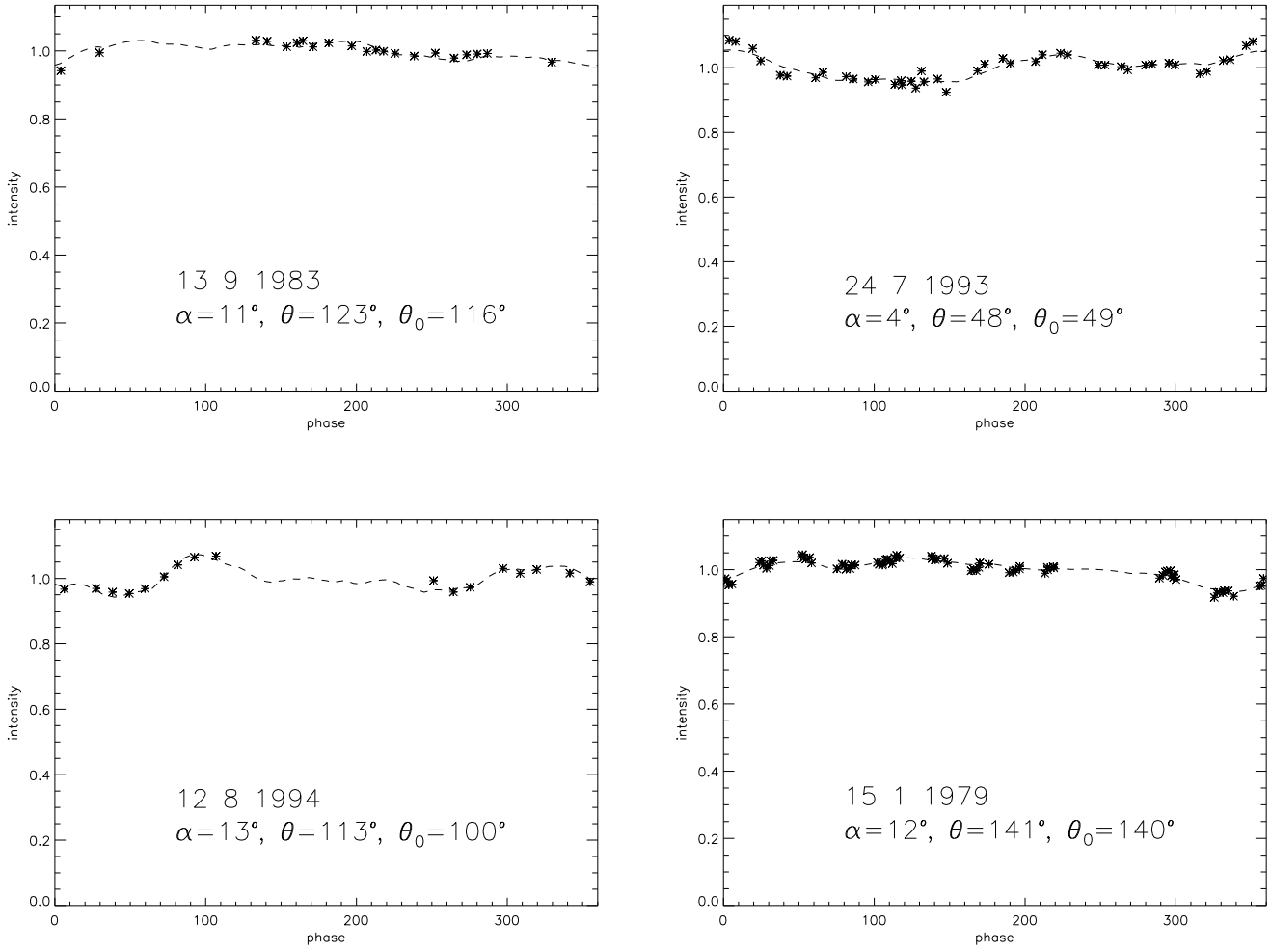
intensity
phase
13 9 1983
α=11°, θ=123°, θ0=116°
24 7 1993
α=4°, θ=48°, θ0=49°
12 8 1994
α=13°, θ=113°, θ0=100°
15 1 1979
α=12°, θ=141°, θ0=140°

Fig. 52

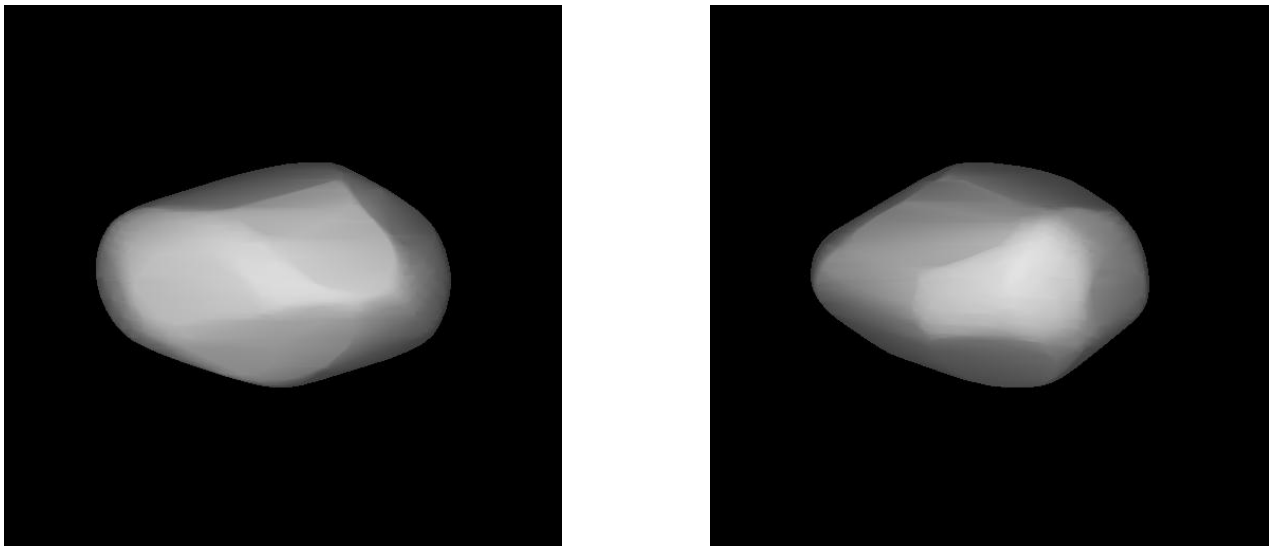

Fig. 53

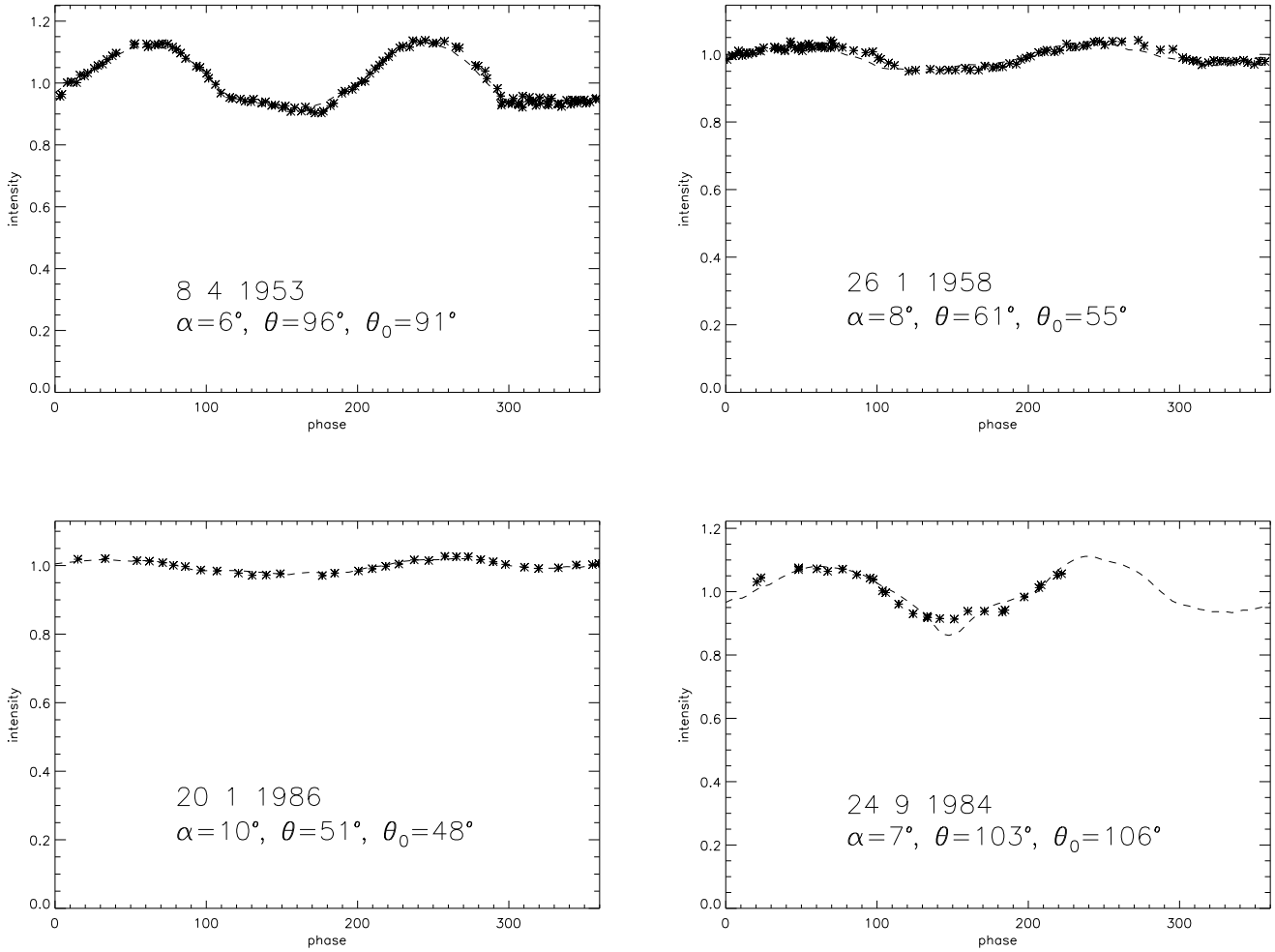
8 4 1953
α=6°, θ=96°, θ0=91°
26 1 1958
α=8°, θ=61°, θ0=55°
20 1 1986
α=10°, θ=51°, θ0=48°
24 9 1984
α=7°, θ=103°, θ0=106°
intensity
phase

Fig. 54

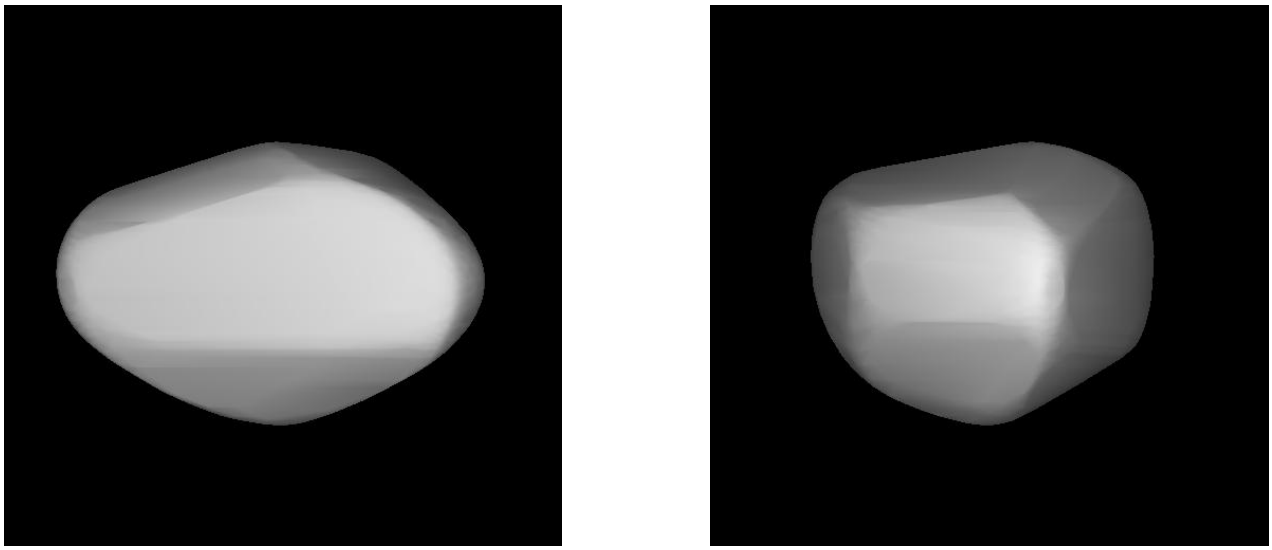

Fig. 55

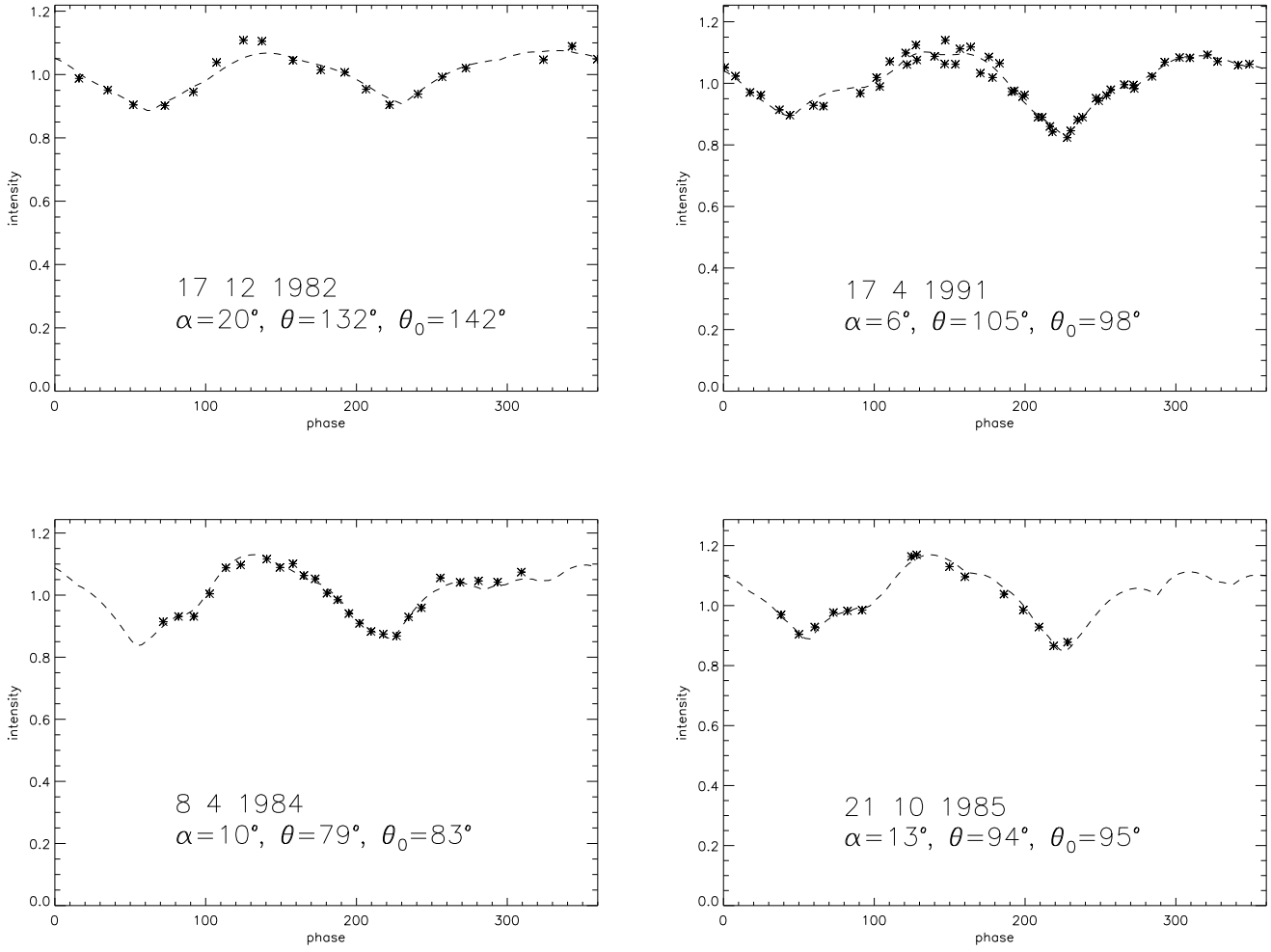
17 12 1982
α=20°, θ=132°, θ0=142°
17 4 1991
α=6°, θ=105°, θ0=98°
8 4 1984
α=10°, θ=79°, θ0=83°
21 10 1985
α=13°, θ=94°, θ0=95°
intensity
phase

Fig. 56

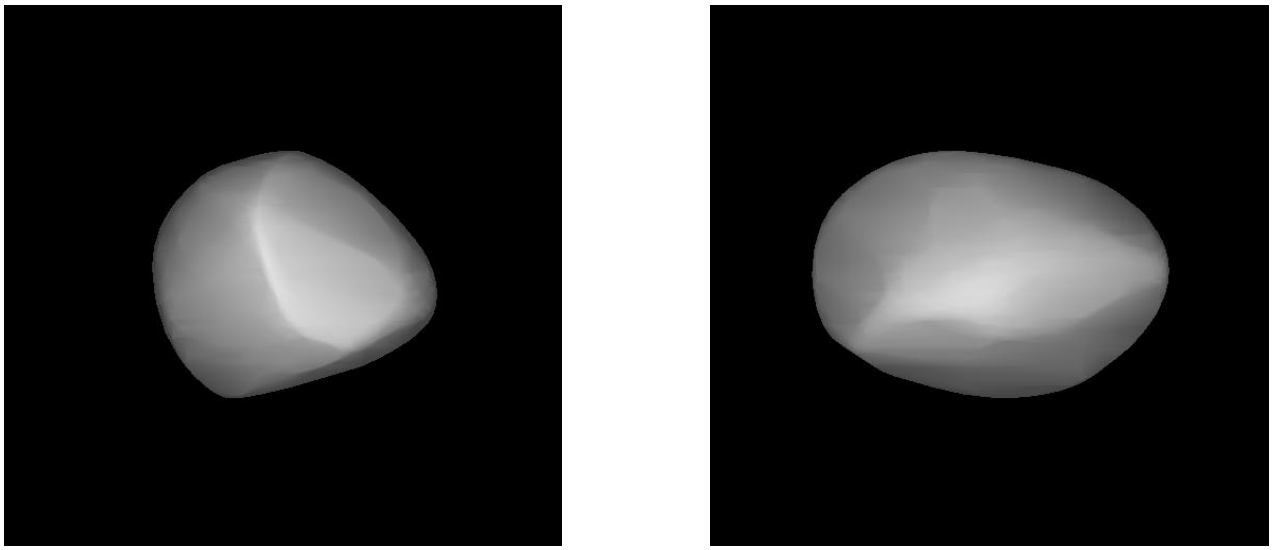

Fig. 57

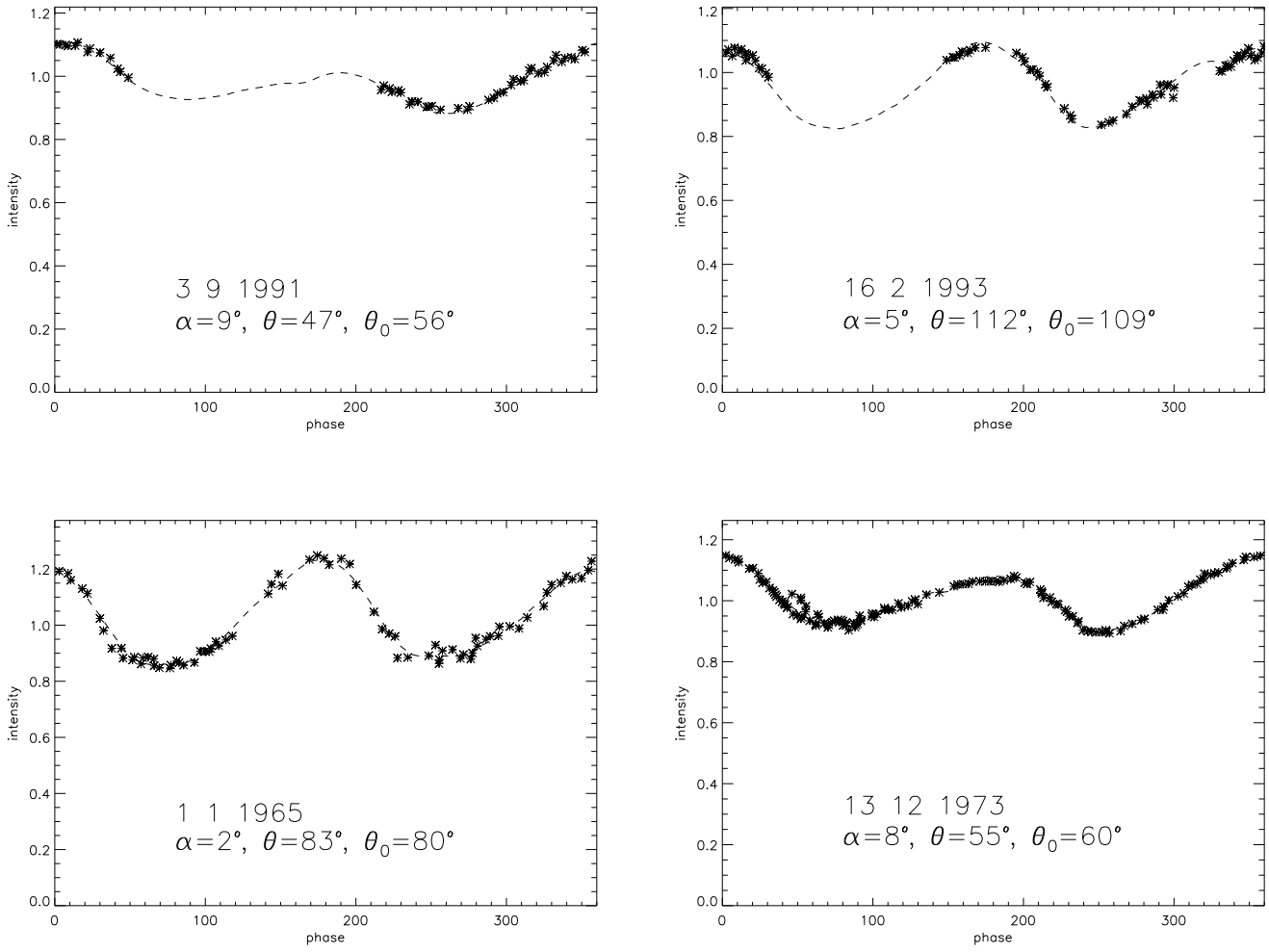
intensity
phase
3 9 1991
α=9°, θ=47°, θ0=56°
16 2 1993
α=5°, θ=112°, θ0=109°
1 1 1965
α=2°, θ=83°, θ0=80°
13 12 1973
α=8°, θ=55°, θ0=60°

Fig. 58

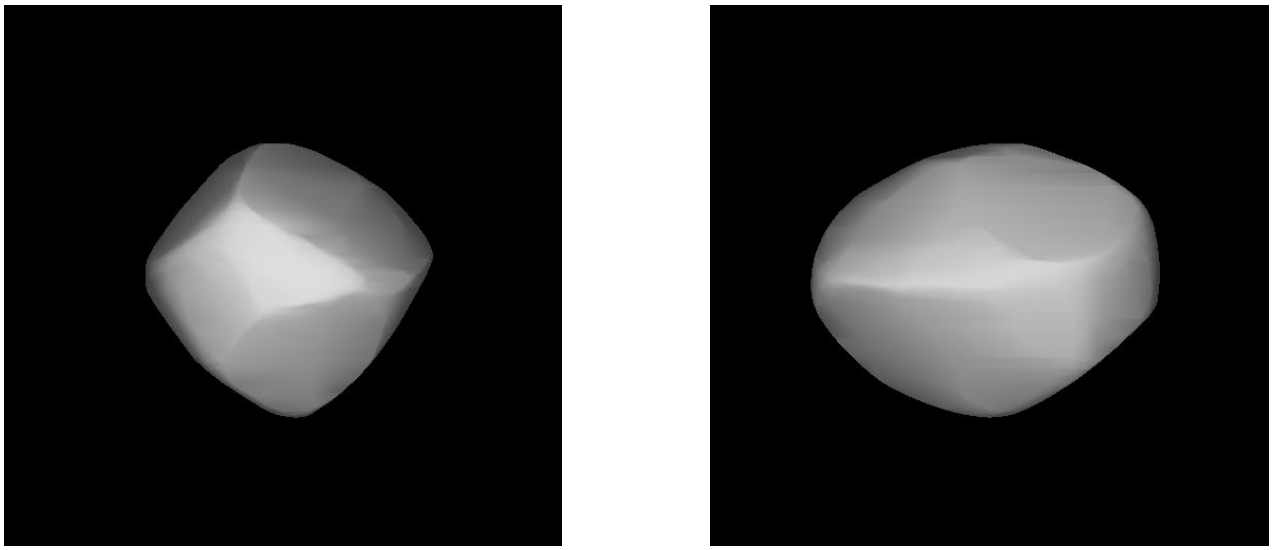

Fig. 59

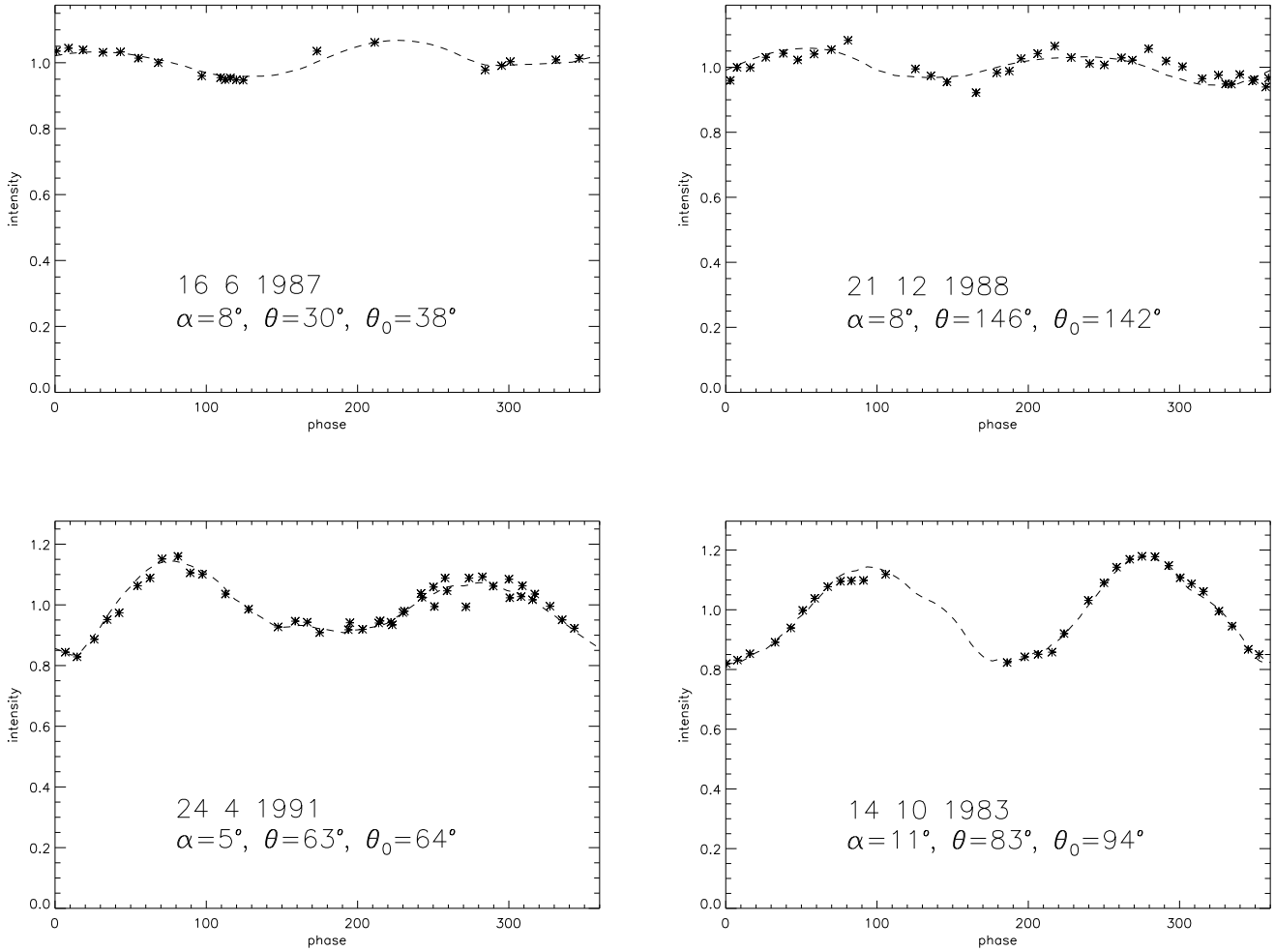
intensity
phase
16 6 1987
α=8°, θ=30°, θ0=38°
21 12 1988
α=8°, θ=146°, θ0=142°
24 4 1991
α=5°, θ=63°, θ0=64°
14 10 1983
α=11°, θ=83°, θ0=94°

Fig. 60

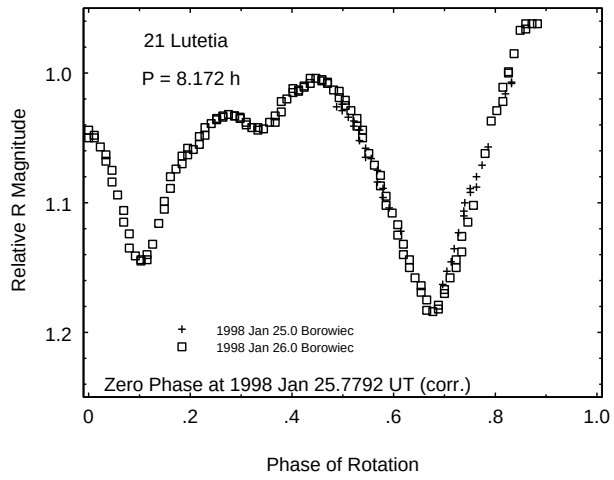

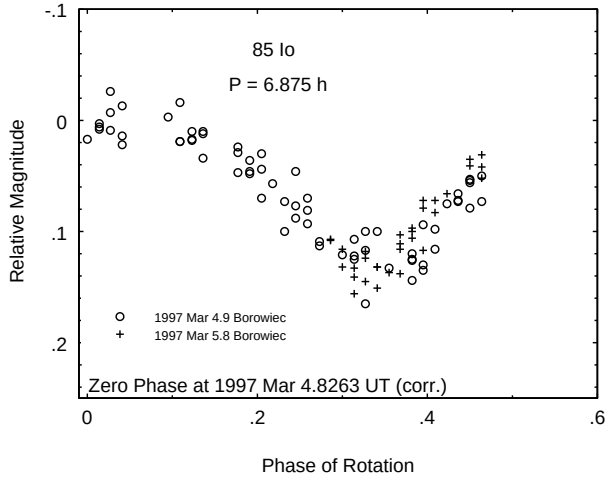

Fig. 61

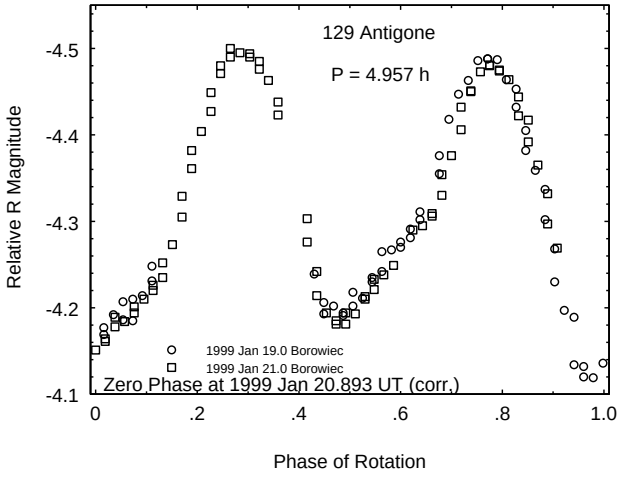

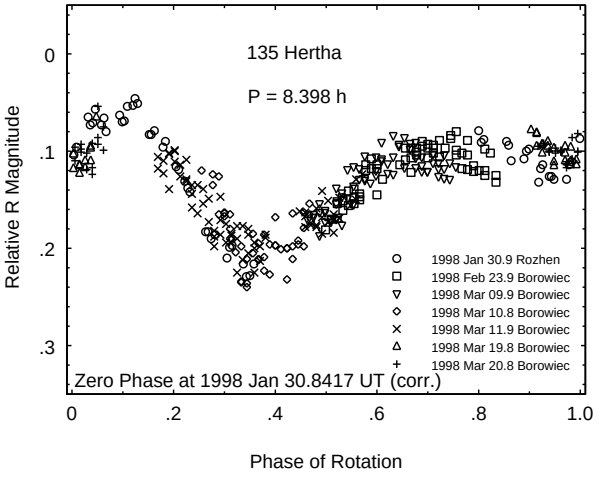

Fig. 62

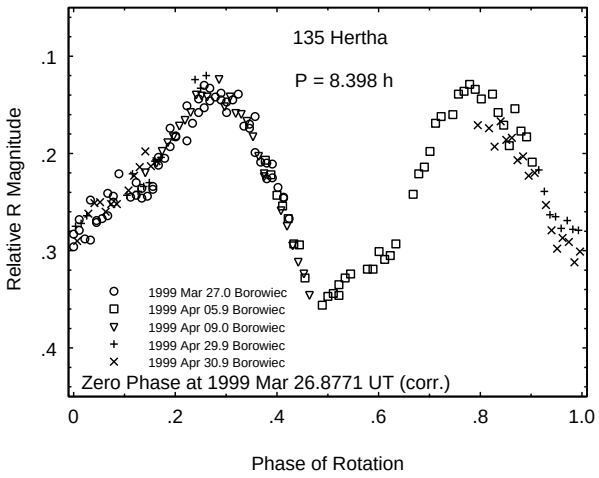

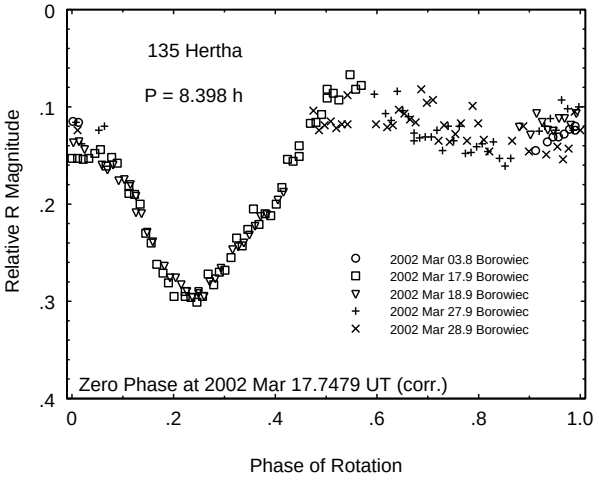

Fig. 63

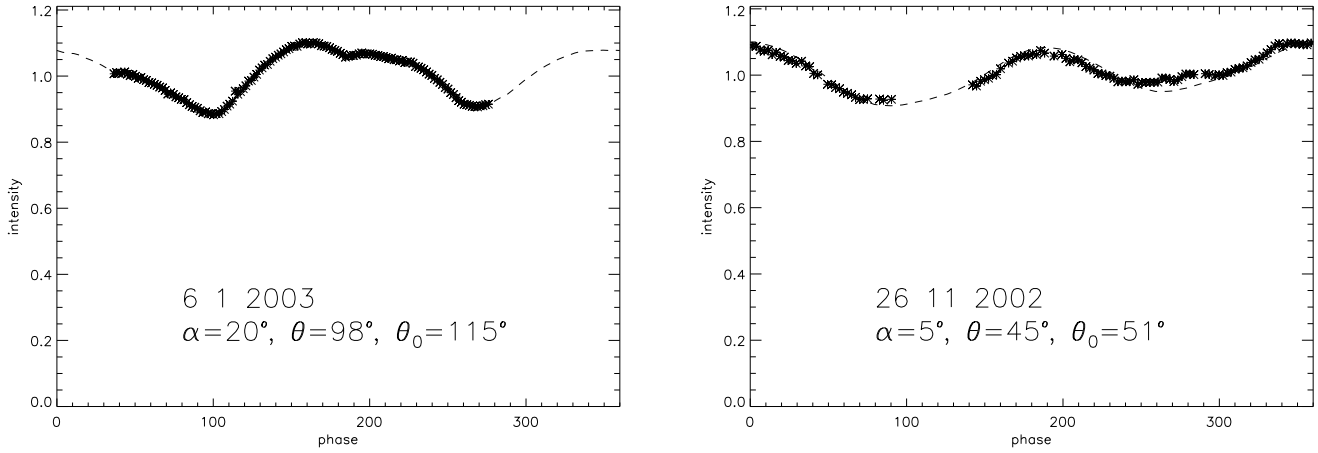

Fig. 64